



# UNIwersytet PRZYRODNICZY WE WROCLAWIU

**mgr inż. Weronika Ptak**

## **Ocena oddziaływania wybranych opon rolniczych na podłoże z wykorzystaniem cyfrowej analizy obrazu 3D**

Evaluation of the impact of selected agricultural tires on the ground  
using digital 3D image analysis

**(zestawienie publikacji naukowych stanowiących rozprawę doktorską)**

Rozprawa doktorska wykonana  
w Instytucie Inżynierii Rolniczej,  
Wydziału Przyrodniczo-Technologicznego,  
pod kierunkiem  
promotora: dr. hab. inż. Jarosława Czarneckiego, prof. uczelni  
oraz  
promotora pomocniczego: dr. inż. Marka Brennensthula

Wrocław, 2023

## Spis treści

<b>1. Streszczenie</b> .....	<b>3</b>
<b>2. Streszczenie w języku angielskim</b> .....	<b>5</b>
<b>3. Powiązane tematycznie publikacje naukowe stanowiące rozprawę doktorską</b> .....	<b>7</b>
3.1. Use of 3D scanning technique to determine tire deformation in static conditions .....	7
3.2. Evaluation of agriculture tires deformation using innovative 3D scanning method.....	15
3.3. Evaluation of tire footprint in soil using innovative 3D scanning method.....	31
3.4. Evaluation of tires acting on soil in field conditions using 3D scanning method .....	47
<b>4. Oświadczenia współautorów</b> .....	<b>62</b>
4.1. Use of 3D scanning technique to determine tire deformation in static conditions .....	62
4.2. Evaluation of agriculture tires deformation using innovative 3D scanning method.....	66
4.3. Evaluation of tire footprint in soil using innovative 3D scanning method.....	72
4.4. Evaluation of tires acting on soil in field conditions using 3D scanning method .....	78

## 1. Streszczenie

Zagęszczenie gleb spowodowane oddziaływaniem układów jezdnych pojazdów i maszyn rolniczych jest problemem trudnym do opisanego, ale zarazem ciągle aktualnym. Zachodzi zatem potrzeba dokładnego rozpoznania zjawisk zachodzących w układzie opona-gleba i poszukiwania technik pomiarowych, pozwalających na szybką i precyzyjną analizę skutków oddziaływania opon na glebę.

Niniejsza rozprawa doktorska powstała na podstawie monotematycznego cyklu czterech artykułów naukowych opublikowanych w czasopiśmie z listy Journal Citations Reports. Głównym celem badań było wyznaczenie wpływu wybranych parametrów konstrukcyjnych i eksploatacyjnych opon rolniczych na deformację gleby identyfikowaną przy użyciu innowacyjnej techniki skanowania 3D oraz komputerowej analizy obrazu. Cel ten osiągnięto poprzez realizację czterech celów cząstkowych.

W publikacji 1 przedstawiono opracowaną metodę pomiaru deformacji opony z wykorzystaniem skanowania 3D, która umożliwiła wyznaczenie wpływu ciśnienia powietrza i obciążenia pionowego koła na deformację pionową i poziomą opon rolniczych konstrukcji diagonalnej i radialnej na podłożu nieodkształcalnym (publikacja 2). W pierwszej kolejności sporządzono przekrój pionowy profilu opony. Odczytanymi parametrami była wysokość profilu oraz wysokość odpowiadająca maksymalnej deformacji poprzecznej opony – na tej wysokości sporządzono przekrój poziomy profilu, a następnie zmierzono jego szerokość i pole powierzchni. Wykazano, że wartości wysokości profilu i wysokości odpowiadającej maksymalnej deformacji poprzecznej opony były niższe dla opony radialnej w porównaniu z oponą diagonalną.

W dalszej kolejności wyznaczono wpływ ciśnienia powietrza w oponie i obciążenia pionowego koła na odkształcenia gleby spowodowane oddziaływaniem opon w warunkach laboratoryjnych. Dokonano pomiaru wymiarów geometrycznych odcisku opony na glebie, tj. długość, szerokość, głębokość determinujących powierzchnię kontaktu opony z glebą. Interpretując wyniki badań przedstawionych w publikacji 3 stwierdzono, że głębokość odcisku znacząco wpływała na jego powierzchnię. Przy stałej wartości obciążenia pionowego koła redukcja ciśnienia powietrza w oponie radialnej powodowała wzrost jej powierzchni kontaktu z glebą we wszystkich przypadkach, zaś dla opony diagonalnej nie stwierdzono takiej tendencji.

Na podstawie wyników badań opisanych w publikacji 4 wyznaczano wpływ oddziaływania opon rolniczych na glebę w warunkach polowych przy przyjętych wartościach ciśnienia powietrza w oponie i obciążenia pionowego koła. Pomiaru obejmowały te same

parametry odcisku jak w części laboratoryjnej. W przypadku opony radialnej potwierdzona została jej monotoniczność w aspekcie oddziaływania na glebę. Z kolei dla opony diagonalnej tylko w zakresie najwyższego z przyjętych ciśnień powietrza stwierdzono wzrost wszystkich parametrów na skutek kolejnych przyrostów obciążenia pionowego. W przypadku pozostałych kombinacji czynników mierzone parametry zmieniały się według niejednoznacznej tendencji.

Ostatni cel cząstkowy zrealizowano na podstawie wyników badań przedstawionych w publikacji 3 oraz publikacji 4. W pierwszej kolejności opracowano modele matematyczne (osobne dla każdej z opon) opisujące powierzchnię kontaktu opony z glebą w funkcji obciążenia pionowego koła i ciśnienia powietrza w oponie w oparciu o wyniki z części laboratoryjnej. Następnie zweryfikowano ich przydatność w części polowej. Stwierdzono, że w większym stopniu odzwierciedlenie w warunkach polowych znajdował model opracowany dla opony radialnej (współczynnik korelacji  $R^2$  był równy 0,92), zaś w przypadku opony diagonalnej przydatność modelu kształtowała się na niższym poziomie, jednak potwierdzono statystycznie istotność dopasowania modelu.

Wiadome jest, że ze względu na szereg czynników opisujących oddziaływanie opon rolniczych na glebę jednoznaczne rozwiązanie problemu jej zagęszczenia jest niemożliwe. Przeprowadzone badania umożliwiły osiągnięcie wyznaczonych celów i poszerzenie wiedzy na temat układu opona-gleba, co z pewnością przyczyni się do realizacji dalszych badań w tym zakresie.

**Słowa kluczowe:** deformacja opony; deformacja gleby; powierzchnia kontaktu opony z glebą; opony rolnicze; skanowanie 3D

## **2. Streszczenie w języku angielskim**

Soil compaction caused by the impact of the movement chassis of agricultural vehicles and machinery is a difficult issue to describe, however, is still topical. Therefore, there is a need for precise recognition of the phenomena occurring in the tire-soil system and a search for measurement techniques that allow rapid and precise analysis of the effects of tires on the soil.

This dissertation is based on a monothematic series of four scientific papers published in journals from the Journal Citations Reports list. The main objective of the research was to determine the influence of selected design and operational parameters of agricultural tires on soil deformation identified using an innovative 3D scanning technique and computer image analysis. This objective was achieved through four sub-objectives.

Publication 1 presents the developed method for measuring tire deformation using 3D scanning, which enabled the determination of the influence of air pressure and wheel vertical load on the vertical and horizontal deformation of agricultural tires of bias-ply and radial construction on the non-deformable surface (publication 2). First, a vertical cross-section of the tire profile was taken. The parameters read were the height of the profile and the height corresponding to the maximum deflection of the tire - at this height, a horizontal cross-section of the profile was drawn up and its width and area were measured. It was shown that the values for profile height and height of maximum tire deformation were lower for a radial tire compared to a bias-ply tire.

The effect of tire pressure and vertical wheel load on soil deformation caused by tire impact under laboratory conditions was then determined. The geometric dimensions of the tire footprint on the soil were measured, i.e. length, width and depth determining the tire-soil contact area. Interpreting the test results presented in publication 3, it was found that the depth of the footprint significantly affected its area. At a constant value of the vertical wheel load, a reduction in air pressure in the radial tire resulted in an increase in tire-soil contact area in all cases, while no such trend was found for the bias-ply tire.

Based on the results of the tests described in publication 4, the effect of the impact of agricultural tires on the soil under field conditions was determined at the assumed values of tire pressure and vertical wheel load. The measurements included the same footprint parameters as in the laboratory section. In the case of the radial tire, its predictability in terms of the impact on the soil was confirmed. For the bias-ply tire, on the other hand, only in the range of the highest air pressure adopted was there an increase in all parameters as a result

of successive increases in vertical load. The measured parameters changed according to an ambiguous trend for the other factor combinations.

The last sub-objective was achieved on the basis of the research results presented in publication 3 and publication 4. First, mathematical models (separate for each tire) were developed to describe the tire-soil contact area as a function of vertical wheel load and tire pressure based on the results from the laboratory part. Their suitability was then verified under the field conditions. It was found that the model developed for the radial tire was more closely reflected under the field conditions (correlation coefficient  $R^2$  was equal to 0.92), while the suitability of the model for the bias-ply tire was at a lower level, however, the statistical significance of the model was confirmed.

It is known that due to a number of factors describing the impact of agricultural tires on the soil, an unambiguous solution to the problem of soil compaction is impossible. The research has made it possible to achieve the set objectives and broaden knowledge of the tire-soil system, which will certainly contribute to further research in this area.

**Keywords:** tire deformation; soil deformation; tire-soil contact area; agriculture tires; 3D scanning

### **3. Powiązane tematycznie publikacje naukowe stanowiące rozprawę doktorską**

#### 3.1. Use of 3D scanning technique to determine tire deformation in static conditions

Autorzy: **Weronika Ptak**, Jarosław Czarnecki, Marek Brennensthul

Czasopismo: Journal of Agriculture Engineering, 2022, 53, 1-7

Doi: 10.4081/jae.2022.1221

# Use of 3D scanning technique to determine tire deformation in static conditions

Weronika Ptak, Jaroslaw Czarnecki, Marek Brennensthul

Wroclaw University of Environmental and Life Sciences, Institute of Agricultural Engineering, Wroclaw, Poland

## Abstract

This paper presents an innovative digital method to analyse agricultural tire profiles based on pictures. From this method, we can conclude that the tire deformation is caused by the changes in vertical load and inflation pressure. The first stage in this method is 3D-scanning; the vertical cross-section is created from the obtained picture of the tested tire. From this cross-section, the deflection of the tire can be determined. Then, the horizontal cross-section is created - this operation allows determining the tire's contact area at the highest vertical deformation. Obtained results can be useful to create the tire deformation characteristic. In turn, the contact pressure values can be determined (even through laboratory testing, without research in field conditions). The knowledge about contact pressure allows taking some actions to reduce soil compaction. In the description of the method, the radial tire was used, but the structure and equipment of the test bench allow the use of cross-ply tires with different dimensions.

## Introduction

Nowadays, in farming production, the choice of appropriate technologies is a very important factor. Moreover, in the case of agricultural vehicles, the choice of technical-exploitation parameters of the tires is essential. Consequences of inadequate choice of these parameters can be reflected in excessive soil compaction; further, the soil environment can be exposed to severe disturbances (Ani *et al.*, 2018; Guimarães Júnnyor *et al.*, 2019; Keller and *et al.*, 2019). For this reason, information about phenomena in

the tire-surface system is required.

Recently, two main types of agricultural tires (with different internal structures) are available in the market. The first type consists of bias-ply tires that have greater mechanical strength - these tires are more resistant to damages, but are less flexible. The second type is composed of the radial tires - in this case, the flexibility is higher than in bias-ply tires, so the possibility of use of low inflation pressures is higher too (Lindemuth, 2006). Due to the farming practice, the appropriate total range of the inflation pressure is 0.8-2.0 bar. At the field operations, the inflation pressure should be in the range 0.8-1.2 bar, while at the transportation, inflation pressure can be higher (above 1.2 to 2.0 or even higher - in the case of tires with higher dimensions). It is related to different deformability - on the soft surfaces, a tire with low pressure can have a greater contact area than a tire with high pressure. In turn, it limits the sinkage of the tire - as a result, the compaction is lower. On the other hand, inflation pressure should be higher than in the field at the transportation because it can reduce rolling resistance. Manufacturers of the agricultural tires recommend specific inflation pressure values depending on tire dimensions, load, and velocity (Kowalski, 2006). These changeable parameters determine the deformation of the tire and, as a consequence, they affect the tire-surface area (Arvidsson and Keller, 2007; Diserens *et al.*, 2011; Taghavifar and Mardani, 2013).

Due to the different stiffness of tires, their action on surfaces will be changeable. For this reason, it is necessary to research tires in the aspect of flexibility (Misiewicz *et al.*, 2016; Anifantis *et al.*, 2020). In the same cases, the deflection is measured by sensors (Song *et al.* 2018), while in other research, more complex methods are used - for example, in (Anifantis *et al.*, 2020). However, it can be stated that the parameters of the tires (*i.e.*, sizes, design, internal structure) are so different that the determination of flexibility is a complex issue. For this reason, in literature, there are more publications about the impact of tires on surfaces.

Many authors use different methods to measure the tire-surface contact area and soil deformation resulting from wheels' static and dynamic effects (Błaszkiwicz, 1990; Wulfsohn and Upadhyaya, 1992). The simplest are based on tires footprints measurements (Grečenko, 1995). In general, based on mathematical and geometric models as well as on the elasticity theory, they determine the contact area using a rectangular coordinate system and elliptical estimation. By means of a profilometer, Jurga (2008) studied soil deformation, performing measurements of the rut formed by the passage of wheels. Diserens (2009) used a photometric method, taking pictures of the tire-soil contact surfaces and then analysing them in the Adobe Photoshop Elements software. Derafshpour *et al.* (2019) filmed the passage of a tire on glass covered with a special liquid to observe the change in the area of the tire contact with the surface using the technique of image processing. Kumar *et al.* (2018) used carbon paper between two sheets of white paper, placing them under a tire.

The latest methods to study changes in shape, dimensions, and

Correspondence: Weronika Ptak, Wroclaw University of Environmental and Life Sciences, Institute of Agricultural Engineering, 51-630, Wroclaw, Poland.

E-mail: weronika.ptak@upwr.edu.pl

Key words: Agricultural tire; 3D scanning; contact pressure; tire deformation.

Received for publication: 24 June 2021.

Accepted for publication: 2 December 2021.

© Copyright: the Author(s), 2022

Licensee PAGEPress, Italy

Journal of Agricultural Engineering 2022; LIII:1221

doi:10.4081/jae.2022.1221

This article is distributed under the terms of the Creative Commons Attribution Noncommercial License (by-nc 4.0) which permits any non-commercial use, distribution, and reproduction in any medium, provided the original author(s) and source are credited.



area include digital image analysis technology with 3D scanning. This method has been widely used, among others, in medicine, materials science, assembly lines, or the machine wear testing (Stawicki, 2018; Lazarević *et al.*, 2019; Alontseva *et al.*, 2020; Zhang *et al.*, 2020). For example, Farhadi *et al.* (2018) used a 3D scan to measure plaster of Paris moulds of tire footprints on the soil to study the volume of the rut, with its width and depth.

According to the literature, the studies of the wheel-surface contact are carried out by different methods, but only a small part of them allow spatial analysis already at the experiment stage. Moreover, only some of them allow immediate visualization of the spatial image of the tire (during the experiment). In these methods, individual analysis of each plane is realised; then the spatial picture is created. Whereas in these methods, a three-dimensional picture of tire profile is applied (during the experiment) - the individual analysis of separate planes is not needed. Most often, what is analysed is planes, which are used to create spatial models at a later stage. Therefore, it has become appropriate to develop a method that allows for quick spatial imagery of objects (wheel and surface interacting with each other). Based on such a spatial model, any number of planes, like tire cross-section or tire-soil contact surface, will be analysed. For these reasons, this paper aimed to present the innovative method of digital analysis of agricultural tires, especially to evaluate their deformation at different vertical loads and inflation pressures.

## Materials and methods

The overall concept of the experiment was to develop a method of static tests of agricultural tires through digital analysis of the spatial image of their profile. In this way, applying various vertical loads and air pressure, it was possible to characterize tires in terms of their horizontal and vertical deformation and of their contact with the surface. Various vertical loads and air pressure in the tire were used as experimental factors. It was assumed that the first stage static tests would be carried out under laboratory conditions on a non-deformable surface - during this test, the tire footprint was created with no torque applied. The test bench allowed testing tires of different sizes and designs. The one used in the present experiment was the radial 500/50R17 tire, and its technical parameters are presented in Table 1.

### Characteristics of the test bench

The design of the test bench made it possible to carry out tests on two types of surfaces: i) non-deformable surfaces - intended to predetermine the characteristics of the tire, mainly related to its deformability; such tests can be used as a model for further research; ii) deformable surfaces - intended to study the interaction of the tire with a particular surface. It will be possible to determine both the deformation of the tire and the surface. The surface material (*e.g.*, soil) will be placed in the so-called soil bathtub; iii) the present article sets out the principles of measuring and analysing the results for the non-deformable surface.

The research tools consist of two main parts: i) universal test bench for various static vertical load values, which was self-designed and made from standard elements of the steel. The only pieces from the market were the sensor (to measure vertical load) and the hydraulic jack; ii) a kit for creating and analysing a digital image of the tire profile.

With its outline presented in Figure 1A and its overall view in Figure 1B, the test bench allows applying various load values to

non-drive wheels of agricultural trailers, spreaders, or balers, *i.e.*, machinery causing soil compaction. In this experiment, only non-driving wheels were tested because the test bench was not fitted in the driving mechanism of the tire. The presented test bench is appropriate to static tests - their results will allow creating the characteristics of tire deformation. Moreover, the tests of non-driving wheels have practical justification because these tires can be exposed to the highest loads; the driving wheels in the tractors are sometimes equipped in systems to inflation pressure control, while the tires in trailers/balers/spreaders are not equipped in these systems. The design of the test bench is based on a vertical frame (3) made of steel closed profiles (Figure 1A). The tested tire (2) is mounted on a shaft with bearings, which in turn, is fixed to the inner frame (4). As a result of the use of linear steel guides, the inner frame can only move vertically, eliminating the risk of unintentional movement of the wheel.

The smooth change in the vertical load of the tire is achieved through a hydraulic cylinder (6) located between the main frame and the inner frame. The vertical load is measured using the TecSis dynamometer (5) with a measurement accuracy of 50 N and a measuring range of 0-100 kN. Therefore, the maximum vertical load that can be obtained with the hydraulic cylinder is 50 kN. This value is within the range of the vertical load of an agricultural machinery tire, often found in practice (Brennenstul, 2016). It is also in line with the maximum tire load capacity recommended by the manufacturer (described in the load index and in the catalogue data). The screw mechanisms (7) mounted at the top of the test bench are used to lock the position of the inner frame (4). The test bench allows the research of tires with a maximum external diameter of 1500 mm and a maximum width of 500 mm. Due to the recommendations of tires manufacturers and the ETRTO book, the values of the vertical loads for the tires with described dimensions do not exceed 4000-4500 kg. For this reason, the elements of the test bench (in the aspect of mechanical strength) were chosen to a maximum load of about 5000 kg. Therefore, the maximum capacity of the hydraulic jack was 4500 kg. Technical parameters of the tested bench are presented in Table 2.

**Table 1. Technical parameters of the tested tire.**

Parameter	Radial tire
Construction	Radial tire
External diameter (mm)	932
Profile width (mm)	500
Profile indicator (%)	50
Rim diameter (inch/mm)	17/432
Profile height (mm)	250
Load index (-)	146
Max load (kg)	3250



The kit for creating and analysing a digital tire profile image consists of a 3D scanner (SMARTTECH3D UNIVERSE, SMARTTECH3D, Poland, Warsaw, www.smarttech3d.com/), whose technical parameters are presented in Table 3. The scanner was connected to a laptop with dedicated Smarttech3D measure software, enabling continuous real-time data visualization.

### Scanning process

The tests began with the installation of the wheel at the test bench, with the scanner placed on the ground. Scanning was carried out from 12 different positions around the tire to cover its different parts and contact with the surface. Before scanning, parameters such as tire air pressure and vertical load were preset. The load, *i.e.*, the force produced by the hydraulic cylinder, changed smoothly, and its values were available on the laptop. Once the required load value was reached, the inner frame was mechanically locked by means of the screw mechanism, eliminating the risk of inadvertently reducing the vertical load due to a drop in pressure in the hydraulic cylinder (*e.g.*, due to internal leaks). Because the tire was black, it was covered with anti-glare spray coating (with white matt surface) to achieve greater contrast so that the light of the scanner could more accurately record the scanned object.

Such procedure is used to scan dark objects - an alternative to coating is painting the object white. Since the scanner can only be used up to a specific volumetric size, larger objects are divided into parts to be scanned; then all those scans are combined using the scanner software. The result is a spatial image of the tire profile.

Before scanning, an ellipse was drawn around the test bench on the ground, with 12 marked points indicating where the scanner had to be positioned when scanning parts of the tire. The connection of the many scans was a native function of the scanning laser equipment. The ellipse with the scanner's location was developed based on previous tests - the distance between the scanner and tire was determined by measuring the volume of the scanner. Figure 2 shows the layout of the scanner locations to ensure that the full spatial image of the tire was obtained. These positions opposite the tread are closer to each other due to the different geometry of this

part of the tire, requiring more images to be taken. The optimal distance of the scanner (its working distance) was when three light beams emitted by the projector met, indicating the centre of the scanning volume. Figure 3 (left part) shows the scanning effect when the location points of the scanner were evenly spaced, with red colour indicating parts of the tire not captured by the scanning volume. This was due to the positions of the scanner, in general, angled with respect to the tire median plane. With the scanner positions opposite the thread closer to each other, it was possible to fill in the 'blank spaces'. The effects are highlighted in green in Figure 3 (right part), with the tire's shoulders clearly visible.

**Table 2. Technical parameters of the tested bench.**

Parameter	Value
Height (mm)	2100
Width (mm)	950
Length (mm)	700
Max external diameter of tested tire (mm)	1500
Max width of tested tire (mm)	500
Max displacement achievable by the hydraulic jack (mm)	320
Weight (without tire) (kg)	90

**Table 3. Technical specification of 3D scanner.**

Parameter	Description
Scanning technology	white structural light - LED
Measuring volume (x*y*z) (mm)	400×300×240
Distance between points (x*y) (mm)	0.156
Accuracy (mm)	0.08
Power consumption during measurement (W)	200
Weight (kg)	4.40
Working temperature (°C)	20+/-0.5

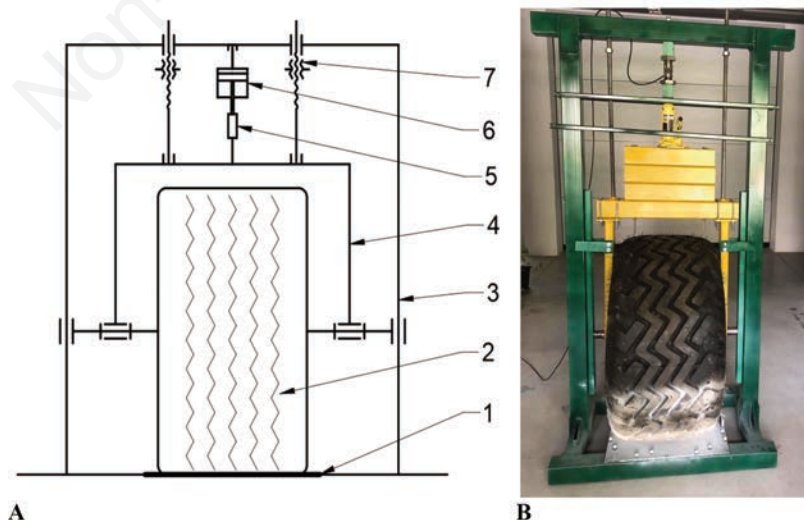


**Figure 1. A) The outline of a test bench to study tires with different loads applied: 1- surface, 2- wheel with tire, 3- main frame, 4- inner frame, 5- dynamometer, 6- hydraulic cylinder, 7- screw mechanism for locking the position of the inner frame. B) Overall view of a test bench to study tires with different loads applied.**

The scanner software allows filling blank spaces, but the two extreme edges of the tire tread need to be scanned to use it. The blank spaces could be caused by a lack of continuity of the picture created after scanning. It can negatively influence the created spatial picture of the tire. Therefore, it is better if the positions of the scanner are closer to each other. Based on previous tests, it was assumed that for a tire approximately 500 mm wide and approximately 900 mm in diameter, the optimum number of the positions would be 12. With fewer scanner locations, the scanning process would be faster, but the images obtained (particularly the tire tread) would not be sufficiently mapped. On the other hand, it would be too time-consuming to perform more scans, and the resulting tire image would not differ in accuracy compared to the number of scans finally taken. Of course, this method can also be used for tires with other external dimensions, but it is advisable to predetermine the number of the scanner positions beforehand.

The result of the combination of individual scans of different parts was a spatial image of the tire profile consisting of a point cloud (Figure 4A). This image allowed creating a mesh of triangles (Figure 4B) that was the basis for determining horizontal and ver-

tical sections of the tire profile. An essential element for scanning was the surface as a reference plane to help further analyse the image. The surface scan included a view of its front part (the surface was made up of a flat piece of sheet metal 4 mm thick).

The mesh of triangles was used to draw cross-sections, which were then exported to AutoCad 2019 (Auto-Desk), where detailed results were obtained from the analysis of tire deformation depending on vertical load and tire air pressure. First, the A-A vertical plane cross-section passing through the tire-surface contact was analysed (Figure 5). Based on this section, it was possible to determine both the vertical deformation of the profile (flattening) and the horizontal deformation (the tire sidewalls move away from each other). Horizontal section B-B was then analysed with a plane parallel to the surface, with its distance from the surface, or height (hp), at the largest horizontal deformation of the tire after the load was applied.

Based on the vertical section analysis (A-A, Figure 5), the width of the tire profile (b) and vertical deformation or flattening (h) were read from the graphics program. An example of a vertical section is presented in Figure 6A.

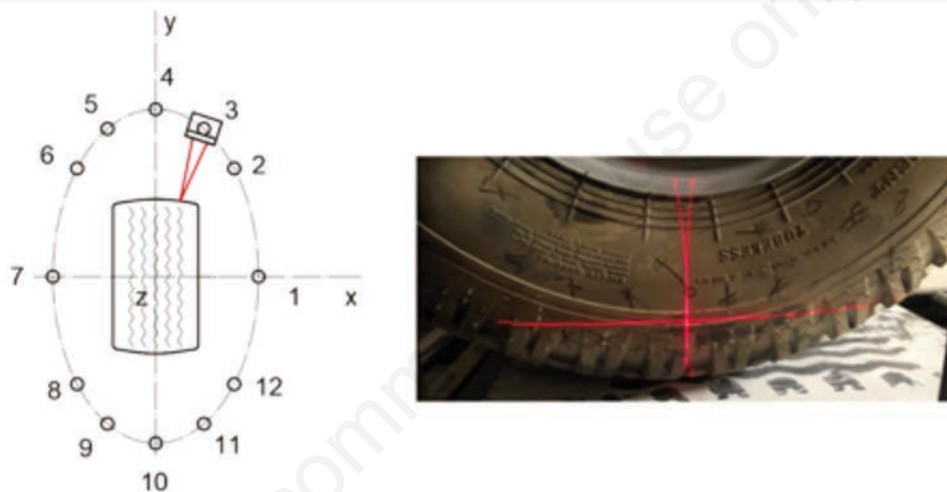


Figure 2. Positions of the scanner around the tire (left), the view of the laser beams on the scanned tire (right).



Figure 3. Tread scanning effects: the effect with scanner location points evenly spaced (left), the effect with scanner location points unevenly spaced (right).



From the horizontal section (B-B, Figure 5) it was possible to read its precise area using geometric dimensions (length, width). Then, based on the previously known vertical load value and the calculated area, it was possible to predict the contact pressure at a given rut depth. An example horizontal section made at a height corresponding to the maximum horizontal deformation of the tire is presented in Figure 6B.

It is recommended at least three repetitions for each of all combinations. The accuracy of our method is so high because the experiment is conducted in the same conditions (the same place, the same time). Therefore, in addition to the very high resolution of the scanner, the high accuracy of the whole method can be obtained. The availability of the method is dependent on the cost of the scanner - it is the most expensive element of the whole test bench. Other parts of the test bench were made from typical elements with low costs.



Figure 4. A) A spatial image of a tire profile consisting of a point cloud. B) View of the created triangle mesh prepared for cross-sectional processing (left), the effect of zooming triangle mesh (right).

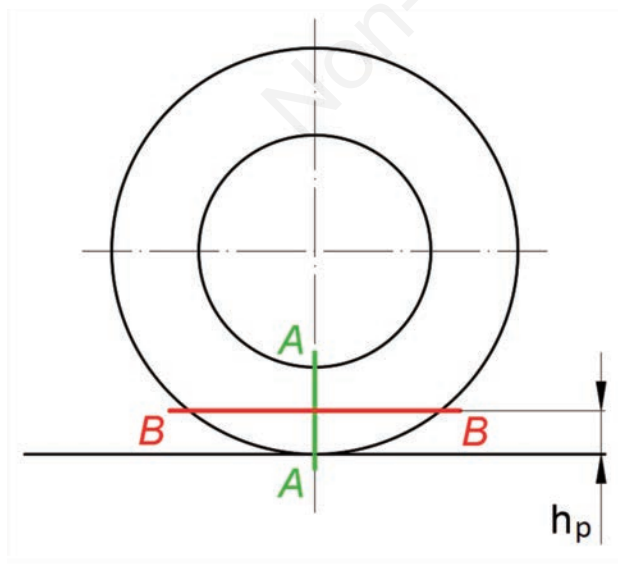


Figure 5. Location of planes making tire profile sections: A-A - vertical section plane, B-B - horizontal section plane,  $h_p$  - horizontal section plane distance from the surface.

## Results

Based on the scans and cross-sections, it was possible to determine the geometrical dimensions of the widest cross-section of the tire on a plane parallel to the support plane. In the first place, the vertical deformation values were determined using vertical section analysis. A comparison of the cross-sections for the loaded and unloaded tire is presented in Figure 7A.

According to Figure 7A, at the initial load of 1275 N (resulting only from the weight of the tire and the internal frame of the test bench), the profile height was 239.6 mm, and the width was 485.0 mm. After increasing the load to 14,715 N (it was reflected the mass of 1500 kg), a flattened profile was observed, with the height lower by 25.1 mm, or about 12%. At the same time, an increase in the horizontal section area was recorded, with the width increasing by 20.2 mm (about 4%). The figure also shows the height at the greatest horizontal deformation, which amounted to 122.8 mm for the unloaded tire and 98.9 mm for the loaded tire. At these heights, horizontal sections presented in Figure 7B were subsequently drawn (in a plane parallel to the surface).

Using geometric dimensions, it was possible to measure the area of a horizontal section, which in the later stages of the analysis allowed the calculation of the tire-surface contact pressure. For the tire with the lower load, the length of the footprint was 239.6 mm, and the cross-sectional area was 89,389.2 mm<sup>2</sup> (approx. 0.089 m<sup>2</sup>). The calculated contact pressure would be 0.014 MPa in this case

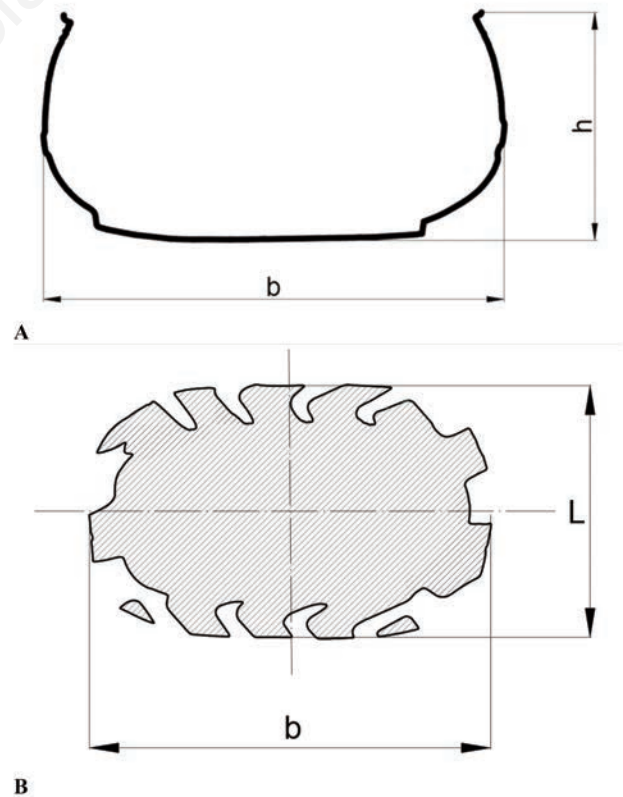


Figure 6. A) An example of a vertical section of a tire profile created in the graphics program; b- profile width (horizontal deformation), h- profile height (vertical deformation). B) An example of a horizontal section of a tire with dimensions: L- length, b-width.

(hypothesizing a sinking of the tire up to the indicated section). After increasing the load to 14,715 N, the footprint length increased by 80.1 mm (33%) and its width by 20.2 mm (4%). The cross-sectional area was 123,291.3 mm<sup>2</sup> (approx. 0.12 m<sup>2</sup>), increasing by approximately 33,902 mm<sup>2</sup> (approx. 0.03 m<sup>2</sup>), or 37.9%. With an applied load level of 14,715 N, under the same hypothesis, the contact pressure was 0.119 MPa. The significant increase in contact pressure (compared to the load of 1275 N) was mainly a result of a significant increase in vertical force. In such an experiment, it is, of course, possible to use other vertical load values in the range of up to 50,000 N, which will allow more complete studies of changes in the contact area and contact pressure.

Geometrical parameters of the tire in two different load states are presented in Figure 8. The parameter with the most significant increase due to an increase in vertical load was the length of the horizontal section - in this case, it was 32.9%. Its width increased by about 4% and the profile height by just over 14%.

Figure 9 presents the tire-surface contact area and contact pressure for two different load values. According to the graph, an increase in vertical load from 1275 to 14,715 N resulted in an increase in the contact area by 0.034 m<sup>2</sup>. In addition, a significant increase in contact pressure, by 0.105 MPa, was recorded, mainly due to a significant increase in vertical load.

## Discussion and conclusions

Since this is a methodological paper, it aims to present the innovative method of analysis of agricultural tires deformation. The proposed method of digital image analysis allows studying vertical and horizontal deformation of a tire with various loads and pressure applied. Thanks to the use of computer software, it was possible to measure the deflection of the tire and the area of its contact with the surface at any load applied. The data collected in the experiment can be used to study changes of such parameters in laboratory conditions without the need for time-consuming and costly field tests.

To evaluate the parameters in the tire-surface system, many methods have high accuracy (Wulfsohn and Upadhyaya, 1992; Diserens *et al.*, 2011; Taghavifar and Mardani, 2013). Unfortunately, they often allow analysing just single parameters - for example, rut depth (Diserens, 2009) or contact area (Sivarajan *et al.*, 2018; Derafshpour *et al.*, 2019). In comparison with other methods, the proposed method is complex because it can be used to quickly assess the main parameters of tire-surface systems. Because the 3D-scanning methods are becoming more popular (Farhadi *et al.*, 2018; Stawicki, 2018; Lazarević *et al.*, 2019), the presented method is rational for further use. Moreover, it can be used to evaluate deformation both the tire and soil - it will be helpful at the choice of optimal conditions of agricultural tire use.

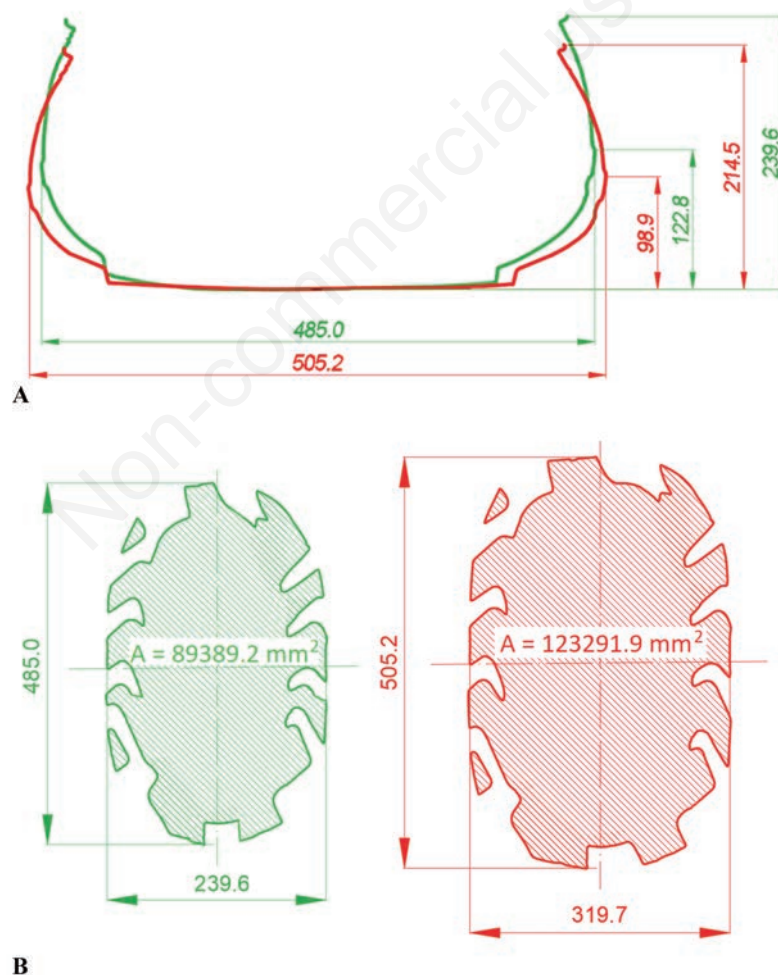
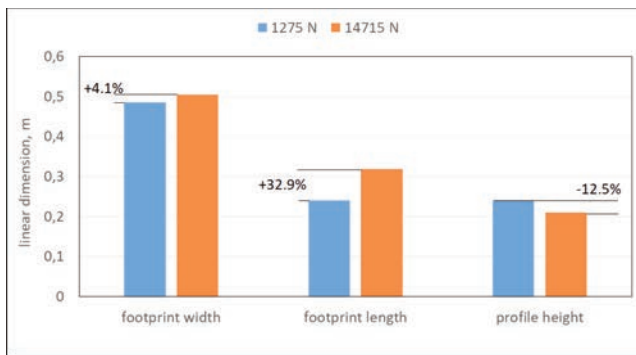
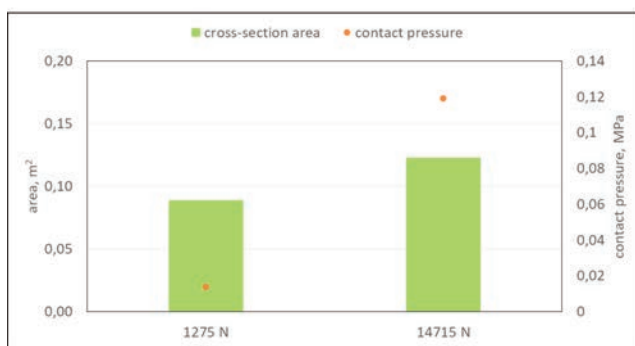


Figure 7. A) Cross-section width and height at both vertical load values: green- tire loaded with 1275 N, red- tire loaded with 14715 N. B) Horizontal sections of tire 500/50R17 profile: green- tire with 1275 N load, red- tire with 14715 N load.



**Figure 8.** The effect of two vertical load levels on the width, length, and height of the tire 500/50R17 footprint and on the tire profile height at the surface-tire contact section %.



**Figure 9.** The tire-surface contact area and contact pressure for both vertical load values.

## References

- Alontseva D.L., Ghassemieh E., Krasavin A.L., Kadyroldina A.T. 2020. Development of 3D scanning system for robotic plasma processing of medical products with complex geometries. *J. Electron. Sci. Technol.* 100057.
- Ani O.A., Uzoejinwa B.B., Ezeama A.O., Onwualu A.P., Ugwu S.N., Ohagwu C.J. 2018. Overview of soil-machine interaction studies in soil bins. *Soil Till. Res.* 175:13-27.
- Anifantis A.S., Cutini M., Bietresato M. 2020. An experimental-numerical approach for modelling the mechanical behaviour of a pneumatic tyre for agricultural machines. *Appl. Sci.* 10:3481.
- Arvidsson J., Keller T. 2007. Soil stress as affected by wheel load and tire inflation pressure. *Soil Till. Res.* 96:284-91.
- Błaszkiwicz Z. 1990. A method for the determination of the contact area between a tire and the ground. *J. Terramechan.* 27:263-82.
- Brennensthal M. 2016. Co warto wiedzieć o oponach? *AgroProfil* 6/2016.
- Da Silva Guimarães Júnnyor W., Diserens E., De Maria I.C., Junior C.F.A., Farhate C.V.V., de Souza Z.M. 2019. Prediction of soil stresses and compaction due to agricultural machines in sugarcane cultivation systems with and without crop rotation. *Sci.Total Environ.* 681:424-34.
- Derafshpour S., Valizadeh M., Mardani A., Saray M.T. 2019. A novel system developed based on image processing techniques for dynamical measurement of tire-surface contact area. *Measurement.* 139:270-6.
- Diserens E. 2009. Calculating the contact area of trailer tyres in the field. *Soil Till. Res.* 103:302-9.
- Diserens E., Défossez P., Duboisset A., Alaoui A. 2011. Prediction of the contact area of agricultural traction tires on firm soil. *Biosyst. Engine.* 110:73-82.
- Farhadi P., Golmohammadi A., Sharifi A., Shahgholi G. 2018. Potential of three-dimensional footprint mold in investigating the effect of tractor tire contact volume changes on rolling resistance. *J. Terramechan.* 78:63-72.
- Grečenko A. 1995. Tyre footprint area on hard ground computed from catalogue values. *J. Terramechan.* 32:325-33.
- Jurga J. 2008. Wpływ głębokości koleiny i ciśnienia powietrza w ogumieniu na naciski jednostkowe kół ciągników na glebę. *Inżynieria Rolnicza* 4:347-51.
- Keller T., Sandin M., Colombi T., Horn R., Or D. 2019. Historical increase in agricultural machinery weights enhanced soil stress levels and adversely affected soil functioning. *Soil Till. Res.* 194: 104293.
- Kowalski B. 2006. *Rolnictwo na kołach.* Farmer 21/2006.
- Kumar S., Pandey K.P., Kumar R., Kuma A. 2018. Effect of ballasting on performance characteristics of bias and radial ply tyres with zero sinkage. *Measurement* 121:218-24.
- Lazarević D., Nedić B., Jović S., Šarkoćević Ž., Blagojević M. 2019. Optical inspection of cutting parts by 3D scanning. *Physica A Stat. Mechan. Appl.* 121583.
- Lindemuth B.E. 2006. An overview of tire technology. *The Pneumatic Tire*, U.S. Department of Transportation, 3-7.
- Misiewicz P.A., Richards T.E., Blackburn K., Godwin R.J. 2016. Comparison of methods for estimating the carcass stiffness of agricultural tyres on hard surfaces. *Biosyst. Engine.* 147:183-92.
- Sivarajan S., Maharlooei M., Bajwa S.G., Nowatzki J. 2018. Impact of soil compaction due to wheel traffic on corn and soybean growth, development and yield. *Soil Till. Res.* 175:234-43.
- Song H.S., Sim K.S., Park T.W. 2018. Optimal tread design for agricultural lug tires determined through failure analysis. *J. Agric. Engine.* 49:64-70.
- Stawicki T. 2018. Limit wear of working parts of subsoil shanks with regard to their design solutions. *J. Res. Appl. Agric. Engine.* 63:115-20.
- Taghavifar H., Mardani A. 2013. Investigating the effect of velocity, inflation pressure, and vertical load on rolling resistance of a radial ply tire. *J. Terramechan.* 50:99-106.
- Wulfsohn D., Upadhyaya S.K. 1992. Determination of dynamic three-dimensional soil-tire contact profile. *J. Terramechan.* 29:433-64.
- Zhang J., Huang J., Fu C., Huang L., Ye H. 2020. Characterization of steel reinforcement corrosion in concrete using 3D laser scanning techniques. *Constr. Build. Mat.* 270:121402.

### 3.2. Evaluation of agriculture tires deformation using innovative 3D scanning method

Autorzy: **Weronika Ptak**, Jarosław Czarnecki, Marek Brennensthul,  
Krzysztof Lejman, Agata Małecka

Czasopismo: Agriculture, 2022, 12(8), 1108

Doi: [10.3390/agriculture12081108](https://doi.org/10.3390/agriculture12081108)

## Article

# Evaluation of Agriculture Tires Deformation Using Innovative 3D Scanning Method

Weronika Ptak <sup>\*</sup>, Jarosław Czarnecki, Marek Brennenstul , Krzysztof Lejman and Agata Małecka

Institute of Agricultural Engineering, Wrocław University of Environmental and Life Sciences, 51-630 Wrocław, Poland; jaroslaw.czarnecki@upwr.edu.pl (J.C.); marek.brennenstul@upwr.edu.pl (M.B.); krzysztof.lejman@upwr.edu.pl (K.L.); 113322@student.upwr.edu.pl (A.M.)

\* Correspondence: weronika.ptak@upwr.edu.pl

**Abstract:** This study presents the results of research related to agriculture tire deformation under variable vertical load and inflation pressure. The research objects were two tires of the same size and different internal structures. Three levels of inflation pressure and five levels of vertical load were used. The loaded tire with each inflation pressure was scanned using the 3D scanner—the effect of this operation was a three-dimensional image of a tire part (near the place of contact with the surface). The next step was the creation of vertical and horizontal cross-sections of the tire profile, which allowed the analysis of tested parameters: profile height, location of the point of maximum tire deflection, the width of the tire profile, and the area of horizontal cross-sections. Finally, the mathematical model was formulated, describing contact areas of horizontal cross-sections as a function of the factors. Based on the conducted research, it was stated that an increase in vertical load caused reductions in both types of heights. Moreover, the width of tire profiles and the area of horizontal cross-sections increased due to the increase in vertical load (for bias-ply, increases were smaller than for radial tires). Similar changes were observed after the reduction of inflation pressure.

**Keywords:** agricultural vehicle; tire deformation; radial tire; bias-ply tire; contact area; 3D scanning



**Citation:** Ptak, W.; Czarnecki, J.; Brennenstul, M.; Lejman, K.; Małecka, A. Evaluation of Agriculture Tires Deformation Using Innovative 3D Scanning Method. *Agriculture* **2022**, *12*, 1108. <https://doi.org/10.3390/agriculture12081108>

Academic Editor: Yanbo Huang

Received: 17 June 2022

Accepted: 26 July 2022

Published: 27 July 2022

**Publisher's Note:** MDPI stays neutral with regard to jurisdictional claims in published maps and institutional affiliations.



**Copyright:** © 2022 by the authors. Licensee MDPI, Basel, Switzerland. This article is an open access article distributed under the terms and conditions of the Creative Commons Attribution (CC BY) license (<https://creativecommons.org/licenses/by/4.0/>).

## 1. Introduction

The development of modern agriculture and intensification of production has caused a need for new machines with higher operational width [1,2]. These make it possible to achieve high efficiency in field operations, but they can cause higher vertical load (often, machines with greater width have higher masses) [3]. The use of these machines can lead to higher contact pressure, and the soil can be exposed to damage related to high compaction [4,5]. The results of previous research emphasize serious changes in the physical and mechanical properties of the soil compacted by the wheels of agricultural vehicles [6,7]. Compaction of the soil is a major problem influencing (in a destructive way) natural environment functioning [8–10]. The ability to uptake nutrients by plants is disturbed [11], which can lead to insufficient contents of carbon dioxide and rainwater. These disruptions often make field operations difficult and lower the yield of the plants [12,13]. On the other hand, high energy losses of agricultural machinery can occur [14].

Environmental protection requirements create new demands to reduce the negative consequences of the compaction of the soil by tractor wheels [15]. One agronomical way to improve the management of the compaction is the cultivation of deep-rooted plants, which can have a positive effect by loosening the soil structure [16]. However, attention to the technical and operational parameters of the machines is needed (especially in the aspect of the chassis parameters) [17].

Nowadays in agriculture, wheeled and tracked chassis are used. The most popular type is a wheeled system with the tire as the main element—it has direct contact with the ground [18]. Agricultural tires are divided into two types depending on their internal



structure. The first is bias-ply tires, which have the same quantity of material in each part of the profile. Bias-ply tires are characterized by relatively high mechanical strength, but they are relatively stiff. The second type of agricultural tire has a radial structure. In this case, the material near the tread is thicker than on the side walls. These can cause better grip and lower soil compaction, but on the other hand, radial tires are more prone to mechanical damage [19,20].

The tire, as an element of the chassis, plays an important role in generating pressure on the soil. Its values are dependent on the contact area, which is determined by the type of the tire, the size of the wheel, inflation pressure, and vertical load [21–23]. The problem of excessive compaction has been the subject of intensive scientific research. One of the frequently described factors is the internal design of the tire. Originally, in agricultural vehicles, bias-ply tires were used. They are characterized by higher mechanical strength, but their traction abilities are worse than radial tires [24]. Moreover, due to their higher stiffness, bias-ply tires cause higher compactness than radial tires. It was reported that the use of radial tires in agriculture made it possible to obtain lower unit pressure and, as a consequence, less intensive compactness [25,26]. Other significant factors in the research concerning the tire–surface system are inflation pressure and the vertical load of the wheel [27,28]. Renčín et al. [29] concluded that even a small increase in inflation pressure (from 90 kPa to 120 kPa) led to large increases in the values of unit pressure on the soil. In the same research, a non-linear increase in the contact area of a tire (as a consequence of vertical load increases) was reported. Filipovic et al. [30] also analyzed the inflation pressure and stated that this factor is crucial for unit pressure and has an impact on the risk of excessive compactness.

In the literature, there are many publications regarding the contact area between the tire and the ground, but this problem is complex and hard to describe [31,32]. Most of the research is based on measuring the tire's footprint on the soil [33,34]. In research conducted by Lamande et al. [35], loaded tires were placed on the soil, and the surface around them was sprinkled with gypsum. After lifting a tire, the footprint was drawn on foil, and then it was measured. Another method was used by Kumar et al. [18]. In this case, two sheets of carbon paper were placed between the tire and soil, and then the footprint generated on the paper was measured. The development of digital technology gave new possibilities to measure the tire–surface contact area [36]. One is a photometric method in which photographs of the footprints are analyzed in special software [37]. In research conducted by Farhadi et al. [14], a 3D scanner was used to measure a previously created gypsum imprint.

Those methods of assessing the tire's impact on the soil are based on measurements in the place of the contact, and deformable surfaces are often needed. Due to the differences between the tire's designs, their deformability will differ, so their impact on the soil will also differ. This confirms the need to conduct further research aimed at the assessment of the unit pressure generated by tires on the soil. For this reason, the aim of this study was the evaluation of changes related to tire deformation using a three-dimensional scanning method. In the first stage, the relationship between parameters (inflation pressure and vertical load of the tire) and dimensions of the vertical cross-sections of the tire will be analyzed. Then, the area of horizontal cross-sections at different exploitation parameters will be analyzed. Finally, the mathematical models will be formulated (separately for each of the tires).

## 2. Materials and Methods

The research was conducted in laboratory conditions on a non-deformable surface. Two types of tires (bias-ply and radial) of the same size were tested, with a profile width: 500 mm, profile height: 250 mm, rim diameter: 17 inches. Variable parameters used in the experiment were inflation pressure (3 levels: 0.8 bar, 1.6 bar, and 2.4 bar) and vertical load acting on the tires (5 levels of forces corresponding to the following masses: 800, 1200, 1600,

2000, and 2400 kg). The method of research was based on the scheme proposed by Ptak et al. [38], but some modifications related to the scanning process were used.

### 2.1. Test Bench

The test bench made it possible to study non-driven tires in static conditions; the scheme of the bench is presented in Figure 1. It was built from steel elements. The basis of the design was an external frame (3) connected to an internal frame (4). A hydraulic jack (6) was mounted between both frames because it was necessary to implement smooth changes in the vertical load on the tires. Vertical load values were measured using a TecSisforce sensor (5) with an accuracy of 50 N and a measurement range of 0–100 kN. The tire was placed on the shaft, which was mounted (using bearings) on the internal frame. Screw mechanisms (7) were intended to lock the internal frame (i.e., in the case of the accidental reduction of oil pressure in the hydraulic jack). The surface used in the experiment (1) was a flat steel bar 4 mm thick; this element was the reference basis in the optical analysis of the tire profile. The changes in inflation pressure were obtained using an HLO 215-25 compressor.

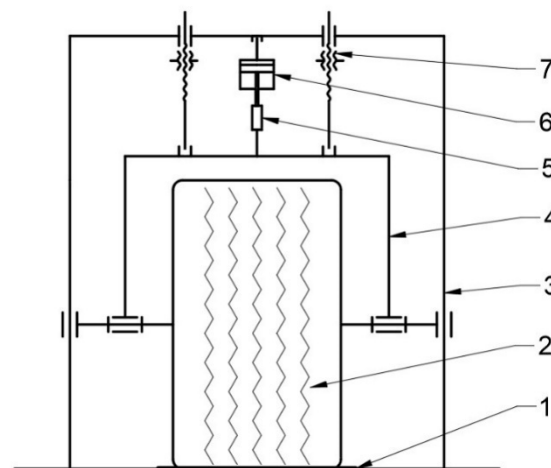


**Figure 1.** Scheme of the test bench: 1—non-deformable surface, 2—wheel with tested tire, 3—external frame, 4—internal frame, 5—force sensor, 6—hydraulic jack, 7—screw mechanism.

### 2.2. Scanning Process

A SMARTTECH3D scanner was used for the scanning process, the main parameters of which are presented in Table 1. The scanner was connected to a notebook fitted with special SMARTTECH3D measuring software. Before the start of the scanning process, the tested tire was covered with a white matte layer, which made it possible to obtain higher contrast. After mounting the tire, the test bench was placed on a rotary table connected to the software of the scanner, and then the main parameters, such as vertical load and inflation pressure, were entered. The rotary table made it possible to determine the basic parameters of the scanning process, i.e., the angular range of the scanning, angles of each rotation, and the number of scanning steps. In the experiment, the angular range of 360° was used, and a single step corresponded to the rotation of 20°. The effects of this operation were 18 individual scans with the ground created by clouds of points. As an effect of rotational scanning, a spatial picture of the tire was obtained. The process was applied in each factor combination (tire—inflation pressure—vertical load).

**Table 1.** Technical specification of 3D scanner.

Parameter	Description
Scanning technology	white structural light-LED
Measuring volume (x, y, z) [mm]	400 × 300 × 240
Distance between points [mm]	0.156
Accuracy [mm]	0.08
Power consumption during measurement [W]	200
Weight [kg]	4.40
Working temperature [°C]	20 ± 0.5

### 2.3. Management of Obtained Data

The effects of the scanning process were represented by a cloud of points which reflected the geometry and shape of the tire in real conditions. Performing further analysis was possible after the transformation of the cloud into a triangular mesh. In turn, the mesh was used to draw a vertical and horizontal cross-section of the tire profile. The cross-section was exported to the AutoCad software, which made it possible to determine specific dimensions of the tire profile. The plane used to perform the vertical cross-section was perpendicular to the surface, and it covered the center line of the tire. Figure 2 shows an example of a vertical cross-section with typical dimensions (total height of the profile and height measured at the maximum transverse deformation of the profile). In Figure 2, red lines show the part of the tire tread that could not be scanned (due to the lack of access to laser beams). However, this part was not the subject of the research—the main attention was paid to the edges of the profile and their deformations.

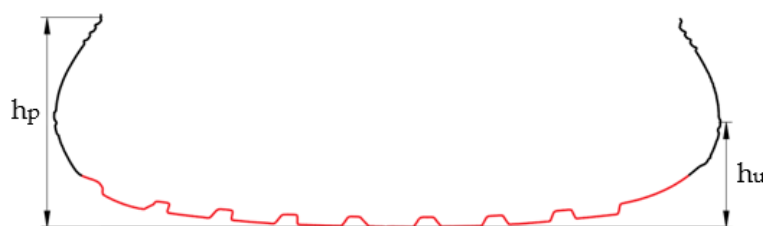


**Figure 2.** Vertical cross-section of the tire profile:  $h_p$ —total height of the profile,  $h_u$ —height measured at the maximum vertical deformation.

At the height corresponding to the maximum deformation, the horizontal cross-section was made, which was further used to read the width of the profile. Then, in AutoCad software, the area of the cross-section at the maximum deflection was read; it was assumed that it would be the area of the tire's contact with the surface (at the maximum deformation). The example of the horizontal cross-section is presented in Figure 3.

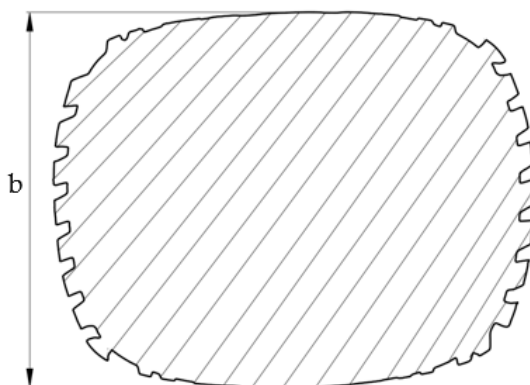


**Figure 3.** Horizontal cross-section with dimension b (width of tire profile).

### 2.4. Statistical Analysis of Results

The results were examined using statistical analysis. The first part included the evaluation of the factor's impact on tire dimensions and the area of horizontal cross-section. First, the test of distribution normality was done (using the Shapiro–Wilk test at the significance level  $\alpha = 0.05$ ). Then, the test of variance homogeneity was conducted (Levene test at the significance level  $\alpha = 0.05$ ). The statistical procedures had to determine the possibility of ANOVA use to evaluate the influence of the factors on the parameters. When the criterion was fulfilled (distributions in accordance with normal distribution, homogeneous variances), the two-factor ANOVA test at the significance level  $\alpha = 0.05$  was used. In other cases, the evaluation was conducted using the non-parametrical Kruskal–Wallis test at the significance level  $\alpha = 0.05$ . Both in the first and other cases, the statistical procedure included post-hoc tests—they had to show significant differences between each of the levels of the factors.

The statistical analysis also included formulating a mathematical model separately for each of the tires. These models had to describe the relationship between the factors (vertical load, inflation pressure) and the horizontal cross-section area. Mathematical models were created using TableCurve 3D software.

### 3. Results

The experiment led to the results regarding vertical and horizontal deformation of two tires with the same external dimensions and different internal structures. The variable factors were inflation pressure and the vertical load of the wheel.

Figure 4 shows the visualization of vertical cross-sections of both tires with all values of vertical load and inflation pressure. The highest deflection of the tire was observed at the vertical load of 2400 kg (gray color). However, at the lowest inflation pressure (0.8 bar) in the case of the radial tire, differences in deflections were quite low. It can be stated that in these cases, the deflection was not dependent on vertical load. The bias-ply tire with the inflation pressure of 1.6 bar had greater differences in deflection; the two lowest levels of vertical load (800 kg and 1200 kg) caused a significant difference compared to other levels of the load (1600 kg, 2000 kg, and 2400 kg).

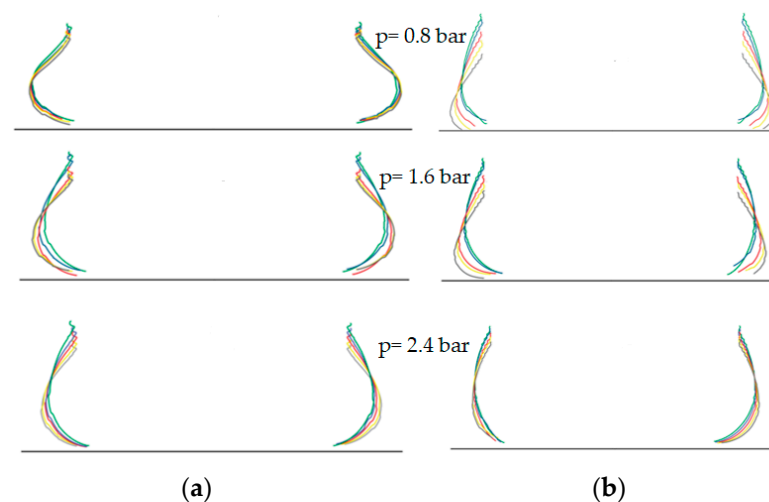


**Figure 4.** Visualization of vertical cross-sections at different levels of vertical load and inflation pressures: radial tire (a); bias—ply tire (b), p—inflation pressure; gray—2400 kg, yellow—2000 kg, red—1600 kg, blue—1200 kg, 800 kg—green.

Parameters read from vertical cross-sections were height of the tire profile ( $h_p$ ) and height corresponded to maximum deflection ( $h_u$ ). Figure 5 shows the values of  $h_p$  and  $h_u$  at all factor combinations (inflation pressure, vertical load) for both tires. In each case, decreases in heights due to an increase in vertical load were different. The highest value of

total profile height of the bias-ply tire was observed at the inflation pressure of 2.4 bar, and the lowest vertical load, 205 mm. For the radial tire at the same vertical load and inflation pressure, the height of the profile was 197 mm. In the case of the radial tire at 0.8 bar inflation pressure, an increase in vertical load from 1200 to 2400 kg caused a reduction in deflection by 6.4 mm. It was a relatively small difference, and it could be assumed that there is some limit to deflection; a further increase in vertical load, especially at low inflation pressure, will not cause high changes in deflection. These changes do not have to be related to the changes in the height of maximum deflection ( $h_u$ ). The comparison of both tires made it possible to conclude that the  $h_u$  parameter for the radial tire was more differentiated than for the bias-ply tire. In the latter case, the height of maximum deflection decreased due to an increase in vertical load; this tendency was observed at all levels of inflation pressure. The lowest value of the  $h_u$  parameter was observed at the inflation pressure of 0.8 bar. In the case of the radial tire, it was observed at the vertical load of 1600 kg (the  $h_u$  value was 50.4 mm), while for the bias-ply tire, this situation occurred at the vertical load of 2400 kg ( $h_u = 37.2$  mm). At the highest vertical load and highest inflation pressure, the heights of maximum deflection were 68.2 mm and 74.4 mm for the radial tire and bias-ply tire, respectively. Similar values were observed for the radial tire at the inflation pressure of 2.4 bar and vertical load of 800 kg. For the bias-ply tire, this tendency occurred at the inflation pressure of 0.8 bar and vertical load of 1200 kg.

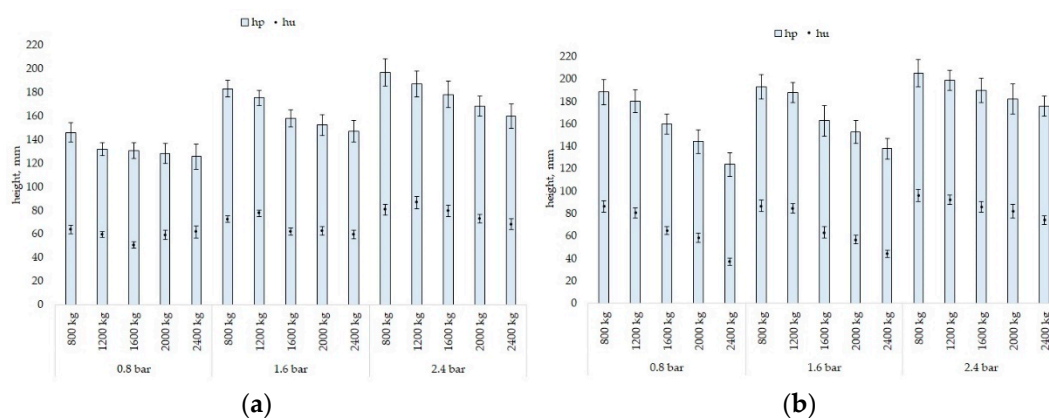


**Figure 5.** The values of the heights of tire profiles: radial tire (a); bias-ply tire (b);  $h_p$ —total height of tire profile,  $h_u$ —height of maximum deflection of the tire; linear markers mean standard deviation.

The next step in the research description was the preparation of horizontal cross-sections at the height of maximum deflection, shown in Figure 6. The cross-sections correspond to vertical cross-sections and confirm the previously described tendency concerning tire deformation. Moreover, Figure 6 shows the difference in the thread-parts of the tire with their edges at different distances from each other. It shows that the points of maximum deflection were located at different heights.

The parameters read from horizontal cross-sections were their total area ( $A_{hu}$ ) and the width ( $b_{hu}$ ). Figure 7 shows the values of the area of horizontal cross-sections. The highest values of the parameter were observed for both tires at the highest vertical load (2400 kg) and the lowest inflation pressure (0.8 bar). The areas were 0.325 m<sup>2</sup> and 0.316 m<sup>2</sup> for the radial and bias-ply tire, respectively. At the highest (2.4 bar) and lowest (0.8 bar) inflation pressures for each vertical load, higher cross-section areas were observed for the radial tire. Only in the case of the inflation pressure of 1.6 bar and vertical load of 800 kg was the area of cross-section higher for the bias-ply tire.

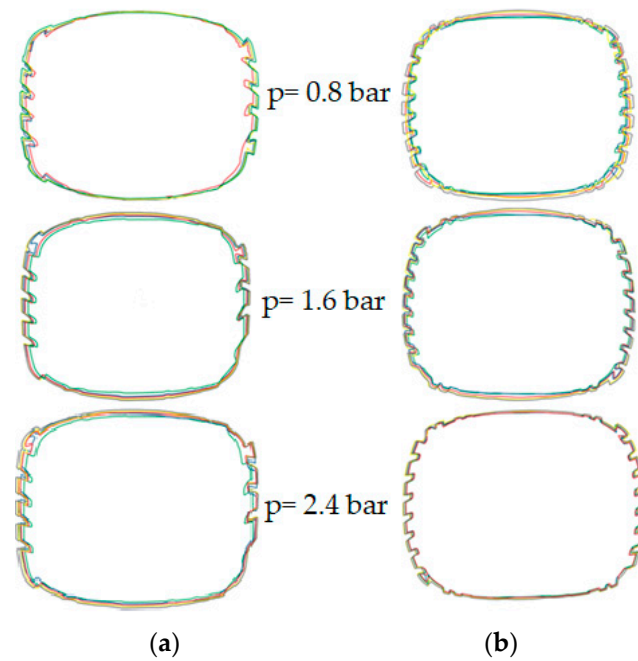


**Figure 6.** Visualization of horizontal cross-sections according to inflation pressure and vertical load: radial tire (a); bias-ply tire (b).

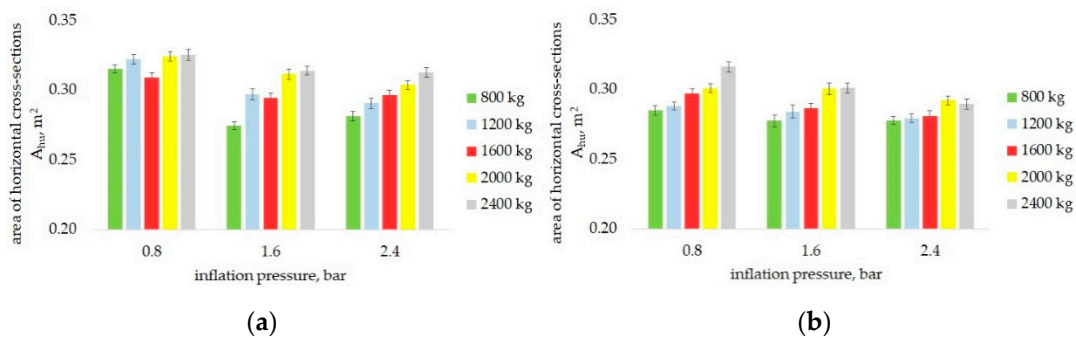


**Figure 7.** The values of areas of horizontal cross-sections: radial tire (a); bias-ply tire (b).

Figure 8 shows the values of cross-section width ( $b_{hu}$  parameter). The highest values of this parameter were obtained at the inflation pressure of 0.8 bar, which was observed for both tires. In the case of the radial tire, similar values of areas were observed at the vertical loads of 1200 kg, 2000 kg, and 2400 kg; in each of these three cases, they were about 540 mm (0.54 m). For the radial tire, the values higher than 540 mm were obtained only at the vertical load of 2400 kg (546 mm). The proportional increase in the cross-section area due to a load increase was observed in each inflation pressure and vertical load combination for both tires; the exception was the radial tire at the inflation pressure of 0.8 bar. Comparison of both tires made it possible to conclude that higher values of the cross-section area were obtained for the radial tire. It can be the basis for the statement that the radial tire is more elastic and more exposed to deformations.



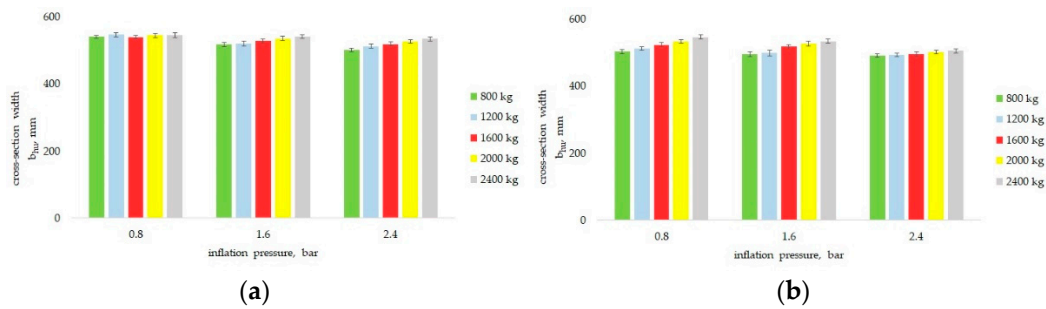


Figure 8. The values of width of cross-sections: radial tire (a); bias-ply tire (b).

The results were confirmed using statistical analysis. The first step was the evaluation of the possibility of using ANOVA tests to describe the factor impact on the analyzed parameters. Then, two-factor ANOVA tests were conducted separately for each of the tires. Table 2 shows the results of the statistical analysis for the radial tire. The  $p$ -value describes the probability of acceptance of the hypothesis about the lack of significant impact of the factor. When the  $p$ -value is greater than the significance level (in this case,  $\alpha = 0.05$ ), the factor is not significant for the parameter. Homogenous groups are denoted by letters A–D, and they mean the levels of factors which did not cause significant differences in the analyzed parameters.

Table 2. Results of statistical analysis for radial tire, significance level  $\alpha = 0.05$ , SD—standard deviation.

Analyzed Parameter	Factor	Factor Level	Arithmetic Mean	$\pm$ SD	$p$ -Value
Height of tire profile ( $h_p$ ), mm	Vertical load	800 kg	175.1 <sup>A</sup>	24.03	<0.00001
		1200 kg	164.7 <sup>B</sup>	26.41	
		1600 kg	155.8 <sup>C</sup>	22.01	
		2000 kg	149.8 <sup>CD</sup>	18.21	
		2400 kg	143.9 <sup>D</sup>	17.25	
	Inflation pressure	0.08 MPa	132.6 <sup>A</sup>	9.89	<0.00001
0.16 MPa	163.3 <sup>B</sup>	15.71			
0.24 MPa	177.9 <sup>C</sup>	16.35			
Height of maximum deformation of the tire ( $h_u$ ), mm	Vertical load	800 kg	72.2 <sup>A</sup>	7.92	0.00008
		1200 kg	74.4 <sup>A</sup>	12.58	
		1600 kg	64.1 <sup>B</sup>	13.02	
		2000 kg	64.9 <sup>B</sup>	6.82	
		2400 kg	63.1 <sup>B</sup>	5.42	
	Inflation pressure	0.08 MPa	58.9 <sup>A</sup>	5.58	<0.00001
0.16 MPa	66.8 <sup>B</sup>	7.71			
0.24 MPa	77.5 <sup>C</sup>	7.70			
Width of the tire ( $b_{hu}$ ), mm	Vertical load	800 kg	522.5 <sup>A</sup>	17.87	0.00002
		1200 kg	527.4 <sup>A</sup>	16.57	
		1600 kg	529.2 <sup>AB</sup>	10.50	
		2000 kg	536.5 <sup>B</sup>	9.35	
		2400 kg	541.5 <sup>C</sup>	7.08	
	Inflation pressure	0.08 MPa	544.1 <sup>A</sup>	5.68	<0.00001
0.16 MPa	530.8 <sup>B</sup>	9.60			
0.24 MPa	519.3 <sup>C</sup>	13.07			
Area of cross-section ( $A_{hu}$ ) m <sup>2</sup>	Vertical load	800 kg	0.290 <sup>A</sup>	0.019	<0.00001
		1200 kg	0.300 <sup>B</sup>	0.015	
		1600 kg	0.303 <sup>B</sup>	0.008	
		2000 kg	0.313 <sup>C</sup>	0.009	
		2400 kg	0.317 <sup>C</sup>	0.007	
	Inflation pressure	0.08 MPa	0.319 <sup>A</sup>	0.007	<0.00001
0.16 MPa	0.298 <sup>B</sup>	0.015			
0.24 MPa	0.297 <sup>B</sup>	0.011			

The letters at arithmetic means (A, B, C, D) denote separate homogenous groups.

Based on Table 2, it can be stated that both vertical load and inflation pressure had a significant impact on all parameters (in all cases, *p*-values were much lower than the significance level). Post-hoc tests conducted for the first factor (vertical load) showed that significant differences in  $h_p$  values were observed between each of the first four levels. Only the two highest levels of vertical load (2000 kg and 2400 kg) were classified into one homogeneous group, which means that there were no significant differences in  $h_p$  values between these levels. In the case of  $h_u$  values, homogenous groups were observed for the two first levels (800, 1200 kg) and the other three levels (1600, 2000, 2400 kg). Analysis of changes in tire width showed that the first homogeneous group was observed for the first three levels of vertical loads. The next homogeneous group was created by levels 1600 and 2000 kg (1600 kg was classified to the first homogeneous group, while the last homogeneous group was characterized by the highest vertical load (2400 kg)). Significant differences for the last parameter (the area of cross-section) were observed between the lowest level, two medium levels (1200, 1600 kg) and two highest levels (2000, 2400 kg). A post-hoc test for the second factor (inflation pressure) showed the differences in  $h_p$  values between each of the levels. The same situation was observed for  $h_u$  values and the values of tire width ( $b_{hu}$ ). Significant differences in the cross-section area were observed between the lowest level (0.8 bar) and two other levels (1.6, 2.4 bar).

The statistical analysis for the bias-ply tire is presented in Table 3. Explanations of symbols are the same as in Table 2.

**Table 3.** Results of statistical analysis for bias-ply tire, the significance level  $\alpha = 0.05$ , SD—standard deviation.

Analyzed Parameter	Factor	Factor Level	Arithmetic Mean	± SD	<i>p</i> -Value
Height of tire profile ( $h_p$ ), mm	Vertical load	800 kg	195.3 <sup>A</sup>	12.34	<0.00001
		1200 kg	188.9 <sup>A</sup>	11.32	
		1600 kg	170.7 <sup>B</sup>	17.38	
		2000 kg	159.7 <sup>B</sup>	19.72	
		2400 kg	145.7 <sup>C</sup>	24.88	
	Inflation pressure	0.08 MPa	159.2 <sup>A</sup>	25.94	<0.00001
0.16 MPa	166.8 <sup>A</sup>	23.33			
0.24 MPa	190.2 <sup>B</sup>	14.40			
Height of maximum deformation of the tire ( $h_u$ ), mm	Vertical load	800 kg	89.8 <sup>A</sup>	6.54	<0.00001
		1200 kg	85.6 <sup>A</sup>	6.15	
		1600 kg	71.3 <sup>B</sup>	11.63	
		2000 kg	65.7 <sup>B</sup>	12.92	
		2400 kg	51.9 <sup>C</sup>	17.33	
	Inflation pressure	0.08 MPa	65.5 <sup>A</sup>	18.40	<0.00001
0.16 MPa	67.0 <sup>A</sup>	17.33			
0.24 MPa	86.0 <sup>B</sup>	8.94			
Width of the tire ( $b_{hu}$ ), mm	Vertical load	800 kg	497.5 <sup>A</sup>	7.38	<0.00001
		1200 kg	501.8 <sup>A</sup>	10.05	
		1600 kg	512.8 <sup>B</sup>	14.14	
		2000 kg	521.0 <sup>B</sup>	15.38	
		2400 kg	528.9 <sup>C</sup>	19.04	
	Inflation pressure	0.08 MPa	524.2 <sup>A</sup>	16.56	<0.00001
0.16 MPa	515.1 <sup>B</sup>	16.55			
0.24 MPa	497.9 <sup>C</sup>	7.27			
Area of cross-section ( $A_{hu}$ ), m <sup>2</sup>	Vertical load	800 kg	0.280 <sup>A</sup>	0.005	<0.00001
		1200 kg	0.284 <sup>AB</sup>	0.005	
		1600 kg	0.288 <sup>B</sup>	0.008	
		2000 kg	0.297 <sup>C</sup>	0.005	
		2400 kg	0.302 <sup>C</sup>	0.012	
	Inflation pressure	0.08 MPa	0.297 <sup>A</sup>	0.012	<0.00001
0.16 MPa	0.290 <sup>B</sup>	0.010			
0.24 MPa	0.283 <sup>C</sup>	0.007			

The letters at arithmetic means (A, B, C) denote separate homogenous groups.



Statistical analysis of the results obtained for the bias-ply tire showed that all factors had a significant impact on all analyzed parameters ( $p$ -values were smaller than the significance level  $\alpha$ ). Post-hoc tests for  $h_p$  values showed that the two lowest levels created a separate group, then the levels 1600 kg and 2000 kg created the next homogeneous group; finally, the higher vertical load level created a separate group. Moreover, significant differences were observed between the two groups—the first was created by the lowest inflation pressure while the second by the highest pressure. Post-hoc tests for  $h_u$  values made it possible to conclude that non-significant differences in this parameter were observed at the two first levels of vertical load (they created one homogeneous group). A similar situation was observed for the two next levels (1600 kg and 2000 kg); the highest level of the load created a separate homogeneous group. For the second factor (inflation pressure), significant differences were observed between the highest level (2.4 bar) and two other levels. In the case of tire width, the influence of vertical load was the same as in the case of the  $h_p$  parameter (homogeneous groups were created by the same levels of vertical load). A post-hoc test for the second factor showed significant differences between each of the levels. Significant differences in values of areas of cross-sections were observed between three groups: the first was created by two lowest levels, the second group included the levels of 1200 kg and 1600 kg, while the third group was created by two highest levels. The second factor (inflation pressure) caused significant differences between all three levels (at each inflation pressure value, there were significant differences between the cross-section areas).

Statistical analysis included both analysis of variance and mathematical model formulation. After verification of factor significance, equations describing the cross-section area as a function of vertical load and inflation pressure were created. The models were formulated separately for the radial and bias-ply tire.

### 3.1. Model for Radial Tire

The overall form of the equation (Equation (1)) is:

$$A_{hu} = a + b \cdot \ln G + c \cdot (\ln G)^2 + \frac{d}{p} \quad (1)$$

$$R^2 = 0.881$$

where:

$A_{hu}$ —area of horizontal cross-section ( $m^2$ ),

$G$ —vertical load (kg),

$p$ —inflation pressure (bar),

$a, b, c, d$ —parameters (constants of equation).

The final form of the equation (Equation (2)) is:

$$A_{hu} = 0.491 - 0.081 \cdot \ln G + 0.007 \cdot (\ln G)^2 + \frac{0.028}{p} \quad (2)$$

In Table 4 the values of parameters of Equation (2) are presented while Table 5 shows the results of the verification of the model concerning the radial tire. It includes a comparison of measured values of the cross-section area (the arithmetic mean from the replications) and values calculated from the mathematical model. Moreover, the values of an estimation error were presented; the error was calculated from the following equation (Equation (3)):

$$\text{Err} = 100 \times \left( \frac{A_m - A_c}{A_m} \right), \% \quad (3)$$

where:

Err—error of estimation, %,

$A_m$ —measured area of cross-section,  $m^2$ ,

$A_c$ —calculated area of cross-section,  $m^2$ .

Analysis of obtained results made it possible to conclude that the highest error was 4.68%, the lowest error was 0.17%, and the mean error was at the level of 1.62%.

**Table 4.** Values of equation parameters for radial tire.

Parameter	Value
a	0.491
b	−0.081
c	0.007
d	0.028

**Table 5.** Verification of mathematical model for radial tire.

Vertical Load, kg	Inflation Pressure, bar	Area of Cross-Section (Measured)	Area of Cross-Section (Calculated from Model)	Error, %
800	0.8	0.315	0.305	3.22
1200	0.8	0.322	0.313	2.93
1600	0.8	0.309	0.319	3.21
2000	0.8	0.324	0.325	0.29
2400	0.8	0.325	0.331	1.71
800	1.6	0.275	0.288	4.68
1200	1.6	0.297	0.295	0.73
1600	1.6	0.294	0.302	2.47
2000	1.6	0.312	0.308	1.32
2400	1.6	0.314	0.313	0.34
800	2.4	0.281	0.282	0.17
1200	2.4	0.291	0.289	0.59
1600	2.4	0.296	0.296	0.22
2000	2.4	0.304	0.302	0.72
2400	2.4	0.313	0.307	1.76

### 3.2. Model for Bias-Ply Tire

The overall form of the equation (Equation (4)) is:

$$A_{hu} = a + b \cdot \ln G + c \cdot (\ln G)^2 + d \cdot (\ln G)^3 + e \cdot p \quad (4)$$

$$R^2 = 0.895$$

where:

$A_{hu}$ —area of horizontal cross-section ( $m^2$ ),

$G$ —vertical load (kg),

$p$ —inflation pressure (bar),

$a, b, c, d, e$ —parameters (constants of equation).

The final form of the equation (Equation (5)) is:

$$A_{hu} = 3.523 - 1.250 \cdot G + 0.158 \cdot (\ln G)^2 - 0.006 \cdot (\ln G)^3 - 0.008 \cdot p \quad (5)$$

Table 6 presents the values of parameters of Equation (4). Table 7 shows the results of the verification of the model for the bias-ply tire. The error of estimation was calculated using the same formula as in the case of the radial tire.

**Table 6.** Values of equation parameters for bias-ply tire.

Parameter	Value
a	3.523
b	−1.250
c	0.158
d	−0.006
e	−0.008

**Table 7.** Verification of mathematical model for bias-ply tire.

Vertical Load, kg	Inflation Pressure, bar	Area of Cross-Section (Measured)	Area of Cross-Section (Calculated from Model)	Error, %
800	0.8	0.285	0.287	0.65
1200	0.8	0.288	0.290	0.66
1600	0.8	0.295	0.296	0.17
2000	0.8	0.301	0.303	0.78
2400	0.8	0.316	0.310	2.14
800	1.6	0.278	0.280	0.95
1200	1.6	0.284	0.283	0.29
1600	1.6	0.287	0.290	1.03
2000	1.6	0.301	0.296	1.39
2400	1.6	0.301	0.303	0.54
800	2.4	0.278	0.274	1.52
1200	2.4	0.280	0.277	1.10
1600	2.4	0.281	0.283	0.71
2000	2.4	0.292	0.290	0.84
2400	2.4	0.290	0.296	2.27

Based on the results (Table 7), it can be concluded that the highest value of the error was 2.27%, while the lowest error was 0.17%. The mean error calculated from all cases was 1.01%.

#### 4. Discussion

The results made it possible to determine the differences in the deformation of radial and bias-ply tires with the same dimensions at different levels of vertical load and inflation pressure. The experiment was conducted on a non-deformable surface. Based on obtained results, two mathematical models were created. Similar experiments were conducted by other researchers. Sharma and Pandey [39] and Grečenko [40] created models and formulas describing the deformation of agricultural tires. However, these authors found that mathematical models needed large amounts of data obtained from experiments conducted on many tires under different conditions. In addition, there are studies describing the deformation of tires and the contact area on deformable surfaces (often on agricultural soil). The main advantage of the present models is related to their simple form. Unlike other models, they used just two initial parameters (inflation pressure and vertical load, while other models also need parameters of the surface).

It was concluded that an increase in vertical load caused an increase in the cross-section area (it can be equated with the contact area). In turn, an increase in inflation pressure caused a reduction in the cross-section area. This tendency is also confirmed by Teimourlou and Taghavifar [41]. In an experiment conducted by Renčín et al. [29], the reduction in inflation pressure of a radial tire (from 1.6 bar to 0.8 bar) caused an increase in the tire imprint area by 21%. In our research, a similar change in inflation pressure caused increases in the cross-section area by 6–13% (it was dependent on vertical load). Different results were obtained by Raper et al. [28]. In this case, the changes in contact area after the change in inflation pressure were significantly smaller than in our research. However, the impact of a vertical load increase (reported by Raper et al. [28]) was different from the results of our research (an increase in vertical load by 90% caused an increase in the area by more

than 30%, while in our research an increase in vertical load by 100% caused an increase in the area by 1–4%, dependent on inflation pressure).

Some studies described the accuracy of methods; according to one of them, using only the tire size to determine the contact area [42] can produce an error of 70% [43]. Schjønning et al. [44] compared two radial tires with different dimensions (650/65R30.5 and 800/50R34) from different manufacturers. Based on an elliptical model of the tire contact area, they concluded that a tire with a lower size caused a much higher footprint than a tire with larger dimensions. In turn, Way and Kishimoto [45] tested an 18.4R38 tire, and they observed very similar values of the contact area in each factor combination (described by different values of vertical load and inflation pressure).

In summary, comparing changes in tire performance under variable vertical load and inflation pressure is necessary to obtain information about tire deformation and the area of its contact with the surface. Knowledge about the relationship between tire elasticity and the contact area is crucial to obtaining better soil protection.

## 5. Conclusions

The analysis of the relationship between exploitation factors and deformability of the tires made it possible to conclude that both inflation pressure and vertical load were significant factors affecting the analyzed parameters.

1. An increase in vertical load of the wheel caused reductions in analyzed heights (both height of tire profile and height of maximum deflection of the tire). This tendency was observed for both tires, but in the case of the radial tire, the values of the heights were lower than for the bias-ply tire.

2. A reduction in inflation pressure led to reductions in values of the heights (height of tire profile and height of maximum deflection) both for the radial and bias-ply tire. For the radial tire, the impact of inflation pressure on the heights was lower than in the case of the bias-ply tire.

3. The values of width of the tire profile were comparable for the radial and bias-ply tire. An increase in vertical load of the wheel with the radial tire caused an increase in the width of the tire profile—higher differences were observed at high values of inflation pressure. However, an increase in vertical load of the bias-ply tire caused an increase in profile width only at two lower levels of inflation pressure (0.8 bar and 1.6 bar).

4. In the case of the radial tire, the area of the horizontal cross-section was higher than for the bias-ply tire. A reduction in inflation pressure of the radial tire caused significant increases in the area of horizontal cross-sections. The highest differences were observed after the reduction of inflation pressure from 1.6 bar to 0.8 bar. In the case of the bias-ply tire, an inflation pressure reduction caused lower increases in the area of cross-section. This tire was more exposed to the changes in the area of cross-section after the changes in vertical load. At each inflation pressure, proportional increases in the cross-section area due to the increases in vertical load were observed.

**Author Contributions:** Conceptualization, J.C. and W.P.; methodology, J.C.; software, M.B. and W.P.; validation, M.B., A.M.; formal analysis, J.C. and K.L.; investigation, W.P., M.B. and A.M.; resources, W.P.; data curation, M.B.; writing—original draft preparation, W.P. and M.B.; writing—review and editing, M.B.; visualization, W.P.; supervision, J.C.; project administration, J.C. and K.L.; funding acquisition, J.C. and K.L. All authors have read and agreed to the published version of the manuscript.

**Funding:** The Article Processing Charge is financed by the Wrocław University of Environmental and Life Sciences.

**Institutional Review Board Statement:** Not applicable.

**Informed Consent Statement:** Not applicable.

**Data Availability Statement:** Not applicable.

**Conflicts of Interest:** The authors declare no conflict of interest. The funders had no role in the design of the study; in the collection, analyses, or interpretation of data; in the writing of the manuscript; or in the decision to publish the results.

## References

- Lyu, X.; Peng, W.; Niu, S.; Qu, Y.; Xin, Z. Evaluation of sustainable intensification of cultivated land use according to farming households' livelihood type. *Ecol. Ind.* **2022**, *138*, 108848. [\[CrossRef\]](#)
- Zhou, K.; Bochtis, D.; Jensen, A.L.; Kateris, D.; Soerensen, C.G. Introduction of a New Index of Field Operations Efficiency. *Appl. Sci.* **2020**, *10*, 329. [\[CrossRef\]](#)
- Keller, T.; Sandin, M.; Colombi, T.; Horn, R.; Or, D. Historical increase in agricultural machinery weights enhanced soil stress levels and adversely affected soil functioning. *Soil Till. Res.* **2019**, *194*, 104293. [\[CrossRef\]](#)
- Moinfara, A.; Ghoalmhossein, M.; Yousef, S.; Gilandeha, A.; Kavehb, M.; Szymanek, M. Investigating the effect of the tractor driving system type on soil compaction using different methods of ANN, ANFIS and step wise regression. *Soil Till. Res.* **2022**, *222*, 105444. [\[CrossRef\]](#)
- Carman, K. Compaction characteristics of towed wheels on clay loam in a soil bin. *Soil Till. Res.* **2002**, *65*, 37–43. [\[CrossRef\]](#)
- Da Silva Guimarães Júnnyor, W.; Diserens, E.; De Maria, I.C.; Junior, C.F.A.; Farhate, C.V.V.; de Souza, Z.M. Prediction of soil stresses and compaction due to agricultural machines in sugarcane cultivation systems with and without crop rotation. *Sci. Total Environ.* **2019**, *681*, 424–434. [\[CrossRef\]](#)
- Berisso, F.E.; Schjøning, P.; Lamandé, M.; Weisskopf, P.; Stettler, M.; Keller, T. Effects of the stress field induced by a running tyre on the soil pore system. *Soil Till. Res.* **2013**, *131*, 36–46. [\[CrossRef\]](#)
- Augustin, K.; Kuhwald, M.; Brunotte, J.; Duttman, R. Wheel Load and Wheel Pass Frequency as Indicators for Soil Compaction Risk: A Four-Year Analysis of Traffic Intensity at Field Scale. *Geosciences* **2020**, *10*, 292. [\[CrossRef\]](#)
- Ren, L.; Vanden Nest, T.; Ruysschaert, G.; D'Hose, T.; Wim Cornelis, W. Short-term effects of cover crops and tillage methods on soil physical properties and maize growth in a sandy loam soil. *Soil Till. Res.* **2019**, *192*, 76–86. [\[CrossRef\]](#)
- Hamza, M.A.; Anderson, W.K. Soil compaction in cropping systems. *Soil Till. Res.* **2005**, *82*, 121–145. [\[CrossRef\]](#)
- Botta, G.F.; Tolon-Becerra, A.; Lastra-Bravo, X.; Tourn, M. Tillage and traffic effects (planters and tractors) on soil compaction and soybean (*Glycine max* L.) yields in Argentinean pampas. *Soil Till. Res.* **2010**, *110*, 167–174. [\[CrossRef\]](#)
- Naujokienė, V.; Šarauskis, E.; Lekavičienė, K.; Adamavičienė, A.; Buragienė, S.; Kriaučiūnienė, Z. The influence of biopreparations on the reduction of energy consumption and CO<sub>2</sub> emissions in shallow and deep soil tillage. *Sci. Total Environ.* **2018**, *626*, 1402–1413. [\[CrossRef\]](#)
- Sivarajan, S.; Maharlooei, M.; Bajwa, S.; Nowatzki, J. Impact of soil compaction due to wheel traffic on corn and soybean growth, development and yield. *Soil Till. Res.* **2018**, *175*, 234–243. [\[CrossRef\]](#)
- Farhadi, P.; Golmohammadi, A.; Sharifi, A.; Shahgholi, G. Potential of three-dimensional footprint mold in investigating the effect of tractor tire contact volume changes on rolling resistance. *J. Terramech.* **2018**, *78*, 63–72. [\[CrossRef\]](#)
- Ungureanu, N.; Vladut, V.; Biris, S.; Matache, M. Research in distribution of pressure in soil depth under wheels of different machines. In Proceedings of the 17th International Scientific Conference Engineering for Rural Development, Jelgava, Latvia, 23–25 May 2018. [\[CrossRef\]](#)
- Elkins, C.B. Plant roots as tillage tools. *J. Terramech.* **1985**, *22*, 177–178. [\[CrossRef\]](#)
- Keller, T.; Arvidsson, J. Technical solutions to reduce the risk of subsoil compaction: Effects of dual wheels, tandem wheels and tyre inflation pressure on stress propagation in soil. *Soil Till. Res.* **2004**, *79*, 191–205. [\[CrossRef\]](#)
- Becker, C.; Schalk, E. Agricultural tyre stiffness change as a function of tyre wear. *J. Terramech.* **2022**, *102*, 1–15. [\[CrossRef\]](#)
- Khemis, C.; Abrougui, K.; Ren, L.; Mutuku, E.A.; Chehaibi, S.; Cornelis, W. Effects of tractor loads and tyre pressures on soil compaction in Tunisia under different moisture conditions. In Proceedings of the European Geosciences Union General Assembly, Vienna, Austria, 23–28 April 2017.
- Lindemuth, B.E. An overview of tire technology. In *The Pneumatic Tire*; U.S. Department of Transportation, National Highway Traffic Safety Administration: Washington, DC, USA, 2006; pp. 3–7.
- Taghavifar, H.; Mardani, A. Investigating the effect of velocity, inflation pressure, and vertical load on rolling resistance of a radial ply tire. *J. Terramech.* **2013**, *50*, 99–106. [\[CrossRef\]](#)
- Diserens, E.; Défossez, P.; Duboisset, A.; Alaoui, A. Prediction of the contact area of agricultural traction tires on firm soil. *Biosyst. Engine* **2011**, *110*, 73–82. [\[CrossRef\]](#)
- Arvidsson, J.; Keller, T. Soil stress as affected by wheel load and tire inflation pressure. *Soil Till. Res.* **2007**, *96*, 284–291. [\[CrossRef\]](#)
- Ten Damme, L.; Stettler, M.; Pinet, F.; Vervaet, P.; Keller, T.; Munkholm, L.J.; Lamandé, M. The contribution of tyre evolution to the reduction of soil compaction risks. *Soil Till. Res.* **2019**, *194*, 104283. [\[CrossRef\]](#)
- Kumar, S.; Pandey, K.P.; Kumar, R.; Ashok Kumar, A. Effect of ballasting on performance characteristics of bias and radial ply tyres with zero sinkage. *Measurement* **2018**, *121*, 218–224. [\[CrossRef\]](#)
- Botta, G.F.; Rivero, D.; Tourn, M.; Bellora Melcona, F.; Pozzolo, O.; Nardon, G.; Balbuena, R.; Tolon Becerra, A.; Rosatto, H.; Stadler, S. Soil compaction produced by tractor with radial and cross-ply tyres in two tillage regimes. *Soil Till. Res.* **2008**, *101*, 44–51. [\[CrossRef\]](#)

27. Svoboda, M.; Brennenstul, M.; Pospíšil, J. Evaluation of changes in soil compaction due to the passage of combine harvester. *Acta Univ. Agric. Silvic. Mendel. Brun.* **2016**, *64*, 877–882. [[CrossRef](#)]
28. Raper, R.L.; Bailey, A.C.; Burt, E.C.; Way, T.R.; Liberati, P. Inflation pressure and dynamic load effects on soil deformation and soil-tire interface stresses. *Trans. ASAE* **1995**, *38*, 685–689. [[CrossRef](#)]
29. Renčín, L.; Polcar, A.; Bauer, F. The Effect of the Tractor Tires Load on the Ground Loading Pressure. *Acta Univ. Agric. Silvic. Mendel. Brun.* **2017**, *65*, 1607–1614. [[CrossRef](#)]
30. Filipovic, D.; Kovacev, I.; Copec, K.; Fabijanic, G.; Kosutic, S.; Husnjak, S. Effects of Tractor Bias-ply Tyre Inflation Pressure on Stress Distribution in Silty Loam Soil. *Soil Water Res.* **2016**, *11*, 190–195. [[CrossRef](#)]
31. Kenarsari, A.E.; Vitton, S.J.; Beard, J.E. Creating 3D models of tractor tire footprints using close-range digital photogrammetry. *J. Terramech.* **2017**, *74*, 1–11. [[CrossRef](#)]
32. Schwanghart, H. Measurement of contact area, contact pressure and compaction under tires in soft soil. *J. Terramech.* **1991**, *28*, 309–318. [[CrossRef](#)]
33. Derafshpour, S.; Valizadeh, M.; Mardani, A.; Saray, M.T. A novel system developed based on image processing techniques for dynamical measurement of tire-surface contact area. *Measurement* **2019**, *139*, 270–276. [[CrossRef](#)]
34. Błaszkiwicz, Z. A method for the determination of the contact area between a tyre and the ground. *J. Terramech.* **1990**, *27*, 263–282. [[CrossRef](#)]
35. Lamande, M.; Schjøanning, P.; Tøgersen, F.A. Mechanical behaviour of an undisturbed soil subjected to loadings: Effects of load and contact area. *Soil Till. Res.* **2007**, *97*, 91–106. [[CrossRef](#)]
36. Bagnall, D.K.; Morgan, C.S. SLAKES and 3D Scans characterize management effects on soil structure in farm fields. *Soil Till. Res.* **2021**, *208*, 104893. [[CrossRef](#)]
37. Diserens, E. Calculating the contact area of trailer tyres in the field. *Soil Till. Res.* **2009**, *103*, 302–309. [[CrossRef](#)]
38. Ptak, W.; Czarnecki, J.; Brennenstul, M. Use of 3D scanning technique to determine tire deformation in static conditions. *J. Agric. Eng.* **2022**, *53*, 1–7. [[CrossRef](#)]
39. Sharma, A.K.; Pandey, K.P. The deflection and contact characteristics of some agricultural tyres with zero sinkage. *J. Terramech.* **1996**, *33*, 293–299. [[CrossRef](#)]
40. Grečenko, A. Tyre footprint area on hard ground computed from catalogue values. *J. Terramech.* **1995**, *32*, 325–333. [[CrossRef](#)]
41. Teimourlou, R.F.; Taghavifar, H. Determination of the Super-Elliptic Shape of Tire-Soil Contact Area Using Image Processing Method. *Cercet. Agron. Mold.* **2015**, *48*, 5–14. [[CrossRef](#)]
42. McKyes, E. *Soil Cutting and Tillage*; Developments in Agricultural Science Elsevier Science: Amsterdam, The Netherlands, 1985; Volume 7, pp. 140–141.
43. Godin, T.; Defossez, P.; Leveque, E.; Le Bas, C.; Boizard, H.; Debuisson, S. Evaluation des contraintes engendrées par les engins dans les systèmes de grandes cultures, viticoles et forestiers français. In Proceedings of the 69th Congress e Brussels, Brussels, Belgium, 15–16 February 2006.
44. Schjøanning, P.; Lamandé, M.; Tøgersen, F.A.; Arvidsson, J.; Keller, T. Modelling effects of tyre inflation pressure on the stress distribution near the soil–tyre interface. *Biosyst. Engine* **2008**, *99*, 119–133. [[CrossRef](#)]
45. Way, T.R.; Kishimoto, T. Interface pressures of a tractor drive tyre on structured and loose soils. *Biosyst. Engine* **2004**, *87*, 375–386. [[CrossRef](#)]

### 3.3. Evaluation of tire footprint in soil using innovative 3D scanning method

Autorzy: **Weronika Ptak**, Jarosław Czarnecki, Marek Brennenstul,  
Krzysztof Lejman, Agata Małecka

Czasopismo: Agriculture, 2023, 13(3), 514

Doi: 10.3390/agriculture13030514



## Article

# Evaluation of Tire Footprint in Soil Using an Innovative 3D Scanning Method

Weronika Ptak <sup>\*</sup>, Jarosław Czarnecki, Marek Brennenstul , Krzysztof Lejman and Agata Małecka

Institute of Agricultural Engineering, Wrocław University of Environmental and Life Sciences, 37a Józefa Chełmońskiego Street, 51-630 Wrocław, Poland

\* Correspondence: weronika.ptak@upwr.edu.pl

**Abstract:** This paper presents the results of the measurement of tire footprints in soil. The research was conducted under laboratory conditions using soil-filled cases. The research objects were two tires: a radial tire and a bias-ply tire of the same size. The variable parameters were vertical load (7.8 kN, 15.7 kN, 23.5 kN) and inflation pressure (0.8 bar, 1.6 bar, 2.4 bar). Test benches with a mounted tire, a soil case, and a 3D scanner were used in the research. Using the test bench, a tire was loaded with each inflation pressure, and a tire footprint was generated in the soil. Then, a 3D scanner was used to scan the tire footprint, and the parameters of length, width, depth, and tire–soil contact area (as a spatial image) were evaluated using special software. Then, mathematical models were formulated (separately for each type of tire) to describe the tire–soil contact area of the tire footprint as a function of the vertical load and inflation pressure. It was found that the depth of the tire footprint is an important parameter that influences the tire–soil contact area value. However, it was also found that with the right combination of inflation pressure and vertical load, a longer and wider, but shallower, tire footprint can be generated, the contact area value of which is similar to that of a deeper footprint.

**Keywords:** radial tire; bias-ply tire; soil deformation; tire footprint; tire–soil contact area; 3D scanning



**Citation:** Ptak, W.; Czarnecki, J.; Brennenstul, M.; Lejman, K.; Małecka, A. Evaluation of Tire Footprint in Soil Using an Innovative 3D Scanning Method. *Agriculture* **2023**, *13*, 514. <https://doi.org/10.3390/agriculture13030514>

Academic Editor: Kenshi Sakai

Received: 25 January 2023

Revised: 8 February 2023

Accepted: 17 February 2023

Published: 21 February 2023



**Copyright:** © 2023 by the authors. Licensee MDPI, Basel, Switzerland. This article is an open access article distributed under the terms and conditions of the Creative Commons Attribution (CC BY) license (<https://creativecommons.org/licenses/by/4.0/>).

## 1. Introduction

In recent years, a continuous increase in the technical efficiency of agriculture has been observed, thanks to which soil tillage can be carried out more efficiently. Different tillage treatments are often combined and performed with complex agricultural machinery with larger operating widths, and thus a larger mass. Such machinery generates pressure on the soil and compacts it through wheel traffic, which leads to its degradation [1]. In consequence, the water–air balance of the soil is disturbed, the soil’s capacity to absorb rainwater is diminished, and it is insufficiently ventilated, which results in erosion [2–6]. Excessive soil compaction can reduce the yield of plants, as their root system, which is responsible, among other things, for the uptake of water and nutrients from the soil, is not developed sufficiently [7].

The effects of soil compaction are far-reaching, and solutions to mitigate its consequences are being sought. Growing deep-rooted plants might help, as this contributes to soil loosening [8–11]. In agricultural practice, the size and weight of the chassis and wheels of machines used during tillage treatments are important. A typical agricultural machine is based on a wheeled system, the essential element of which is the tire, which is in direct contact with the soil. According to their internal structure, tires can be divided into radial and bias-ply tires. The former is manufactured with an additional layer of material to reinforce the tread part, while the side parts are flexible. On the other hand, the main feature of a bias-ply tire is its greater stiffness, which is due to the same amount of material being evenly spread throughout its cross-section [12]. In practice, this means that a bias-ply tire is more resistant to mechanical damage, but due to its greater stiffness, it can have a more destructive effect on the ground, compacting the soil more than a radial tire.



Due to its having direct contact with the soil, a tire is responsible for the amount of pressure generated by agricultural machines, and the pressure value depends on the tire–soil contact area. This is one of the key tire footprint parameters used to compare the effects of different kinds of tires and the different conditions they operate in [13,14]. Factors that affect the tire–soil contact area include the stiffness of the tire, its size, its inflation pressure, and the vertical load it is subjected to during movement [15]. The literature offers many studies that measured tire contact area with the soil under the influence of variable factors. On the basis of measurements, Grečenko [16] presented formulas predicting the tire–soil contact area, while other authors [17–19] described the tire footprint on the soil as being in the shape of a super-ellipse and included, among other aspects, its length and width in the formula. Technological progress has made it possible to study tire footprints using digital image analysis [20–22]. Kenarsari et al. [23] used photogrammetry to create a 3D model of a tire footprint and then analyzed its length, width, and volume. Farhadi et al. [24] created plaster of Paris molds of a footprint and then used a 3D scanner to obtain information about its dimensions.

According to the literature, many factors, such as tire internal structure, vertical load, and inflation pressure, affect tire contact area with the soil. The area is a very important parameter for determining the distribution of forces applied to the soil. In order to minimize soil compaction, it is advisable to constantly obtain information on the shape and dimensions of the tire footprint in the soil. Many studies analyzed the contact area as a flat surface. However, the tire side edges also interact with the soil, creating a spatial footprint. Today's level of technology makes it possible to obtain information about a three dimensional tire footprint and facilitates a more accurate analysis of the results. Taking into account the above, the aim of the present study was to assess the impact of radial and bias-ply tires subjected to selected conditions on the shape of tire footprints in soil using 3D scanning techniques and digital image analysis.

## 2. Materials and Methods

This research was conducted under laboratory conditions using sandy loam soil. Its moisture and compactness were kept constant throughout, at 25% and 0.9 MPa, respectively. Both were measured with a Penetrologger set produced by Eijkelkamp. The compactness of the soil was measured with a cone, which was part of the set, with a top angle of 60°, a base area of 0.0001 m<sup>2</sup>, and a penetration velocity of 3 cm·s<sup>-1</sup>. The soil moisture was measured with a ThetaProbe, which was also included in the set. Two agricultural tires of the same size but with different structural types, radial and bias-ply, were tested (profile width: 500 mm, profile height: 250 mm, and rim diameter: 17 inches). As part of the tests, three inflation pressure (*p*) levels were used (0.8 bar, 1.6 bar, and 2.4 bar), with three values of vertical load (*G*) acting on the tire: 7.8 kN, 15.7 kN, and 23.5 kN. The research included the measurement of the length (*l*), width (*b*), and depth (*h*) of the tire footprint in the soil and the tire–soil contact area (*A<sub>s</sub>*). The research was conducted using the methodology of Ptak et al. [25] and Ptak et al. [26]. Unlike in the abovementioned research, a tire footprint in the soil was scanned, so the test bench and the scanning process required modification.

### 2.1. Test Bench

To generate a tire footprint in the soil, a unique test bench was used (Figure 1). Its design allowed for a smooth change in vertical load, and at each stage it was also possible to change the tire inflation pressure. The removable part of the test bench was a soil-filled case (1) with a length of 1000 mm, a width of 1000 mm, and a height of 600 mm. Between the outer frame (3) and the inner frame (4), a hydraulic jack (6) was mounted in the vertical plane. The vertical load was smoothly changed with the jack, and its value was measured with a TecSis inductive dynamometer (5), with a accuracy of 50 N and a measuring range of between 0 and 100 kN. The tire was mounted on a shaft with bearings, with the former attached to the inner frame (4). The screw mechanisms (7) allowed for the locking of the

inner frame and the prevention of its movement and pressure drops in the hydraulic jack, which would result in an unintended reduction in the vertical load.

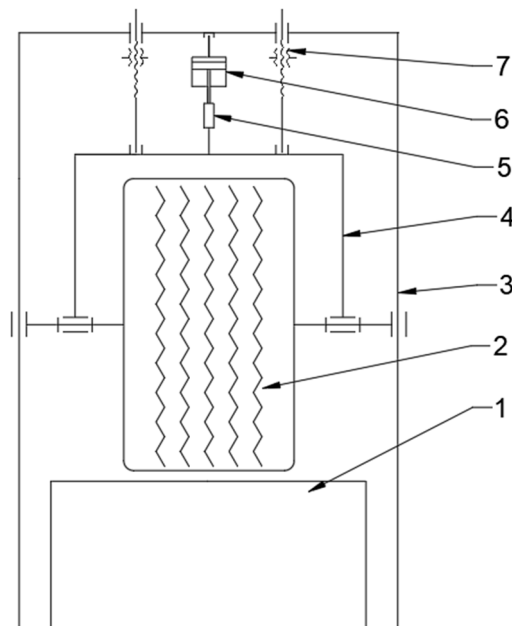


**Figure 1.** The test bench: 1—soil case; 2—wheel with tire; 3—main frame; 4—inner frame; 5—dynamometer; 6—hydraulic cylinder; 7—screw mechanism for locking the inner frame.

The research was conducted in static conditions, so the wheel was placed in the soil case and the tire footprint was generated in the soil without applying torque. There were no driving or braking forces, which could affect the pressure distribution in the soil. After making a footprint in the soil, the soil case was pulled off of the bench. Then, markers indicating the edges were placed around the footprint, which allowed for a more accurate line to be drawn between the footprint and the rest of the soil surface. Before each footprint was created, the soil was mechanically loosened and then compacted to the previous value.

## 2.2. Scanning Process

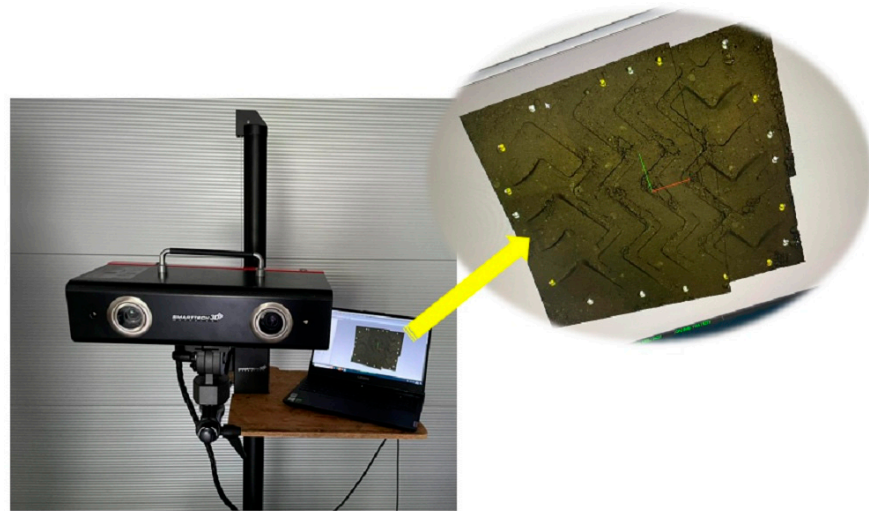
The tire footprint in the soil was scanned with a 3D scanner (SMARTTECH3D Universe), the technical specifications of which are presented in Table 1. The scanner was connected to a laptop with special SMARTTECH3D measuring software, which allows for continuous observation of the acquired data.

**Table 1.** 3D scanner specifications.

Parameter	Description
Scanning technology	white structural light—LED
Measuring volume (x × y × z) (mm)	400 × 300 × 240
Distance between points (mm)	0.156
Accuracy (mm)	0.08
Power consumption during measurement (W)	200
Mass (kg)	4.40
Working temperature (°C)	20 ± 0.5

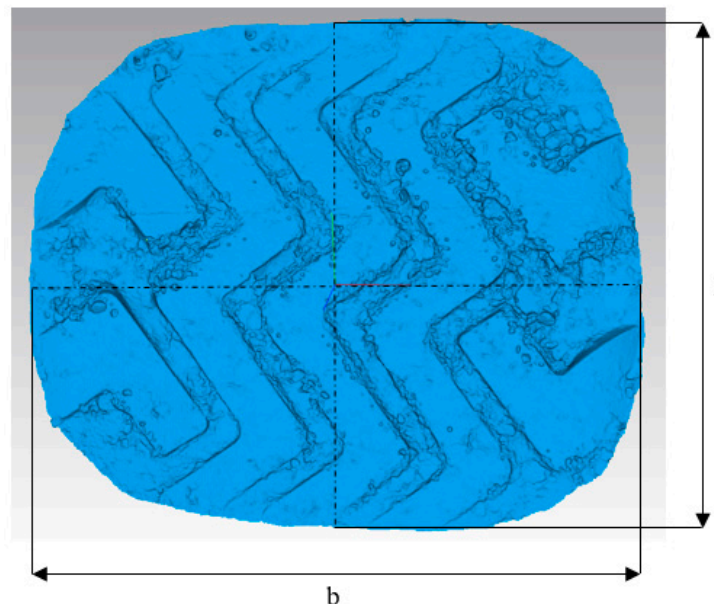
The 3D scanner and laptop (Figure 2) were mounted on a tripod column, which made it possible to maintain a constant height of the scanner's position over the scanned footprint. This helped facilitate the preservation of the measuring volume of the scanner and the efficient movement of the measuring device around the soil case. As a result of the scan, a point cloud was obtained that reproduced the shape and geometry of the tire footprint in

the soil. However, in order to facilitate a proper analysis, it was necessary to first remove the scan of the soil outside the tire footprint, which would disturb the measurement results (for this reason, it was necessary to use the markers mentioned above), and then create a mesh of triangles built from the points.



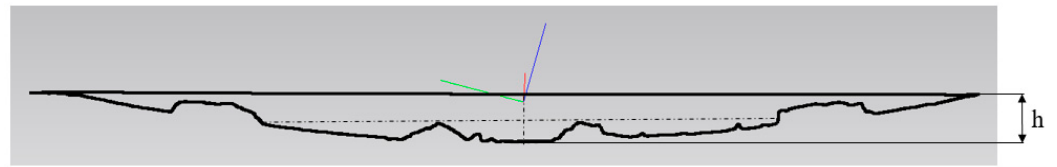
**Figure 2.** 3D scanner and the resulting point cloud.

Figure 3 shows a mesh of triangles of a tire footprint in the soil, with the length and width dimensions taken during the measurement. The tire–soil contact area ( $A_s$ ) was available in the SMARTTECH3D measure software as the whole footprint in three-dimensional space. Scientists usually measure the tire–soil contact area using a simplification, in the form of a two-dimensional projection area. In the case of the presented technique, this a novel approach that makes it possible to present the real shape and size of tire footprints.



**Figure 3.** Mesh of triangles of a tire footprint in soil.  $l$ —length;  $b$ —width.

In order to measure the depth of the footprint ( $h$ ), it was necessary to create its vertical cross-section (Figure 4). Footprint parameters such as length, width, and depth were always measured across the middle of the footprint.



**Figure 4.** Vertical section of the tire footprint in the soil. h—depth of the footprint.

### 2.3. Statistical Analysis

For verification purposes, Statistica 12.5 (StatSoft) was used to perform statistical analyses of the results. As part of this analysis, a homogeneity of variance test was performed, and the compatibility of the data with the normal distribution was assessed. Next, a two-factor analysis of variance at a significance level of  $\alpha = 0.05$  was performed, together with an analysis of the homogeneous groups, as part of a post hoc test. The next step in the statistical analysis was the development of mathematical models describing the footprint area as a function of the operating parameters (vertical load and tire inflation pressure). The model was developed using TableCurve and was verified through standard calculations using an Excel spreadsheet.

### 3. Results

Figure 5 shows the length values of footprints generated by radial and bias-ply tires. The length was the smallest (328 mm for the radial tire and 421 mm for the bias-ply tire) when a vertical load of 7.8 kN was applied at an inflation pressure of 2.4 bar for the radial tire and 1.6 bar for the bias-ply tire. In most cases, with the same load and pressure values, the footprint length was greater for the bias-ply tires. For both tires, the footprint length increased with an increase in the vertical load (with the exception of the bias-ply tire when the vertical load increased to 15.7 kN at an inflation pressure of 1.6 bar, when it decreased by about 4 mm).

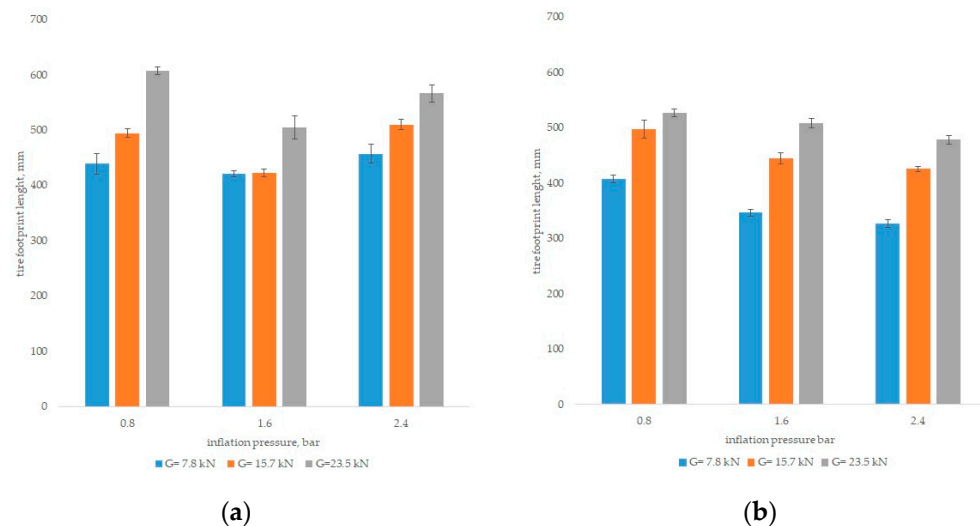


**Figure 5.** Footprint length values: bias-ply tire (a); radial tire (b); the linear markers represent the standard deviation.

For the bias-ply tire, a larger increase in the footprint length was observed when the vertical load was increased from 15.7 kN to 23.5 kN than when it was increased from 7.8 kN to 15.7 kN. In the former case, it increased by 23%, 20%, and 11% for inflation pressures of 0.8 bar, 1.6 bar, and 2.4 bar, respectively. However, after the first increase in load (from 7.8 kN to 15.7 kN), the largest length increase for the bias-ply tire was only 13%. The opposite trend was observed for the radial tire; in this case, the first load increase resulted in a greater increase in footprint length, by 22%, 28%, and 30% for inflation pressures of

0.8 bar, 1.6 bar, and 2.4 bar, respectively, while with a vertical load of 23.5 kN, the maximum increase was only 14%. Unlike for the bias-ply tire, for the radial tire, reducing the pressure always resulted in an increase in the footprint length. Values that were 4–17% larger were recorded when the pressure was decreased from 1.6 bar to 0.8 bar; for the first load increase, the length increase was greater than for the second. In the case of the bias-ply tire, an increase was observed only after the pressure was reduced from 1.6 bar to 0.8 bar (by 4%, 7%, and 20% for vertical loads of 7.8 kN, 15.7 kN, and 23.5 kN, respectively). The pressure reduction from the highest to the middle value resulted in a decrease in the length of the footprint by 7–11%, depending on the vertical load.

Another footprint parameter studied in our research was width (Figure 6). Its highest value was 502 mm for a radial tire with a vertical load of 23.5 kN and an inflation pressure of 0.8 bar. With the same load and pressure, the footprint width for the bias-ply tire was 497 mm. This difference might have been due to the fact that radial tires are only more susceptible to lateral deformation at low inflation pressures. As with the length of the radial tire footprint, its width increased with a reduction in the tire inflation pressure at a given vertical load; after both the first and second pressure reduction, the average increase in the width of the footprint was 4%. For the bias-ply tire, on the other hand, the increase in the footprint width due to the pressure reduction was more pronounced between the levels of 1.6 bar and 0.8 bar (an increase of 2%, 10%, and 7% for loads of 7.8 kN, 15.7 kN, and 23.5 kN, respectively). After reducing the pressure from 2.4 bar to 1.6 bar, an increase in the width of the generated footprint was only found at the lowest vertical load (an increase of 2%). At a load of 15.7 kN, the same pressure drop resulted in a 5% reduction in the width of the footprint, while at the highest vertical load, pressure reduction did not result in any changes.

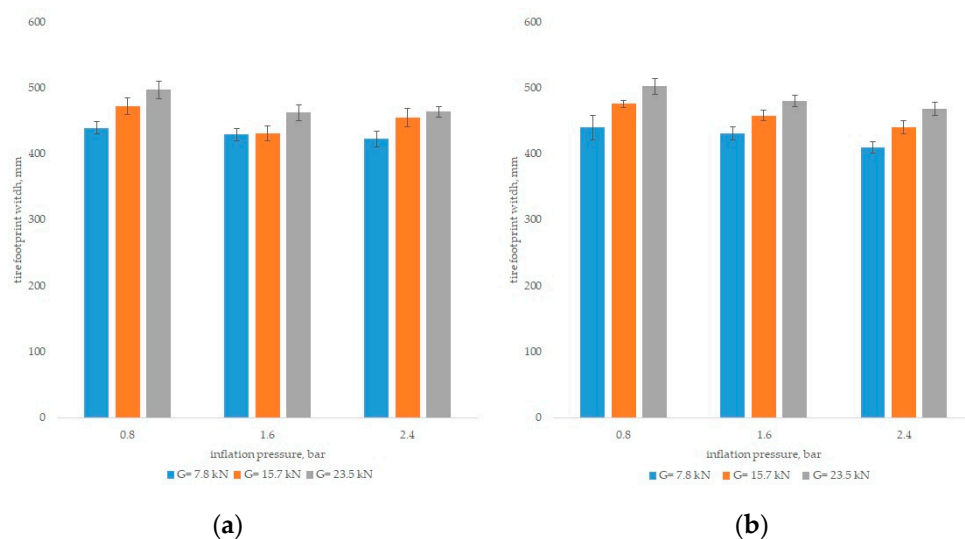


**Figure 6.** Footprint width values: bias-ply tire (a); radial tire (b); the linear markers represent the standard deviation.

Figure 7 presents the depth values of the footprints in the soil for the radial and bias-ply tires. Noticeably, the highest (54 mm) value was observed for the bias-ply tire with an inflation pressure of 2.4 bar and a vertical load of 23.5 kN. With the highest inflation pressure (2.4 bar) for the bias-ply tire, as the vertical load increased, the depth of the footprint also increased, while at lower inflation pressure values (0.8 bar and 1.6 bar), an increase in the vertical load from 7.8 kN to 15.7 kN resulted in a decrease in the depth of the footprint, but it increased again with a vertical load of 23.5 kN. The lowest value of footprint depth of 15 mm for the bias-ply tire was recorded with a vertical load of 15.7 kN and an inflation pressure of 0.8 bar. In addition, for the bias-ply tire, at the highest inflation pressure (2.4 bar), both increases in the vertical load of the tire resulted in an increase in

the footprint depth (increases of 30% and 43%, respectively). At the middle pressure value (1.6 bar), the first increase in vertical load resulted in an 11% decrease in the depth of the footprint, while the next increase resulted in a 10% increase. At the lowest inflation pressure, with a load of 7.8 kN and 15.7 kN for the bias-ply tire, the depth values were practically the same, while after increasing the vertical load to 23.5 kN, an increase of 68% was observed. In the case of the radial tire, the highest depth value was 26 mm (with a load of 23.5 kN and an inflation pressure of 2.4 bar), only slightly different from that produced by 15.7 kN. For each inflation pressure value, an increase in the vertical load resulted in an increase in the depth of the tire footprint. The largest difference of 14 mm (108%) was observed at a pressure of 2.4 bar, between the lowest and highest vertical load. At the two lower inflation pressures, the differences in the depths of the footprints (between sequential load levels) were in the range of 19–39%. For both tires, a clear effect of the inflation pressure on the depth of the generated footprint was noted. In most cases, a pressure drop resulted in a reduction in the depth, while for the bias-ply tire the average reductions in the depth due to the first and second pressure drops were at a similar level (about 30%), whereas for the radial tire, only the pressure reduction from 1.6 bar to 0.8 bar resulted in shallower footprints. On the other hand, at the highest inflation pressure, the radial tire produced a footprint more than twice as shallow as the bias-ply tire.

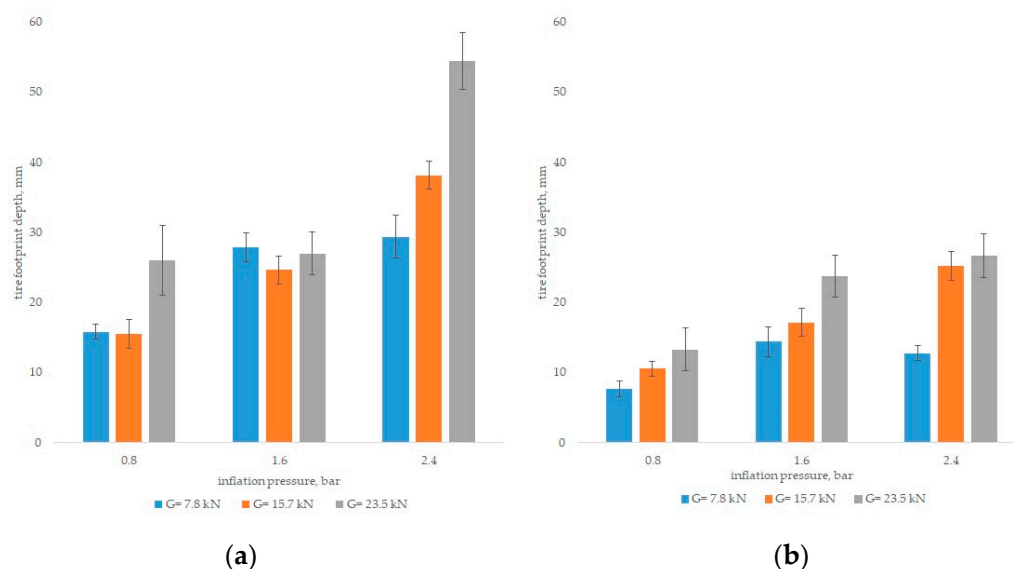


**Figure 7.** Footprint depth values: bias-ply tire (a); radial tire (b); the linear markers represent the standard deviation.

The last footprint parameter was the tire–soil contact area (Figure 8). Its highest value (0.33 m<sup>2</sup>) was observed for the bias-ply tire at the lowest pressure and the highest vertical load. For the bias-ply tire, at the same vertical loads, the lowest value of the footprint area was noted at an inflation pressure of 1.6 bar. However, at each level of inflation pressure, an increase in the vertical load resulted in an increase in the contact area. The highest increases were found at the first change in inflation pressure (by 43% and 23% for increases in load from 7.8 kN to 15.7 kN and from 15.7 kN to 23.5 kN, respectively).

For the radial tire, the lowest contact area of 0.13 m<sup>2</sup> was found with a vertical load of 7.8 kN and an inflation pressure of 2.4 bar. It was also observed that the footprint area for the radial tire changed according to a certain trend; an increase in the vertical load at a given inflation pressure resulted in an increase in the contact area, and at each inflation pressure, the first increase in load (from 7.8 kN to 15.7 kN) resulted in a larger area increase than the second, by 44%, 47%, and 62% for inflation pressures of 0.8, 1.6, and 2.4 bar, respectively. At the same time, a reduction in the inflation pressure in the radial tire at a given vertical load resulted in an increase in the contact area; the largest differences were found for the first



load, with the area increasing by 20% after reducing the pressure from 1.6 bar to 0.8 bar, and by 15% after reducing from 2.4 bar to 1.6 bar. For the first load, reducing the inflation pressure from the highest to the lowest value resulted in an increase in the contact area by 38% (to 0.18 m<sup>2</sup>).

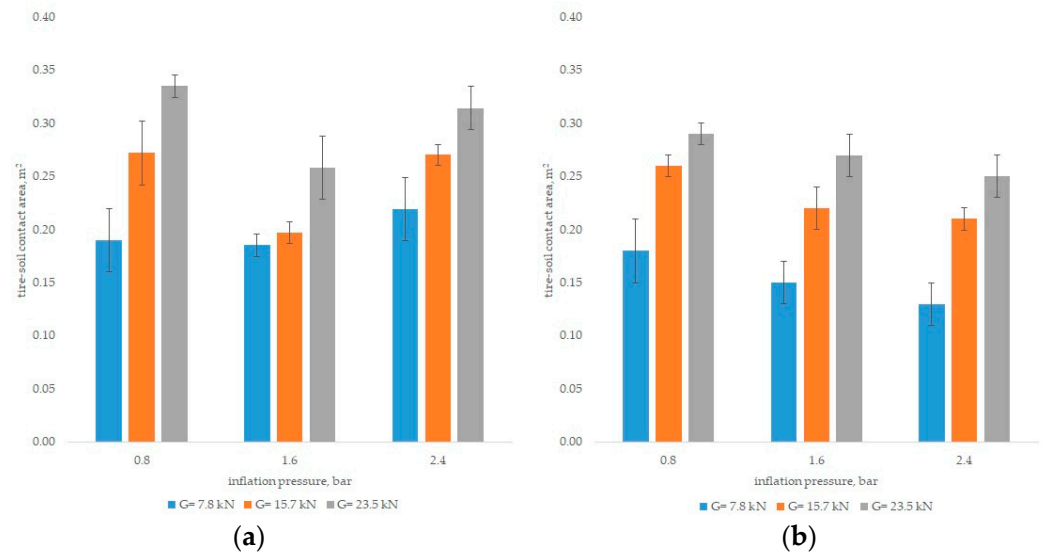


**Figure 8.** Tire–soil contact area values: bias-ply tire (a); radial tire (b); linear markers represent the standard deviation.

Table 2 presents a statistical analysis of the experimental data for the radial tire. The footprint parameters are the width, length, depth, and tire–soil contact area. The *p*-values presented in the table indicate the probability of accepting the hypothesis that the factor does not affect the imprint parameter. If the value of *p* does not exceed the significance level  $\alpha$  (0.05), the factor had a significant influence on the analyzed parameter.

**Table 2.** Statistical analysis of the experimental data for the radial tire. Significance level  $\alpha = 0.05$ . SD—standard deviation.

Footprint Parameter	Factor	Factor Level	Arithmetic Mean	±SD	<i>p</i> -Value
Width of the footprint (b), mm	Vertical load	7.8 kN	426.8 <sup>A</sup>	15.1	<0.0001
		15.7 kN	458.1 <sup>B</sup>	16.6	
		23.5 kN	483.4 <sup>C</sup>	17.5	
	Inflation pressure	0.8 bar	472.6 <sup>A</sup>	29.5	
		1.6 bar	456.2 <sup>B</sup>	22.8	
		2.4 bar	439.6 <sup>C</sup>	22.4	
Length of the footprint (l), mm	Vertical load	7.8 kN	360.6 <sup>A</sup>	36.5	<0.0001
		15.7 kN	456.4 <sup>B</sup>	33.7	
		23.5 kN	504.8 <sup>C</sup>	22.5	
	Inflation pressure	0.8 bar	477.5 <sup>A</sup>	55.1	
		1.6 bar	433.6 <sup>B</sup>	70.8	
		2.4 bar	410.7 <sup>C</sup>	66.6	
Depth of the footprint (h), mm	Vertical load	7.8 kN	11.6 <sup>A</sup>	3.3	<0.0001
		15.7 kN	17.6 <sup>B</sup>	6.5	
		23.5 kN	24.2 <sup>C</sup>	6.6	
	Inflation pressure	0.8 bar	10.5 <sup>A</sup>	3.0	
		1.6 bar	18.4 <sup>B</sup>	4.7	
		2.4 bar	21.6 <sup>C</sup>	6.9	

**Table 2.** *Cont.*

Footprint Parameter	Factor	Factor Level	Arithmetic Mean	±SD	p-Value
Tire–soil contact area (A <sub>s</sub> ), m <sup>2</sup>	Vertical load	7.8 kN	0.154 <sup>A</sup>	0.029	<0.0001
		15.7 kN	0.229 <sup>B</sup>	0.026	
		23.5 kN	0.271 <sup>C</sup>	0.023	
	Inflation pressure	0.8 bar	0.244 <sup>A</sup>	0.053	
		1.6 bar	0.214 <sup>B</sup>	0.055	
		2.4 bar	0.197 <sup>B</sup>	0.055	

The letters in the arithmetic mean column (A, B, C) denote separate homogenous groups.

Based on the footprint generated by the radial tire, it can be concluded that both experimental factors (vertical load and tire inflation pressure) had a significant influence on all footprint dimension values (the *p*-values were much lower than the assumed significance level  $\alpha$ ). In the case of the first factor (vertical load), each of its levels formed a separate homogeneous group; these trends were observed for all four footprint parameters. For the second factor (tire inflation pressure), separate homogeneous groups were identified for each level for the length, width, and depth of the footprint, while for the fourth parameter (contact area), two homogeneous groups were obtained; the first for the lowest tire pressure level (0.8 bar), and the second for the other two levels (1.6 bar and 2.4 bar). In practice, this meant that the change in inflation pressure from 2.4 bar to 1.6 bar did not result in significant changes in the tire–soil contact area.

Table 3 presents the results of the statistical analysis in relation to the footprints generated by the bias-ply tire. Both the experimental factors and the footprint parameters were the same as in the case of the radial tire. First, the effect of the experimental factors on the footprint parameters was determined; in all cases, it was found that both the inflation pressure and vertical load had a significant impact on the footprint parameters. Subsequently, homogeneous group tests were performed. When analyzing the impact of the vertical load, it turned out that a change in its level resulted in significant changes in all footprint parameters, except for the depth; in this case, significant differences were only found between 23.5 kN and the other two levels (there was no significant difference in depth values between 7.8 kN and 15.7 kN). The influence of the tire inflation pressure on the footprint parameters turned out to be slightly smaller; only in the case of the depth of the footprints were three separate homogeneous groups identified, while for the remaining dimensions, two homogeneous groups were observed.

**Table 3.** Statistical analysis of the experimental data for the bias-ply tire. Significance level  $\alpha = 0.05$ . SD—standard deviation.

Footprint Parameters	Factor	Factor Level	Arithmetic Mean	±SD	p-Value
Width of the footprint (b), mm	Vertical load	7.8 kN	430.5 <sup>A</sup>	11.5	<0.0001
		15.7 kN	452.8 <sup>B</sup>	20.9	
		23.5 kN	474.3 <sup>C</sup>	19.6	
	Inflation pressure	0.8 bar	469.6 <sup>A</sup>	26.9	
		1.6 bar	441.1 <sup>B</sup>	18.6	
		2.4 bar	447.0 <sup>B</sup>	21.3	
Length of the footprint (l), mm	Vertical load	7.8 kN	439.1 <sup>A</sup>	20.4	<0.0001
		15.7 kN	475.5 <sup>B</sup>	41.2	
		23.5 kN	559.4 <sup>C</sup>	46.5	
	Inflation pressure	0.8 bar	513.6 <sup>A</sup>	74.9	
		1.6 bar	449.4 <sup>B</sup>	43.1	
		2.4 bar	511.1 <sup>A</sup>	48.9	



**Table 3.** *Cont.*

Footprint Parameters	Factor	Factor Level	Arithmetic Mean	±SD	p-Value
Depth of the footprint (h), mm	Vertical load	7.8 kN	24.3 <sup>A</sup>	6.7	0.0004
		15.7 kN	26.1 <sup>A</sup>	10.0	
		23.5 kN	35.8 <sup>B</sup>	14.5	
	Inflation pressure	0.8 bar	19.1 <sup>A</sup>	5.8	
		1.6 bar	26.5 <sup>B</sup>	2.5	
		2.4 bar	40.7 <sup>C</sup>	11.4	
Tire–soil contact area (A <sub>s</sub> ), m <sup>2</sup>	Vertical load	7.8 kN	0.199 <sup>A</sup>	0.027	<0.0001
		15.7 kN	0.247 <sup>B</sup>	0.039	
		23.5 kN	0.301 <sup>C</sup>	0.038	
	Inflation pressure	0.8 bar	0.264 <sup>A</sup>	0.065	
		1.6 bar	0.216 <sup>B</sup>	0.037	
		2.4 bar	0.267 <sup>A</sup>	0.043	

The letters in the arithmetic mean column (A, B, C) denote separate homogenous groups.

### 3.1. Mathematical Models of Static Soil Deformation

As part of the statistical analysis, mathematical models were developed to describe the contact area as a function of the tire operational parameters. The choice of the contact for the model was dictated by the fact that it is crucial for the value of the force exerted on the soil and for forecasting the risk of soil compaction. Due to the structural differences between the tires, models were developed separately for the radial and bias-ply tires. Mathematical modelling was carried out using Statistica 12.5 (Statsoft) and TableCurve 2D ver. 5.0.1, Systat Software, San Jose, CA, USA.

#### 3.1.1. Mathematical Model for Radial Tire Footprint

After verifying the significance of the experimental factors, a mathematical model was developed. First, the normality of the distribution of the variables (footprint area values) was tested. For this purpose, a Shapiro–Wilk test at a significance level of  $\alpha = 0.05$  was used. The value of the test function  $W$  was 0.94, and the probability  $p$  value was 0.207, which led to the conclusion that the data had a normal distribution (this is the case when the  $p$ -value is greater than the assumed significance level  $\alpha$ ). Subsequently, a general form of the mathematical model (Equation (1)) was developed:

$$A_s = -0.267 - 0.0427 \cdot \ln p + 0.012 \cdot \left( \ln \frac{G}{0.00981} \right)^2 - 0.0035 \cdot \left( \frac{G}{0.00981} \right)^{0.5} \tag{1}$$

where:

- $A_s$ —contact area of the footprint (m<sup>2</sup>),
- $p$ —inflation pressure in the tire generating the footprint (bar),
- $G$ —vertical load of the tire generating the footprint (kN).

The value of the coefficient of determination  $R^2$  for the model was 0.916, and the mean absolute error of estimation was 0.006. As part of the model fit analysis, a significance test of the model variables was performed, formulating a null hypothesis about their insignificance. To verify this hypothesis, a test using the F-Snedecor function at the significance level of  $\alpha = 0.05$  was used (Equation (2)):

$$F = \frac{\frac{R^2}{k}}{\frac{(1-R^2)}{n-k-1}} \tag{2}$$

where:

- $R^2$ —coefficient of determination,
- $n$ —number of cases,
- $k$ —number of variables.

If the value of  $F$  is higher than the critical value ( $F_{crit}$ ), the null hypothesis regarding the insignificance of the variables in the model is rejected. The  $F$  function value calculated on the basis of the above formula was 130.85, and the critical value from the F-Snedecor distribution tables was 4.26; therefore, the null hypothesis was rejected. This means that the variables of the regression model were significant. Subsequently, as part of the model verification, a so-called similarity grid was prepared, i.e., a graph illustrating the relationship between the data calculated from the model and the actual data (Figure 9).

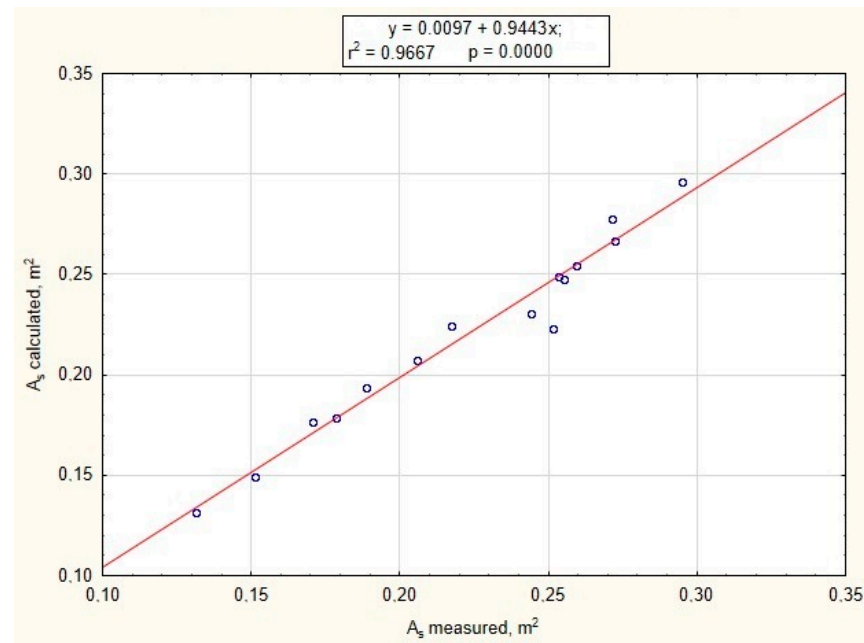


**Figure 9.** Relationship between the model data and the actual data for the radial tire ( $A_s$ —contact area).

By analyzing the graph presented in Figure 9, it turns out that the discrepancy between the actual data and the data calculated from the model is in most cases small. Only the points corresponding to the values of 0.231 and 0.244 m<sup>2</sup> deviate significantly from the trend line. To determine the relationships between the calculated and measured data, evaluation of the regression significance was conducted (F-Fisher test at a significance level of  $\alpha = 0.05$  was used). The null hypothesis stated that the regression coefficient and slope were statistically insignificant. In the case of the coefficient of regression, the value of the test function was  $F_{(1, 13)} = 377.37$  and the probability of the acceptance of the null hypothesis had a value lower than 0.00001. A relatively high test function value and very low level of probability caused us to reject the null hypothesis; for this reason, the regression coefficient was significant. However, the test procedure for the slope showed that it was insignificant (probability  $p = 0.3978$ ).

### 3.1.2. Mathematical Model for the Bias-Ply Tire Footprint

In the case of the bias-ply tire, a mathematical model was developed in the same way as for the radial tire. The test of the normality of the distribution (Shapiro–Wilk at the significance level of  $\alpha = 0.05$ ) confirmed that the data had a distribution that was consistent with a normal distribution; the value of the test function ( $W$ ) was 0.94, and the probability level of the rejection of the hypothesis of no normal distribution was  $p = 0.185$ . For the bias-ply tire, the following mathematical model (Equation (3)) with the contact area as a function of the tire operating parameters was developed:

$$A_s = 0.947 - \frac{1.882}{p^{0.5}} + \frac{1.063}{p} + 7.76 \cdot 10^{-4} G \cdot \ln \frac{G}{0.00981} \quad (3)$$

where:

$A_s$ —contact area of the footprint ( $m^2$ ),

$p$ —inflation pressure in the tire generating the footprint (bar),

$G$ —vertical load of the tire generating the footprint (kN).

The value of the coefficient of determination ( $R^2$ ) for the developed model was 0.812, and the mean absolute error of estimation was 0.014.

The correctness of the model fit was verified using the F-Snedecor function. The calculated value of the function was  $F = 51.83$ , while the critical value in the F-Snedecor distribution tables was 19.45; therefore, it was concluded that the model was well suited to the empirical data. Figure 10 shows the relationship between the model data and the actual data.

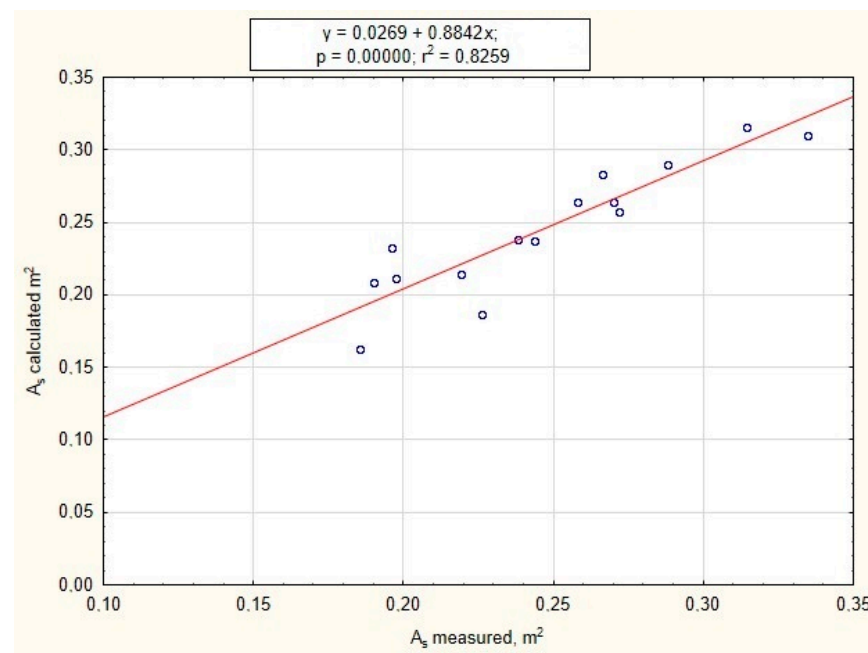


**Figure 10.** Relationship between the model data and the actual data for the bias-ply tire ( $A_s$ —contact area).

In the case of the bias-ply tire model, a slightly worse fit was observed than in the case of the radial tire. This was also evidenced by the lower value of the coefficient of determination  $R^2$  (0.812 for the bias-ply tire model and 0.916 for the radial tire model). When analyzing Figure 10, it can be seen that at higher values of the real area ( $A_s$ ), the match was good, but at lower values, the dispersion of the points from the trend line was large. In the case of the bias-ply tire, verification of the model fit was conducted in the same way as in the case of the radial tire (F-Fisher test at the significance level of  $\alpha = 0.05$ ). The evaluation of the regression coefficient showed that it was significant. The parameters were the values of test function  $F_{(1,13)} = 61.662$ , probability level  $p < 0.00001$ . The slope was an insignificant parameter (probability  $p = 0.3573$ ).

#### 4. Discussion

Our study was carried out using soil as a deformable substrate and different values of tire inflation pressure and vertical load. It was possible to observe changes in the dimensions of the soil footprint of tires with different internal constructions but the same external sizes. Footprint parameters such as length, width, and depth were used to determine the contact area of the tire with the soil (without simplifying it, for example, to the cross-sectional area of the tire at its contact with the ground).

According to our results, the tire inflation pressure and vertical load are the factors that affect the dimensions of the tire footprint in the soil. In most cases, a reduction in

the inflation pressure increases the footprint dimensions, which was confirmed by Shao et al. [27], O'Sullivan et al. [28], and Keller [29]. In addition to the length and width of the footprint, an important parameter is its depth, on which the tire–soil contact area largely depends. Hemmat et al. [30] suggested that the depth of the footprint is the main indicator of soil compaction. According to Moitzi et al. [31], a higher value of vertical load at a lower inflation pressure increases the tire footprint depth in the soil, which was confirmed by Rapper et al. [32]. In the present research, in some cases the same tire–soil contact area was observed for different values of tire inflation pressure and vertical load. For example, a contact area of 0.26 m<sup>2</sup> was recorded at an inflation pressure of 1.6 bar and 23.5 kN vertical load (bias-ply tire) and 0.8 bar and 15.7 kN (radial tire). However, at the same time, for the bias-ply tire, a much greater footprint depth was recorded than for the radial tire (26.99 mm and 10.56 mm, respectively). It was also noted that the same values of inflation pressure and vertical load (0.8 bar and 7.8 kN) resulted in a similar contact area for both tires, but the footprint depth for the bias-ply tire was 15.83 mm, and for the radial tire it was 7.62 mm. These examples show that, under certain conditions, a radial tire has a less destructive effect on the ground. When comparing radial and bias-ply tires, Kurjenluoma et al. [33] found that their internal structure also affects the formation of the rut (tire footprint in the soil) and that lowering the tire pressure reduces the rut depth, but only on soft soil with high humidity. Farhadi et al. [24] took into account soil moisture as a factor influencing the dimensions of the tire footprint in the soil. Similarly, Mohsenimanesh and Ward [34] noted that increasing the soil moisture causes an increase in the tire–soil contact area, but they also found that at any level of soil moisture, the vertical load of the tire also affects this parameter. Comparing the effects of two radial tires, Schjøning et al. [35] noted that a tire with a smaller width generated a longer footprint and was less sensitive to inflation pressure values not recommended by the manufacturer than a wider tire. Botta et al. [36] noted that, in order to increase the contact area of a tire with soil, the size of the tires, the vertical load on the tires, and the soil moisture should be taken into account.

Based on the literature review, our results, and a comparative analysis with those of other authors, it can be concluded that knowledge of the contact area of a tire with the soil and information on factors affecting its value are crucial for protecting soil against the negative impact of agricultural tires. It should also be noted that it is necessary to take into account all the variables described above at the same time, because their selective analysis may lead to erroneous conclusions (e.g., different load values can result in the same contact area and different depths). The right combination of factors, such as load and pressure, can have a positive impact on soil protection and thus improve crop production results.

## 5. Conclusions

Analysis of our results made it possible to conclude that both research factors, i.e., vertical load on the tire and tire inflation pressure, had an impact on the footprint dimension values:

1. An increase in the vertical load, at the same tire inflation, resulted in an increase in the length of the tire footprint. For the radial tire, the length increased steadily with the same load and a decrease in inflation pressure. In the case of the bias-ply tire, the length decreased when the pressure dropped from 2.4 bar to 1.6 bar and then increased when it dropped from 1.6 bar to 0.8 bar. In most cases, at the same pressure and load, greater tire footprint lengths were observed for the bias-ply tire than for the radial tire.
2. At the same inflation pressure, when the vertical load was increased, the width of the footprint also increased for both the radial and bias-ply tires. At the same time, a reduction in the inflation pressure with the same vertical load resulted in an increase in the width of the tire footprint, but only for the radial tire. With the same values of vertical load and inflation pressure, in most cases the radial tire imprint was wider.
3. Reducing the vertical load on the tires resulted in a decrease in the depth of the footprint for all inflation pressure values, but only for the radial tire (for the bias-ply tire, this trend was observed only when the pressure rose to its highest value). In all

cases, at the same values of inflation pressure and vertical load, significantly higher tire footprint depths were observed for the bias-ply tire.

4. Increasing the vertical load at a constant inflation pressure caused an increase in the contact area with the soil of the tested tire footprint. For the radial tire, a reduction in its inflation pressure with a constant vertical load value resulted in an increase in the contact area, but this trend was not observed for the bias-ply tire. The bias-ply tire generated a footprint of a smaller width and length, but a greater depth and contact area, than the radial tire. This indicates that the depth of a tire footprint largely determines the contact area. It was noted that a comparable contact area of the tires could be achieved for different combinations of inflation pressure and vertical load, which means that an ideal combination could reduce the depth of the tire footprint. This is very important information for agricultural practice, because further research will make it possible to use tires on a field while avoiding soil environment degradation.

**Author Contributions:** Conceptualization, J.C. and W.P.; methodology, J.C.; software, M.B. and W.P.; validation, M.B. and A.M.; formal analysis, J.C. and K.L.; investigation, W.P., M.B. and A.M.; resources, W.P.; data curation, M.B.; writing—original draft preparation, W.P. and M.B.; writing—review and editing, M.B.; visualization, W.P.; supervision, J.C.; project administration, J.C. and K.L.; funding acquisition, J.C. and K.L. All authors have read and agreed to the published version of the manuscript.

**Funding:** The article processing charge was financed by Wrocław University of Environmental and Life Sciences.

**Institutional Review Board Statement:** Not applicable.

**Informed Consent Statement:** Not applicable.

**Data Availability Statement:** Not applicable.

**Conflicts of Interest:** The authors declare no conflict of interest. The funders had no role in the design of the study; in the collection, analyses, or interpretation of data; in the writing of the manuscript; or in the decision to publish the results.

## References

1. Keller, T.; Arvidsson, J.; Schjønning, P.; Lamandé, M.; Stettler, M.; Weisskopf, P. In situ subsoil stress-strain behavior in relation to soil precompression stress. *Soil Sci.* **2012**, *177*, 490–497. [[CrossRef](#)]
2. Horn, R.; Domżzał, H.; Słowińska-Jurkiewicz, A.; van Ouwerkerk, C. Soil compaction processes and their effects on the structure of arable soils and the environment. *Soil Tillage Res.* **1995**, *35*, 23–36. [[CrossRef](#)]
3. Bengough, A.G.; McKenzie, B.M.; Hallett, P.D.; Valentine, T.A. Root elongation, water stress, and mechanical impedance: A review of limiting stresses and beneficial root trip traits. *J. Exp. Bot.* **2011**, *62*, 59–68. [[CrossRef](#)]
4. Berisso, F.E.; Schjønning, P.; Keller, T.; Lamandé, M.; Etana, A.; de Jonge, L.W.; Iversen, B.V.; Arvidsson, J.; Forman, J. Persistent effects of subsoil compaction on pore size distribution and gas transport in a loamy soil. *Soil Tillage Res.* **2012**, *122*, 42–51. [[CrossRef](#)]
5. Brus, D.J.; van den Akker, J.J.H. How serious a problem is subsoil compaction in the Netherlands? A survey based on probability sampling. *Soil* **2018**, *4*, 37–45. [[CrossRef](#)]
6. Mossadeghi-Björklund, M.; Jarvis, N.; Larsbo, M.; Forkman, J.; Keller, T. Effects of compaction on soil hydraulic properties, penetration resistance and water flow patterns at the soil profile scale. *Soil Use Manag.* **2019**, *35*, 367–377. [[CrossRef](#)]
7. Lipiec, J.; Stepniewski, W. Effects of soil compaction and tillage systems on uptake and losses of nutrients. *Soil Tillage Res.* **1995**, *35*, 37–52. [[CrossRef](#)]
8. Elkins, C.B. Plant roots as tillage tools. *J. Terramech.* **1985**, *22*, 177–178. [[CrossRef](#)]
9. Materechera, S.A.; Alston, A.M.; Kirby, J.M.; Dexter, A.R. Influence of root diameter on the penetration of seminal roots into a compacted subsoil. *Plant Soil* **1992**, *144*, 297–303. [[CrossRef](#)]
10. Blomquist, J.; Hellgren, O.; Larsson, H. Limiting and promoting factors for high yield in Sweden. *Adv. Sugar Beet Res.* **2003**, *5*, 3–17.
11. Colombi, T.; Keller, T. Developing strategies to recover crop productivity after soil compaction—A plant eco-physiological perspective. *Soil Tillage Res.* **2019**, *191*, 156–161. [[CrossRef](#)]
12. Lindemuth, B.E. An overview of tire technology. In *The Pneumatic Tire*; U.S. Department of Transportation, National Highway Traffic Safety Administration: Washington, DC, USA, 2006; pp. 3–7.

13. Raper, R.L.; Bailey, A.C.; Burt, E.C.; Way, T.R.; Liberati, P. Inflation pressure and dynamic load effects on soil deformation and soil-tire interface stresses. *Trans. ASAE* **1995**, *38*, 685–689. [[CrossRef](#)]
14. Sharma, A.K.; Pandey, K.P. The deflection and contact characteristics of some agricultural tires with zero sinkage. *J. Terramech.* **1996**, *33*, 293–299. [[CrossRef](#)]
15. Botta, G.F.; Jorajuria, D.; Draghi, L.M. Influence of the axle load, tire size and configuration on the compaction of a freshly tilled clayey soil. *J. Terramech.* **2002**, *39*, 47–54. [[CrossRef](#)]
16. Grečenko, A. Tire footprint area on hard ground computed from catalogue values. *J. Terramech.* **1995**, *32*, 325–333. [[CrossRef](#)]
17. Hallonborg, U. Super ellipse as tire-ground contact area. *J. Terramech.* **1996**, *33*, 125–132. [[CrossRef](#)]
18. Keller, T. A model for the prediction of the contact area and the distribution of vertical stress below agricultural tires from readily available tire parameters. *Biosyst. Eng.* **2005**, *92*, 85–96. [[CrossRef](#)]
19. Roșca, R.; Cârlescu, P.; Țenu, I. A semi-empirical traction prediction model for an agricultural tire, based on the super ellipse shape of the contact surface. *Soil Tillage Res.* **2014**, *141*, 10–18. [[CrossRef](#)]
20. Diserens, E. Calculating the contact area of trailer tires in the field. *Soil Tillage Res.* **2009**, *103*, 302–309. [[CrossRef](#)]
21. Diserens, E.; Défossez, P.; Duboisset, A.; Alaoui, A. Prediction of the contact area of agricultural traction tires on firm soil. *Biosyst. Eng.* **2011**, *110*, 73–82. [[CrossRef](#)]
22. Taghavifar, H.; Mardani, A. Investigating the effect of velocity, inflation pressure, and vertical load on rolling resistance of a radial ply tire. *J. Terramech.* **2013**, *50*, 99–106. [[CrossRef](#)]
23. Kenarsari, A.E.; Vitton, S.J.; Beard, J.E. Creating 3D models of tractor tire footprints using close-range digital photogrammetry. *J. Terramech.* **2017**, *74*, 1–11. [[CrossRef](#)]
24. Farhadi, P.; Golmohammadi, A.; Sharifi, A.; Shahgholi, G. Potential of three-dimensional footprint mold in investigating the effect of tractor tire contact volume changes on rolling resistance. *J. Terramech.* **2018**, *78*, 63–72. [[CrossRef](#)]
25. Ptak, W.; Czarnecki, J.; Brennenstul, M. Use of 3D scanning technique to determine tire deformation in static conditions. *J. Agric. Eng.* **2022**, *53*, 1–7. [[CrossRef](#)]
26. Ptak, W.; Czarnecki, J.; Brennenstul, M.; Lejman, K.; Małecka, A. Evaluation of agriculture tires deformation using innovative 3D scanning method. *Agriculture* **2022**, *12*, 1108. [[CrossRef](#)]
27. Shao, X.; Yang, Z.; Mowafy, S.; Zheng, B.; Song, Z.; Luo, Z.; Gou, W. Load characteristics analysis of tractor drivetrain under field plowing operation considering tire-soil interaction. *Soil Tillage Res.* **2023**, *227*, 105620. [[CrossRef](#)]
28. O’Sullivan, M.; Henshall, J.; Dickson, J. A simplified method for estimating soil compaction. *Soil Tillage Res.* **1999**, *49*, 325–335. [[CrossRef](#)]
29. Keller, T. Soil Compaction and Soil Tillage-Studies in Agricultural Soil Mechanics. Ph.D. Thesis, Swedish University of Agricultural Sciences, Uppsala, Sweden, 2004.
30. Hemmat, A.; Yaghoubi-Taskoh, M.; Masoumi, A.; Mosaddeghi, M.R. Relationships between rut depth and soil mechanical properties in a calcareous soil with unstable structure. *Biosyst. Eng.* **2014**, *118*, 147–155. [[CrossRef](#)]
31. Moitzi, G.; Sattler, E.; Wagenristl, H. Effect of cover crop, slurry application with different loads and tire inflation pressures on tire track depth, soil penetration resistance and maize yield. *Agriculture* **2021**, *11*, 641. [[CrossRef](#)]
32. Raper, R.L.; Bailey, A.C.; Burt, E.C.; Way, T.R.; Liberati, P. The effects of reduced inflation pressure on soil-tire interface stresses and soil strength. *J. Terramech.* **1995**, *32*, 43–51. [[CrossRef](#)]
33. Kurjenluoma, J.; Alakukku, L.; Ahokas, J. Rolling resistance and rut formation by implement tires on tilled clay soil. *J. Terramech.* **2009**, *46*, 267–275. [[CrossRef](#)]
34. Mohsenimanesh, A.; Ward, S.M. Estimation of a three-dimensional tire footprint using dynamic soil-tire contact pressures. *J. Terramech.* **2010**, *47*, 415–421. [[CrossRef](#)]
35. Schjøning, P.; Lamandé, M.; Tøgersen, F.A.; Arvidsson, J.; Keller, T. Modelling effects of tire inflation pressure on the stress distribution near the soil-tire interface. *Biosyst. Eng.* **2008**, *99*, 119–133. [[CrossRef](#)]
36. Botta, G.F.; Becerra, A.T.; Tourn, F.B. Effect of the number of tractor passes on soil rut depth and compaction in two tillage regimes. *Soil Tillage Res.* **2009**, *103*, 381–386. [[CrossRef](#)]

**Disclaimer/Publisher’s Note:** The statements, opinions and data contained in all publications are solely those of the individual author(s) and contributor(s) and not of MDPI and/or the editor(s). MDPI and/or the editor(s) disclaim responsibility for any injury to people or property resulting from any ideas, methods, instructions or products referred to in the content.

### 3.4. Evaluation of tires acting on soil in field conditions using 3D scanning method

Autorzy: **Weronika Ptak**, Jarosław Czarnecki, Marek Brennenstul,  
Krzysztof Lejman, Agata Małecka

Czasopismo: Agriculture, 13(5), 1094

Doi: 10.3390/agriculture13051094



## Article

# Evaluation of Tires Acting on Soil in Field Conditions Using the 3D Scanning Method

Weronika Ptak <sup>\*</sup>, Jarosław Czarnecki, Marek Brennenstul , Krzysztof Lejman and Agata Małecka

Institute of Agricultural Engineering, Wrocław University of Environmental and Life Sciences, 51-630 Wrocław, Poland; jaroslaw.czarnecki@upwr.edu.pl (J.C.); marek.brennenstul@upwr.edu.pl (M.B.); krzysztof.lejman@upwr.edu.pl (K.L.); 113322@student.upwr.edu.pl (A.M.)

\* Correspondence: weronika.ptak@upwr.edu.pl

**Abstract:** This research presents the results of tests conducted under field conditions and included measuring the footprint of tires on soil. Two agricultural tires of the same size but different internal structures were tested, 500/50R17 (radial) and 500/50-17 (bias-ply). The factors were tire inflation pressure (0.8 bar, 1.6 bar, and 2.4 bar) and tire vertical load (7.8 kN, 11.8 kN, and 15.7 kN). The footprint made on the soil was scanned with a 3D scanner, resulting in a digital image of the tire footprint on the soil to enable an analysis of the measured parameters: length, width, depth, and contact area (in 3D form). Statistical analysis showed that for radial tire footprints, both inflation pressure and vertical load had a significant effect on all analyzed parameters. For bias-ply tire footprints, it was shown that only inflation pressure had a significant effect on all of the analyzed parameters, while the significance of the effect of the vertical load was not confirmed for the footprint depth. Based on the results obtained, the suitability of models describing the relationship between operating factors and the actual footprint area was verified. It was found that for a radial tire, the model formulated based on laboratory tests can predict the contact surface under field conditions (the correlation coefficient  $R^2$  was equal to 0.9226). In the case of a bias-ply tire, the correlation coefficient  $R^2$  reached a value equal to 0.5828. This indicates a less accurate estimation of the surface area under field conditions based on the model designed after laboratory testing.



**Citation:** Ptak, W.; Czarnecki, J.; Brennenstul, M.; Lejman, K.; Małecka, A. Evaluation of Tires Acting on Soil in Field Conditions Using the 3D Scanning Method. *Agriculture* **2023**, *13*, 1094. <https://doi.org/10.3390/agriculture13051094>

Academic Editor: Kenshi Sakai

Received: 24 April 2023

Revised: 14 May 2023

Accepted: 18 May 2023

Published: 20 May 2023



**Copyright:** © 2023 by the authors. Licensee MDPI, Basel, Switzerland. This article is an open access article distributed under the terms and conditions of the Creative Commons Attribution (CC BY) license (<https://creativecommons.org/licenses/by/4.0/>).

**Keywords:** soil deformation; contact surface; radial tire; bias-ply tire; 3D scanning

## 1. Introduction

The main goal of agriculture is to produce food. This goal can be achieved using various agriculture systems, of which the intensive agriculture system is relatively popular. It is geared toward achieving maximum efficiency in agrotechnical measures [1,2]. Higher efficiency requires using machines with larger widths and the ability to develop higher operational speeds to treat as much area as possible in a given time. This, in turn, creates high power requirements for such machines—so it becomes necessary to use larger tractors. Unfortunately, there are negative side effects of such measures caused by their large weight. The market is responding very quickly to the needs of farmers, and today a trend can be observed—tractors in the middle and upper power range are the most popular, but at the same time, have higher weight than their counterparts of 20–30 years ago [3]. The high weight of field aggregates can cause soil compaction which harms the soil. As a result, the soil's water and air balance is disturbed, the volume of air pores in the soil decreases, rainwater absorption and plant root development are hindered, and the mechanical strength of the soil increases [4,5]. Thus, compacted and more resistant soil requires loosening, which involves energy-intensive procedures, and the fuel consumption of agricultural vehicles consequently increases [6]. For these reasons, there is a need to find solutions to reduce the negative effects of heavy agricultural equipment on the soil.

Soil compaction results from soil stresses caused by the interaction of the chassis system components of agricultural vehicles and machinery. The most popular running



gear in agricultural equipment is the wheeled chassis, which has the tire in direct contact with the soil. The tracked chassis system is also used but is less popular due to its more complicated design and higher price. In the case of a wheeled chassis system, the parameter for determining the amount of pressure generated on the soil is the area of contact between the tire and the soil—this parameter is affected by the stiffness of the tire, its size, and the inflation pressure and vertical load acting on the wheel. Scientific research on the impact of chassis systems on the soil can be divided into two main groups. The first includes experiments conducted under laboratory conditions in soil-filled cases or bins. These studies are not affected by atmospheric conditions and tend to present high repeatability of results (less risk of the influence of random factors). They also generally do not generate high costs for experiments. The disadvantages of laboratory studies include the prior preparation of soil for the experiment and space limitations in laboratory premises. Additionally, some of the factors occurring in real conditions (such as the presence of plant root mass) are not considered. The second group includes research conducted under real conditions, the main and most important advantage of which is obtaining conditions almost identical to those which occur during the operation of agricultural machinery under field conditions. Field research is characterized by greater variability in the results—primarily due to the significant influence of atmospheric conditions and natural processes that would not occur under laboratory conditions. Based on the test results, models are developed to describe the contact area between the tire and the soil. On the one hand, an accurate description of the shape of this area is made—most often super elliptical [7–10].

Sometimes, simplifications are made by introducing an alternate shape similar to a rectangle [11]. On the other hand, a very important result of research on tire–surface interaction is the development of mathematical models that allow the prediction of the parameters of the footprint or rut depending on operating parameters and external conditions [12].

A separate issue concerning the study of the impact of tires on the soil is the technique used when taking measurements. While the measurement of the length or width of the footprint does not present major difficulties, such difficulties may arise when determining the area of the footprint, especially since it is not on a single area (the footprint is three-dimensional). The simplest measurement techniques are based on planimetric techniques or analysis of photographs of the footprint. Diserens [13], Diserens et al. [14], and Taghavifar and Mardani [15] used in their studies an image-processing technique to determine the shape of the contact surface and the parameters affecting that shape. More advanced forms of research use computer techniques—such as the finite element method—to determine soil deformation. For example, González Cueto et al. [16], González Cueto et al. [17], Khot et al. [18], Nakashima and Kobayashi [19], and Smith et al. [20] used the finite element method to analyze tire–soil interaction. In contrast, the work of Nakashima and Oida [21] and Michael et al. [22] used a combination of the finite element method and the discrete element method to represent the model in the tire–soil system. Late experimenting, on the other hand, is based on the use of laser scanning of the footprint surface—such methods require sophisticated equipment and are costly, yet provide very high accuracy during surface representation and the ability to quickly read the basic dimensions of the footprint from the obtained scan [23,24].

Based on the literature review, it can be concluded that the continuous improvement in research methods for the tire–surface system is justified due to the minimization of negative impacts on the soil—primarily avoiding compaction. For the above reasons, this research aims to evaluate the impact of changes in selected operating parameters in tires of different designs on the footprint size of the soil under field conditions using 3D scanning techniques and digital image analysis. An additional goal is to verify the applicability of models developed from laboratory tests to predict soil deformation under field conditions.

## 2. Materials and Methods

This study was carried out under field conditions in an experimental field located at the Institute of Agricultural Engineering of Wrocław University of Environmental and Life

Sciences. The substrate was soil classified as sandy loam soil with a specific density of the soil skeleton of  $2.59 \text{ g/cm}^3$ . During the experiment using a bias-ply tire, the average soil moisture was 22.5%, and the average soil cone index was 0.59 MPa. In contrast, for the part of the experiment with a radial tire, the values of these parameters were 16% and 0.96 MPa. Soil parameters were measured using Eijkelkamp's Penetrologger, which included a ThetaProbe to measure the moisture content and a cone penetrometer to measure soil compactness (the apex angle of the measuring cone was equal to  $60^\circ$ , and the area of its base was equal to  $0.0001 \text{ m}^2$ ). Two agricultural non-drive tires with different internal structures were tested: bias-ply (500/50-17) and radial (500/50R17). The tread type and tire dimensions were the same for both designs: width equal to 500 mm, profile height: 250 mm, rim diameter: 431.8 mm (17 inches), and outside diameter: 931.8 mm. The tires are designed for agricultural machinery such as straw/hay balers, manure spreaders, and forage trailers. Three tire pressures were adopted for the study: 0.8 bar, 1.6 bar, and 2.4 bar, and three values of vertical load on the tire: 7.8 kN, 11.8 kN, and 15.7 kN. The tests included measurement of tire footprint parameters on the soil: length, width, depth, and contact area.

### 2.1. Test Bench

The tire's footprint on the soil was created using the test bench by Ptak et al. (2023) in laboratory research, which required modification for field testing. The modification of the bench consisted mainly of installing elements that provided the possibility of aggregating the bench with a tractor—for this purpose, a three-point linkage was used. A schematic of the stand prepared for imprinting is shown in Figure 1. The vertical load on the tire was obtained using a hydraulic jack (5) which, for the duration of testing, was fitted in the vertical plane between the main frame (2) and the inner frame (3) of the test bench. The value of the vertical load was measured using a TecSis inductive dynamometer (4) with a measurement accuracy of 50 N and a measurement range of 0–100 kN. The tire being tested (1) was mounted on a shaft with bearings in the inner frame (3). Screw mechanisms (6) made it possible to lock the inner frame and its movement in the vertical plane and prevented pressure drops in the hydraulic jack, which could have resulted in an unintended reduction in the vertical load. With the use of weights (7), the test bench's load was achieved. No driving or braking forces were acting on the tire, which could have changed the stress distribution in the soil. After the footprint was created, the hydraulic jack was removed, the test bench with the tire being tested was raised using the tractor's three-point linkage, and then the tractor was driven off to specific locations in the field to create another footprint. The tire's footprint on the soil was created in five repetitions and its outline was marked, which was helpful in the further testing stage.

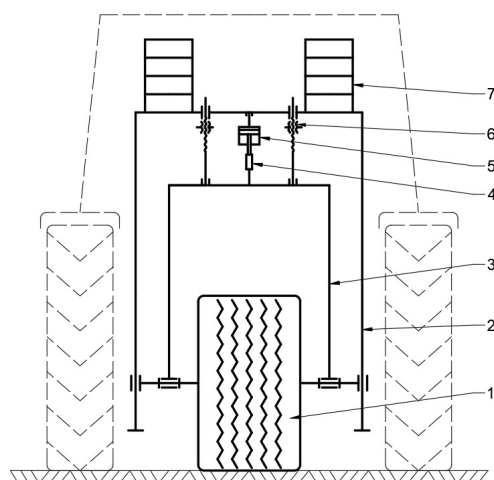


**Figure 1.** Scheme of the test bench: 1—wheel with tested tire, 2—main frame, 3—inner frame, 4—dynamometer, 5—hydraulic jack, 6—screw mechanism for locking the position of the inner frame, and 7—weights.

## 2.2. Scanning Process and Measurement of Footprint Parameters

Each time a footprint was created, it was scanned with a 3D scanner [25], the specifications of which are shown in Table 1. The scanner was connected to a laptop computer with Smarttech3Dmeasure software, which allowed the scanner to be operated. Due to the varying intensity of natural light, the scanning process was carried out in a tent, which ensured a uniform level of illumination of the scanned footprints.

**Table 1.** Technical data of the 3D scanner.

Parameter	Description
Scanning technology	White structural light—LED
Measuring volume (x, y, z) (mm)	400 × 300 × 240
Distance between points (mm)	0.156
Accuracy (mm)	0.08

The scanning process resulted in a digital image of the footprint (in the form of a point cloud), which reflected its actual shape and size. The next step was to create a triangle mesh from the acquired point cloud and measure the parameters for later analysis. To read the depth of the footprint, creating a section in the vertical plane was necessary. Figure 2A shows the triangle mesh of the tire footprint and the intact portion of the soil that served as the reference point and the cross-section when measuring the depth of the footprint.

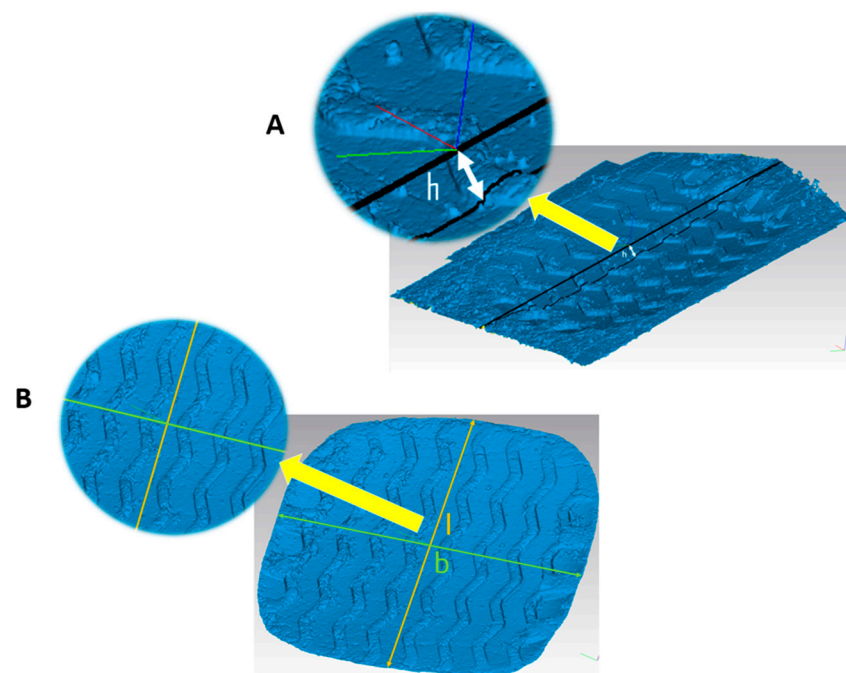


**Figure 2.** Mesh of triangles of the tire footprint on the soil: (A)—with intact soil (h—depth of the footprint); (B)—designated footprint (l—length of the footprint and b—width of the footprint).

The footprint depth was the height of the footprint section. Then, according to the markers surrounding the edge of the footprint, the intact soil part was removed from the image, and the next parameters analyzed in the experiment were determined—namely, the length of the footprint and its width, as shown in Figure 2B. It should be noted that the described parameters were always measured relative to the same measuring point located at the center of the footprint. The real surface was the surface of the footprint in three-dimensional space: not as a simplification in a two-dimensional projection, but as the whole footprint.

### 2.3. Statistical Analysis

Statistical analysis of the results obtained was carried out using Statistica 12.5. First, the results were subjected to analysis of variance at a significance level of  $\alpha = 0.05$  with the separation of homogeneous groups (Fisher's NIR test). Subsequently, the suitability of the models developed for the data obtained in the laboratory part was verified.

### 3. Results

First, the linear dimensions of the footprint were evaluated. Figure 3 shows the results of measurements of the length and width of the footprints generated by the two tires tested.

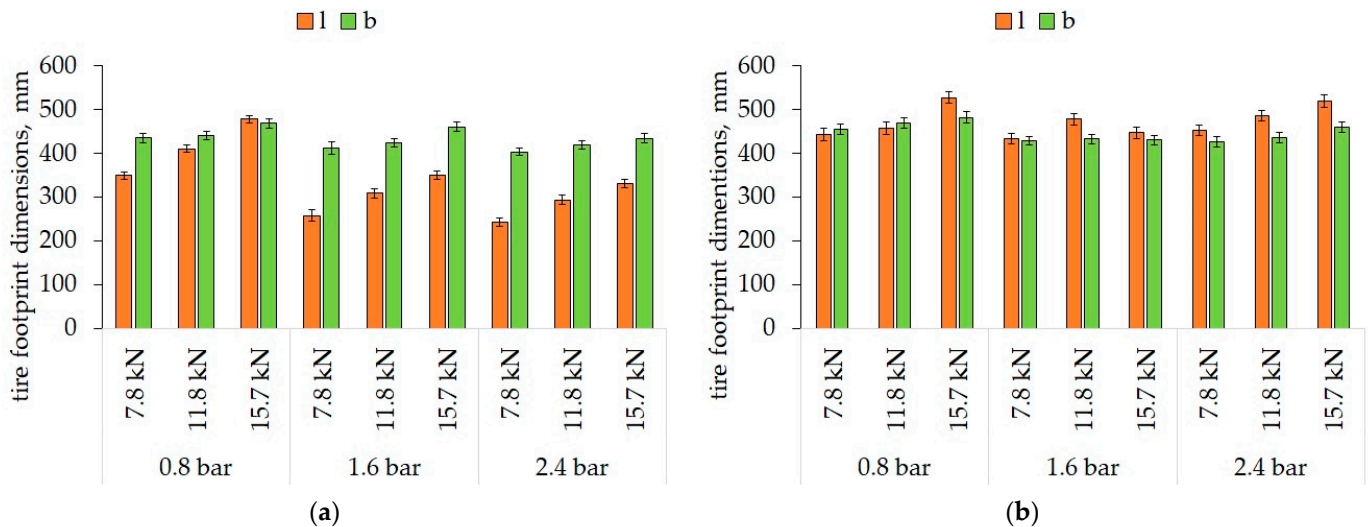


**Figure 3.** Values of tire footprint dimensions: radial tire (a); bias-ply tire (b); l—footprint length and b—footprint width.

In the case of the radial tire, an increase in the vertical load on the tire within the range of the same tire pressure always increased the measured parameters. The highest value of the radial tire's footprint length was 478.8 mm and was achieved at an inflation pressure of 0.8 bar and a vertical load of 15.7 kN. Reducing the vertical load to 11.8 kN and 7.8 kN at the lowest value of air pressure resulted in a decrease in the footprint length by 14% and 27%, accordingly. The lowest value of the footprint length generated by the radial tire was found at a tire pressure of 2.4 bar and a vertical load of 7.8 kN—it was 243.2 mm (49% less compared to the highest value observed for the measured parameter). For the bias-ply tire, the highest value of this parameter (528.2 mm) was observed at an inflation pressure of 0.8 bar and a vertical load of 15.7 kN, and a very similar value (519.8 mm) was found at a load of 15.7 kN and the highest inflation pressure (hence the conclusion that reducing the inflation pressure from 2.4 bar to 0.8 bar at the highest vertical load will result in an insignificant increase in footprint length—of only about 2%). The largest increase in the length of the bias-ply tire footprint with the increase in vertical load was observed at a pressure of 0.8 bar, increasing the vertical load from 11.8 kN to 15.7 kN (it was 16%).

Another analyzed parameter was the width of the footprint. The dynamics of change in this parameter were noticeably smaller than in the case of the footprint length. In the case of the radial tire, the highest value of the width parameter (468.9 mm) was observed at a tire pressure of 0.8 bar and a vertical load of 15.7 kN. By reducing the value of the vertical load to 11.8 kN and 7.8 kN in the range of the lowest inflation pressure, the width of the footprint decreased by 6% and 7%, respectively (to values of 440.5 mm and 435.4 mm, respectively). The largest increase in the measured parameter for the radial tire (8%) was noted at an inflation pressure of 1.6 bar and increasing the vertical load from 11.8 kN to 15.7 kN. At an inflation pressure of 2.4 bar and a load of 7.8 kN, the lowest value of the radial tire footprint width was observed, equal to 404.3 mm (14% less than the highest

value). For a vertical load of 11.8 kN, decreases in footprint width as a result of increasing inflation pressure were in the range of 4–5%, while at the highest vertical load level, changes in inflation pressure induced decreases in footprint width of 2% (an increase in inflation pressure from 0.8 bar to 1.6 bar) and 15% (an increase from 0.8 bar to 2.4 bar). For the bias-ply tire, the highest value of footprint width was observed, while for the radial tire, at an inflation pressure of 0.8 bar and a vertical load of 15.7 kN, a 3% increase (482.9 mm) in comparison with the radial tire. A bias-ply tire loaded at 7.8 kN at the inflation pressure of 2.4 bar generated a footprint width of 426.8 mm, corresponding to the smallest width observed for this tire (about 13% smaller than the largest footprint width). The largest increment (6%) in the current parameter was noticed at the highest inflation pressure level by increasing the vertical load from 11.8 kN to 15.7 kN. In other cases, the increments in footprint length were in the range of 2–3%. Evaluating the values of footprint width as a result of an increase in inflation pressure in the tire for one value of the vertical load, the largest decrease in the described parameter was observed at a vertical load of 15.7 kN and an increase in inflation pressure from 0.8 bar to 1.6 bar—the width of the footprint then decreased from 482.9 mm to 431.0 mm, respectively (a decrease of about 10%). Only a 0.5% decrease in the bias-ply tire’s footprint width value was observed with a constant vertical load of 7.8 kN between the middle and highest adopted inflation pressures (429.0 mm to 426.8 mm).

Figure 4 shows the results of measurements of the next two parameters: depth and tire–soil contact area for the two tires tested.

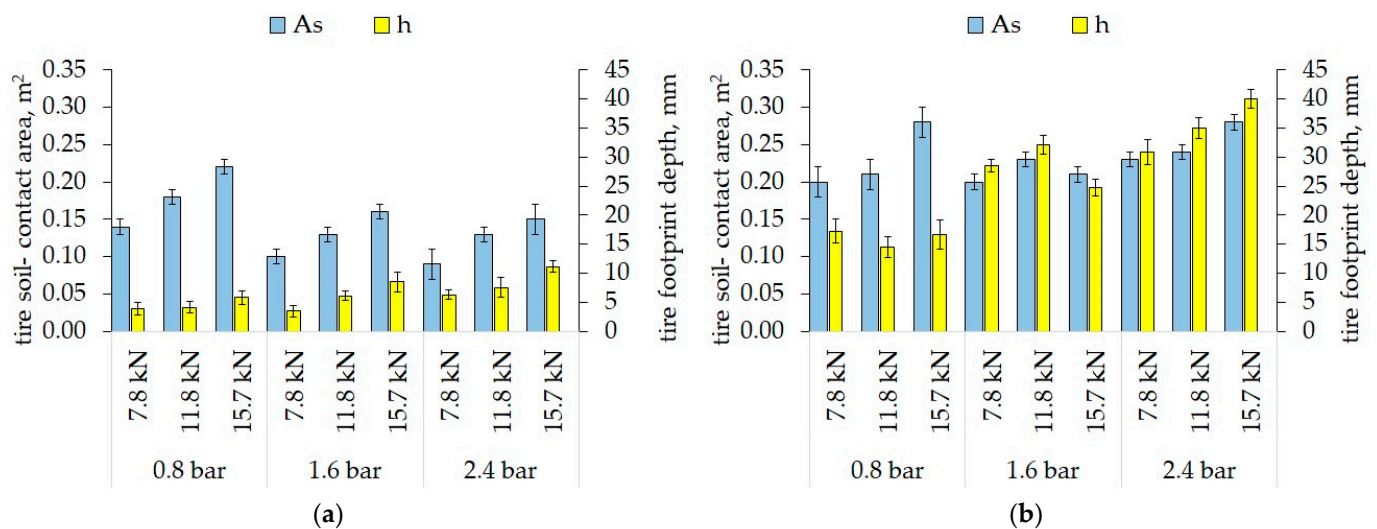


**Figure 4.** Values of tire footprint depth and tire–soil contact area: radial tire (a); bias-ply tire (b);  $A_S$ —tire–soil contact area and  $h$ —footprint depth.

Interpreting the footprint depth of the radial tire, it was noted that in all cases—at a constant value of inflation pressure—as the vertical load increased, the measured parameter increased as well. The smallest radial tire footprint depth (3.5 mm) was found at an inflation pressure of 1.6 bar and the smallest vertical load value. However, increasing the vertical load to 11.8 kN resulted in the greatest depth increase of 74%, resulting in a footprint depth of 6.1 mm. The highest value of the current parameter of 11.1 mm was found at an inflation pressure of 2.4 bar and the highest vertical load. The smallest increase in the current parameter for the radial tire was observed at an inflation pressure of 0.8 bar between the lowest and middle values of the vertical load—it was about 6%, which meant a change in the footprint depth from 3.9 mm to 4.1 mm. Inspecting the change in the value of the footprint depth due to an increase in tire pressure at the same vertical load, an increasing trend was observed in almost all cases. The largest increases in the parameter (48% and 46%) due to increasing the inflation pressure at a constant value of the vertical load were



observed with the first increase in pressure, i.e., from 0.8 bar to 1.6 bar for loads of 11.8 kN and 15.7 kN, respectively.

Analyzing the depth of bias-ply tire footprints, it was observed that in all cases, the footprints reached a depth of more than 10 mm. The smallest value of this parameter, at 14.6 mm, was observed at the lowest inflation pressure (0.8 bar) and at the middle value of the vertical load (11.8 kN). Reducing the vertical load to a value of 7.8 kN caused the bias-ply tire to generate a footprint that was 2.7 mm deeper (an increase of about 15% in the applied parameter). In turn, increasing the vertical load from the middle to the highest value also resulted in an increase in depth (from 14.6 mm to 16.6 mm, which corresponded to 14%). The opposite trend was observed at an inflation pressure of 1.6 bar. At the lowest vertical load, the depth of the footprint was equal to 28.5 mm, and an increase in the vertical load resulted in an increase in depth of about 13% (to a value of 32.2 mm), while as a result of another increase in load (to 15.8 kN), the depth decreased to 24.7 mm. On the other hand, at the highest adopted inflation pressure, the trend of the change in the footprint depth was opposite to the lower inflation pressures. The first increase in the vertical load on the tire to 11.8 kN resulted in an increase in the footprint depth of about 13% to a value of 35.0 mm, while the subsequent increase in the vertical load (to 15.7 kN) resulted in an increase in the footprint depth to a value of 40.0 mm, which was also the greatest footprint depth for a bias-ply tire.

The last parameter analyzed was the contact area between the tire and the soil. The highest value of this parameter for a radial tire ( $0.22 \text{ m}^2$ ) was observed at the lowest inflation pressure and the highest vertical load (0.8 bar and 15.7 kN, respectively). It is noteworthy that in the 0.8 bar inflation pressure, reducing the vertical load to 11.8 kN and then to 7.8 kN resulted in a decrease in the tire–soil contact area each time by a constant  $0.04 \text{ m}^2$  to values of  $0.18 \text{ m}^2$  and  $0.14 \text{ m}^2$  (decreases of 22% and 29%, respectively). A similar trend was observed in the inflation pressure of 1.6 bar, where a reduction in vertical load from 15.7 kN to 11.8 kN and 7.8 kN resulted in a reduction in the tire–soil contact area by  $0.03 \text{ m}^2$  (decreases of 23% and 30%). At the highest vertical load, the tire–soil contact area was equal to  $0.16 \text{ m}^2$ , and with the change in vertical load to lower values, it decreased by  $0.03 \text{ m}^2$  to values of  $0.13 \text{ m}^2$  and  $0.10 \text{ m}^2$ , respectively. The smallest value ( $0.09 \text{ m}^2$ ) of the current parameter was found at an inflation pressure of 2.4 bar and a vertical load of 7.8 kN.

The values of the contact area between the bias-ply tire and the soil were significantly larger compared to the radial tire (at the same inflation pressures and vertical loads). The smallest value of the inspected parameter for the bias-ply tire equal to  $0.20 \text{ m}^2$  was observed at a vertical load of 7.8 kN and the lowest and middle inflation pressure. At an inflation pressure of 0.8 bar, an increase in the vertical load from 7.8 kN to 11.8 kN resulted in a 5% increase in the analyzed parameter. In contrast, a further increase in vertical load resulted in a 33% increase in the contact area to a value of  $0.28 \text{ m}^2$ , the largest observed value of the tire–soil contact area. A value of  $0.28 \text{ m}^2$  was also observed at the highest tire pressure (2.4 bar) and the highest vertical load (15.7 kN). For this pressure, reducing the vertical load to 11.8 kN and then to 7.8 kN resulted in a 14% and 4% decrease in the value of the contact area (to values of  $0.24 \text{ m}^2$  and  $0.23 \text{ m}^2$ ), respectively. In the case of inflation pressure at 1.6 bar, a change in vertical load from the lowest to 11.8 kN resulted in a larger contact area (an increase from  $0.20 \text{ m}^2$  to  $0.23 \text{ m}^2$ , i.e., by 15%), but a subsequent increase in load resulted in a 9% decrease in the current parameter (to a value of  $0.21 \text{ m}^2$ ).

### 3.1. Statistical Analysis Results

#### 3.1.1. Analysis of Variance—Results for Radial Tire

Table 2 shows the results of the multiple analysis of variance for the results obtained for the radial tire. The *p*-values shown indicate the probability of accepting the null hypothesis representing the absence of a significant effect of a factor on the analyzed parameter.

**Table 2.** The statistical analysis of experimental data for the radial tire; the significance level  $\alpha = 0.05$ , and SD—standard deviation.

Footprint Parameter	Factor	Factor Level	Arithmetic Mean	±SD	<i>p</i> -Value
Width of the footprint (b), mm	Vertical load	7.8 kN	417.7 <sup>A</sup>	16.98	<0.00001
		11.8 kN	428.5 <sup>B</sup>	12.63	
		15.7 kN	455.0 <sup>C</sup>	18.04	
	Inflation pressure	0.8 bar	448.3 <sup>A</sup>	17.81	
		1.6 bar	433.3 <sup>B</sup>	23.80	
		2.4 bar	419.5 <sup>C</sup>	15.92	
Length of the footprint (l), mm	Vertical load	7.8 kN	283.9 <sup>A</sup>	50.82	<0.00001
		11.8 kN	338.1 <sup>B</sup>	55.77	
		15.7 kN	387.2 <sup>C</sup>	69.64	
	Inflation pressure	0.8 bar	413.3 <sup>A</sup>	56.29	
		1.6 bar	306.4 <sup>B</sup>	41.18	
		2.4 bar	289.6 <sup>C</sup>	39.53	
Depth of the footprint (h), mm	Vertical load	7.8 kN	4.53 <sup>A</sup>	1.53	<0.00001
		11.8 kN	5.90 <sup>B</sup>	1.86	
		15.7 kN	8.47 <sup>C</sup>	2.58	
	Inflation pressure	0.8 bar	4.59 <sup>A</sup>	1.28	
		1.6 bar	6.00 <sup>B</sup>	2.42	
		2.4 bar	8.31 <sup>C</sup>	2.45	
Tire–soil contact area ( $A_s$ ), m <sup>2</sup>	Vertical load	7.8 kN	0.11 <sup>A</sup>	0.03	<0.00001
		11.8 kN	0.15 <sup>B</sup>	0.03	
		15.7 kN	0.18 <sup>C</sup>	0.04	
	Inflation pressure	0.8 bar	0.18 <sup>A</sup>	0.04	
		1.6 bar	0.13 <sup>B</sup>	0.03	
		2.4 bar	0.12 <sup>B</sup>	0.03	

The letters at the arithmetic mean (<sup>A</sup>, <sup>B</sup>, and <sup>C</sup>) denote separate homogenous groups.

According to the data presented in the table above, it can be concluded that both factors had a significant effect on all four analyzed parameters, as the *p*-values were significantly lower than the accepted significance level  $\alpha$ . Reading the results of the post hoc tests, it was noted that only in the case of the effect of tire inflation pressure on the footprint area were the two levels (1.6 bar and 2.4 bar) classified into one group, which meant that there were no significant differences between these levels in terms of the footprint area. In all other cases, each factor level was classified as a separate homogeneous group.

As part of the statistical analysis, a model describing the relationship between the operating factors and the actual footprint area was verified. This model was developed in the laboratory part of the experiment and is presented in detail by Ptak et al. [26]. Its general form is shown in Equation (1).

$$A_s = -0.267 - 0.0427 \cdot \ln p_i + 0.012 \left( \ln \frac{G}{0.00981} \right)^2 - 0.0035 \left( \frac{G}{0.00981} \right)^{0.5} \quad (1)$$

where:

$A_s$ —contact area of the footprint (m<sup>2</sup>);

$p_i$ —inflation pressure (bar);

$G$ —vertical load (kN).

Verification of the model's suitability was carried out by comparing the experimental data (from the field part of the experiment) with the data calculated from the model. A linear regression analysis (using the F-Fisher test at a significance level of  $\alpha = 0.05$ ) was performed for the resulting data. Figure 5 shows the relationship between the two groups of numerical data.

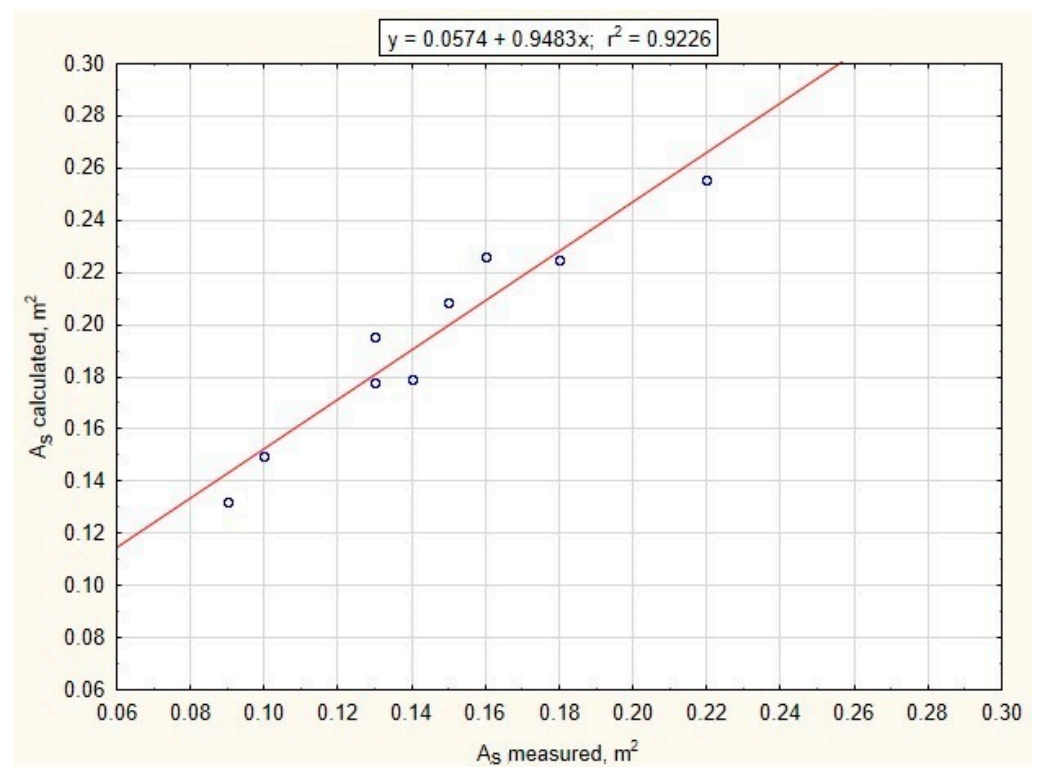


**Figure 5.** Relationship between the area values calculated from the model and the results of measurements under field conditions for footprints generated by the radial tire;  $A_S$ —area of the footprint.

Evaluating the comparison shown in Figure 5, one can see that the clustering of points around the straight line was high. The obtained value of the determination coefficient was 0.9226, which indicates a good fit of the model to the measurement data. Thus, it can be concluded that in the case of a radial tire, the model based on laboratory tests allows forecasting the contact area under field conditions (with known values of vertical load and inflation pressure). This thesis was also confirmed after testing the significance of the regression with the F-Fisher test. In this testing, the null hypothesis of non-significance of the regression coefficient and slope was assumed. The obtained value of the test function was equal to  $F(1,7) = 83.49$ , and the probability level of accepting the null hypothesis was equal to  $p = 0.00004$ . Since the probability level was much lower than the assumed significance level (0.05) and the value of the test function was large, the null hypothesis was rejected—this meant that the correlation coefficient was significant. The slope was also significant ( $p$ -value = 0.0076).

### 3.1.2. Analysis of Variance—Results for Bias-Ply Tire

Table 3 shows the results of the multivariate analysis of variance for the results obtained for the bias-ply tire. As in the previous case, the  $p$ -values denote the probability of accepting the null hypothesis representing the absence of a significant effect of a factor on the analyzed parameter.



**Table 3.** The statistical analysis of experimental data for the bias-ply tire; the significance level  $\alpha = 0.05$ , and SD—standard deviation.

Footprint Parameter	Factor	Factor Level	Arithmetic Mean	$\pm$ SD	<i>p</i> -Value
Width of the footprint (b), mm	Vertical load	7.8 kN	437.3 <sup>A</sup>	17.34	0.00726
		11.8 kN	446.2 <sup>A</sup>	20.04	
		15.7 kN	458.0 <sup>B</sup>	24.90	
	Inflation pressure	0.8 bar	469.4 <sup>A</sup>	15.63	
		1.6 bar	431.1 <sup>B</sup>	9.51	
		2.4 bar	440.9 <sup>B</sup>	18.40	
Length of the footprint (l), mm	Vertical load	7.8 kN	443.7 <sup>A</sup>	14.07	0.00019
		11.8 kN	474.1 <sup>B</sup>	17.36	
		15.7 kN	498.7 <sup>C</sup>	39.89	
	Inflation pressure	0.8 bar	476.4 <sup>A</sup>	41.03	
		1.6 bar	453.7 <sup>B</sup>	22.86	
		2.4 bar	486.5 <sup>A</sup>	30.91	
Depth of the footprint (h), mm	Vertical load	7.8 kN	25.55 <sup>A</sup>	6.50	0.51237
		11.8 kN	27.24 <sup>A</sup>	9.71	
		15.7 kN	27.25 <sup>A</sup>	10.57	
	Inflation pressure	0.8 bar	16.15 <sup>A</sup>	2.22	
		1.6 bar	28.48 <sup>B</sup>	3.45	
		2.4 bar	35.40 <sup>C</sup>	4.43	
Tire–soil contact area ( $A_s$ ), m <sup>2</sup>	Vertical load	7.8 kN	0.21 <sup>A</sup>	0.02	0.00063
		11.8 kN	0.23 <sup>A</sup>	0.02	
		15.7 kN	0.26 <sup>B</sup>	0.04	
	Inflation pressure	0.8 bar	0.23 <sup>A</sup>	0.04	
		1.6 bar	0.21 <sup>A</sup>	0.02	
		2.4 bar	0.25 <sup>B</sup>	0.02	

The letters at the arithmetic mean (<sup>A</sup>, <sup>B</sup>, and <sup>C</sup>) denote separate homogenous groups.

Inspecting the data presented in the table above, it can be concluded that the tire inflation pressure had a significant effect on all the analyzed parameters. In contrast, the second factor (vertical load) was found to have no significant effect on the depth of the footprint generated (in the other analyzed parameters, the significance was maintained). In addition, based on the results of post hoc tests (Fisher's NIR), it was found that in many cases, adjacent levels of the factor were qualified to the same group (e.g., levels of 1.6 bar and 2.4 bar when analyzing the effect of pressure on the width of the footprint, or levels of 7.8 kN and 11.8 kN when evaluating the effect of the load on the footprint area).

Verification of the correctness of the model selection was also carried out for the footprints generated by a bias-ply tire. As in the case of the radial tire, a model was developed based on laboratory tests presented in Ptak et al. [26]. The model had the following form (Equation (2)):

$$A_s = 0.947 - \frac{1.882}{p_i^{0.5}} + \frac{1.063}{p_i} + 7.76 \cdot 10^{-4} G \cdot \ln \frac{G}{0.00981} \quad (2)$$

where:

$A_s$ —contact area of the footprint (m<sup>2</sup>);

$p_i$ —inflation pressure (bar);

$G$ —vertical load (kN).

Figure 6 compares the data calculated from the model with the data acquired during field measurements. As in the case of the model for the radial tire, regression analysis was carried out using the F-Fisher test at a significance level of  $\alpha = 0.05$ .

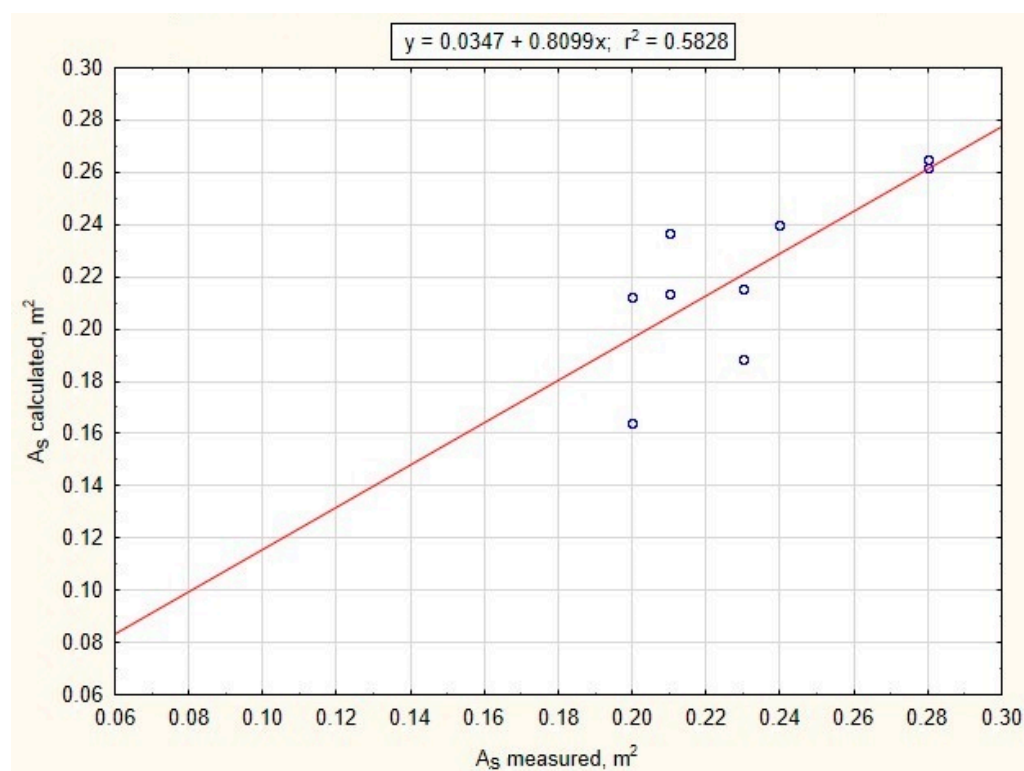


**Figure 6.** Relationship between the area values calculated from the model and the results of measurements under field conditions for footprints generated by a bias-ply tire;  $A_S$ —footprint area.

In the case of the bias-ply tire, a poorer fit between the data calculated from the model and the actual data is evident—there is a greater scattering of points from the regression line. The significance testing of the regression coefficient with the F-Fisher test showed that the value of the test function was equal to  $F(1,7) = 9.778$ , and the probability level of accepting the null hypothesis was equal to  $p = 0.0167$ . This meant that the determination coefficient was considered significant. However, the significance of the slope was not demonstrated (probability level  $p = 0.584$ ). Combined with the relatively low determination coefficient ( $R^2 = 0.58$ ), it can be concluded that the model developed for the bias-ply tire based on laboratory tests has limited applicability under field conditions (only 58% of the model results would coincide with actual results). To better reflect the data, developing a model that would consider additional parameters related to, for example, tire stiffness and parameters describing the ground condition is recommended.

#### 4. Discussion

The experiment conducted under field conditions made it possible to demonstrate differences in the dimensions of the soil footprint created by tires of different internal designs but with the same external dimensions at different vertical wheel loads and inflation pressures. Based on the analysis of the results, the adopted values of the experiment's variable factors differently affect the measured parameters, including the length and width of the footprint; the depth; and, in particular, the area of contact between the tire and the soil. In addition, the suitability of models developed based on laboratory tests for predicting the size of the footprint area under field conditions was evaluated.

Many authors indicate that a reduction in inflation pressure has the effect of increasing tire–soil contact area [27–29]. Diserens [13], examining a range of tires, showed a divergent effect of tire inflation pressure on the tire–soil contact area. Yadav and Raheman [30] showed that the tire–soil contact area increased with the vertical load on the tire. In addition, the rate of increase of the analyzed parameter decreased with an increase in tire size. It was also found that the tire–soil contact area decreased exponentially with an increase in inflation

pressure from 69 kPa to 234 kPa for any vertical tire load. Similar results were observed for both bias-ply and radial tires in the work of Sharma and Pandey [31], Schjønning et al. [27], Schjønning et al. [32], and Kumar et al. [33].

Thus, it seems reasonable to analyze the tire–soil contact surface as a three-dimensional image, also taking into account the depth of the rut formed by the tire. This is because analysis of the footprint as a plane can lead to oversimplifications, and the error will be greater in the depth of the footprint. Studies taking into account this parameter and the amount of soil deformation were conducted by Kenarsari et al. [23] and Pierzchała et al. [34]. This study showed that a similar value of the contact area of radial and bias-ply tires with the soil was obtained at a much greater footprint depth of the bias-ply tire. In the inflation pressure of 0.8 bar, a contact area in the range of 0.21 m<sup>2</sup>–0.22 m<sup>2</sup> was observed with a vertical load of 15.7 kN and 11.8 kN, and the footprint depth for these parameters was equal to 5.8 mm and 14.6 mm (for the radial and bias tire, respectively).

In this case, the footprint depth of the bias-ply tire was about 150% greater compared to the footprint of the other tire tested. The vertical load of the bias-ply tire with a value of 15.7 kN but at an inflation pressure of 1.6 bar resulted in a tire–soil contact area equal to 0.21 m<sup>2</sup>, but the footprint depth was 24.7 mm. It should be noted that a similar value of tire–soil contact area for the tires tested was observed at the same vertical load (15.7 kN) but at a lower pressure for the radial tire (0.8 bar). As a result, the bias-ply tire generated a footprint of 328%, making it more destructive to the soil than the radial tire’s footprint. At an inflation pressure of 1.6 bar, loading the radial tire with the highest accepted load value, a tire–soil contact area of 0.16 m<sup>2</sup> was observed. At the same inflation pressure but with the lowest vertical load, the bias-ply tire had a soil contact area of 0.20 m<sup>2</sup>. This value was only 0.04 m<sup>2</sup> greater compared to the radial tire, but the bias-ply tire’s footprint depth was over 20 mm greater at the same time.

Verifying the validity of the use of models describing the tire footprint area under field conditions, it can be concluded that only in the case of a radial tire can the developed model predict the contact area under real conditions. On the other hand, there are significant limitations to the use of the model developed under laboratory conditions for the bias-ply tire; the model could be used to a limited extent to predict the footprint area under real conditions (only 58% of the real results would agree with the results calculated from the model). To better fit the model to the real data, additional factors would need to be considered—primarily those related to the condition of the soil. This thesis is confirmed in the literature, where models of footprint surface and other parameters related to tire interaction with the soil are discussed [12].

## 5. Conclusions

Based on the conducted tests, it was found that:

1. Unambiguous determination of the factors affecting the tire–soil contact area is difficult due to their diversity. It should also be emphasized that the tire–soil contact area is the overriding parameter responsible for the distribution of stresses in the soil. It is therefore necessary to continue research in this direction, as this will facilitate the selection of appropriate operating parameters of agricultural tires for soil conditions. By verifying the models describing the tire footprint under laboratory conditions, it was found reasonable to use the model under field conditions, but only for a radial tire. In the case of a bias-ply tire, only 58% of the actual results agreed with those calculated from the model.
2. In the range of the same value of inflation pressure, the length and width of the radial tire footprint, in all cases, increased with increasing vertical load. Similarly, at a constant vertical load, a decrease in the discussed parameters was observed with an increase in inflation pressure. In the case of the bias-ply tire footprint, the trend was similar, except for an inflation pressure of 1.6 bar (the first increase in vertical load resulted in a decrease in the length and width of the footprint, and the next again caused an increase in the measured parameters).

3. The footprint depth and contact area of the radial tire increased with increasing vertical load at constant inflation pressure. As with the bias-ply tire's footprint length and width, its footprint depth and contact area increased due to increasing the vertical load at constant inflation pressure. The exception was a tire pressure range of 1.6 bar, at which the first increase in vertical load increased the footprint depth and the area of contact between the tire and the soil, while subsequent increases resulted in a decrease in these parameters.

**Author Contributions:** Conceptualization, J.C. and W.P.; methodology, J.C.; software, M.B. and W.P.; validation, M.B. and A.M.; formal analysis, J.C. and K.L.; investigation, W.P., M.B. and A.M.; resources, W.P.; data curation, M.B.; writing—original draft preparation, W.P. and M.B.; writing—review and editing, M.B.; visualization, W.P.; supervision, J.C.; project administration, J.C. and K.L.; funding acquisition, J.C. and K.L. All authors have read and agreed to the published version of the manuscript.

**Funding:** The article processing charge was financed by the Wrocław University of Environmental and Life Sciences.

**Institutional Review Board Statement:** Not applicable.

**Data Availability Statement:** Not applicable.

**Conflicts of Interest:** The authors declare no conflict of interest. The funders had no role in the design of the study; in the collection, analyses, or interpretation of data; in the writing of the manuscript; or in the decision to publish the results.

## References

1. Cook, R.J. Toward cropping systems that enhance productivity and sustainability. *Proc. Natl. Acad. Sci. USA* **2006**, *103*, 18389–18394. [[CrossRef](#)] [[PubMed](#)]
2. Lyu, X.; Peng, W.; Niu, S.; Qu, Y.; Xin, Z. Evaluation of sustainable intensification of cultivated land use according to farming households' livelihood type. *Ecol. Indic.* **2022**, *138*, 108848. [[CrossRef](#)]
3. Keller, T.; Sandin, M.; Colombi, T.; Horn, R.; Or, D. Historical increase in agricultural machinery weights enhanced soil stress levels and adversely affected soil functioning. *Soil Tillage Res.* **2019**, *194*, 104293. [[CrossRef](#)]
4. Khemis, C.; Abrougui, K.; Ren, L.; Mutuku, E.A.; Chehaibi, S.; Cornelis, W. Effects of tractor loads and tyre pressures on soil compaction in Tunisia under different moisture conditions. *Geophys. Res. Abstr.* **2017**, *19*. [[CrossRef](#)]
5. Botta, G.F.; Tolon-Becerra, A.; Lastra-Bravo, X.; Tourn, M. Tillage and traffic effects (planters and tractors) on soil compaction and soybean (*Glycine max* L.) yields in Argentinean pampas. *Soil Tillage Res.* **2010**, *110*, 167–174. [[CrossRef](#)]
6. Ren, L.; Vanden Nest, T.; Ruysschaert, G.; D'Hose, T.; Wim Cornelis, W. Short-term effects of cover crops and tillage methods on soil physical properties and maize growth in a sandy loam soil. *Soil Tillage Res.* **2019**, *192*, 76–86. [[CrossRef](#)]
7. Grečenko, A. Tyre footprint area on hard ground computed from catalogue values. *J. Terramech.* **1995**, *32*, 325–333. [[CrossRef](#)]
8. Hallonborg, U. Super ellipse as tyre-ground contact area. *J. Terramech.* **1996**, *33*, 125–132. [[CrossRef](#)]
9. Keller, T. A model for the prediction of the contact area and the distribution of vertical stress below agricultural tyres from readily available tyre parameters. *Biosyst. Eng.* **2005**, *92*, 85–96. [[CrossRef](#)]
10. Roşca, R.; Cârlescu, P.; Ţenu, I. A semi-empirical traction prediction model for an agricultural tyre, based on the super ellipse shape of the contact surface. *Soil Tillage Res.* **2014**, *141*, 10–18. [[CrossRef](#)]
11. Yong, R.N.; Boonsinsuk, P.; Fattah, E.A. Tyre load capacity and energy loss with respect to varying soil support stiffness. *J. Terramech.* **1980**, *17*, 131–147. [[CrossRef](#)]
12. Jakliński, L. *Mechanika Układu Pojazd-Teren w Teorii i Badaniach*; Oficyna Wydawnicza Politechniki Warszawskiej: Warszawa, Poland, 2006; pp. 34–35.
13. Diserens, E. Calculating the contact area of trailer tyres in the field. *Soil Tillage Res.* **2009**, *103*, 302–309. [[CrossRef](#)]
14. Diserens, E.; Défossez, P.; Duboisset, A.; Alaoui, A. Prediction of the contact area of agricultural traction tyres on firm soil. *Biosyst. Eng.* **2011**, *110*, 73–82. [[CrossRef](#)]
15. Taghavifar, H.; Mardani, A. Investigating the effect of velocity, inflation pressure, and vertical load on rolling resistance of a radial ply tire. *J. Terramech.* **2013**, *50*, 99–106. [[CrossRef](#)]
16. González Cueto, O.; Iglesias Coronel, C.E.; Recarey Morfa, C.A.; Urriolagoitia Sosa, G.; Hernández Gómez, L.H.; Urriolagoitia Calderón, G.; Herrera Suárez, M. Three dimensional finite element model of soil compaction caused by agricultural tire traffic. *Comput. Electron. Agric.* **2013**, *99*, 146–152. [[CrossRef](#)]
17. González Cueto, O.; Iglesias Coronel, C.E.; López Bravo, E.; Recarey Morfa, C.A.; Herrera Suárez, M. Modelling in FEM the soil pressures distribution caused by a tyre on a Rhodic Ferralsol soil. *J. Terramech.* **2016**, *63*, 61–67. [[CrossRef](#)]
18. Khot, L.R.; Salokhe, V.M.; Jayasuriya, H.P.W.; Nakashima, H. Experimental validation of distinct element simulation for dynamic wheel-soil interaction. *J. Terramech.* **2007**, *44*, 429–437. [[CrossRef](#)]

19. Nakashima, H.; Kobayashi, T. Effects of gravity on rigid rover wheel sinkage and motion resistance assessed using two-dimensional discrete element method. *J. Terramech.* **2014**, *53*, 37–45. [[CrossRef](#)]
20. Smith, W.; Melanz, D.; Senatore, C.; Iagnemma, K.; Peng, H. Comparison of discrete element method and traditional modeling methods for steady-state wheel-terrain interaction of small vehicles. *J. Terramech.* **2014**, *56*, 61–75. [[CrossRef](#)]
21. Nakashima, H.; Oida, A. Algorithm and implementation of soil–tire contact analysis code based on dynamic FE–DE method. *J. Terramech.* **2004**, *41*, 127–137. [[CrossRef](#)]
22. Michael, M.; Vogel, F.; Peters, B. DEM–FEM coupling simulations of the interactions between a tire tread and granular terrain. *Comput. Methods Appl. Mech. Eng.* **2015**, *289*, 227–248. [[CrossRef](#)]
23. Kenarsari, A.E.; Vitton, S.J.; Beard, J.E. Creating 3D models of tractor tire footprints using close-range digital photogrammetry. *J. Terramech.* **2017**, *74*, 1–11. [[CrossRef](#)]
24. Kormanek, M. Determination of rut parameters at various levels of slip of a pneumatic drive wheel—Laboratory research. *Agric. Eng.* **2013**, *4*, 71–81.
25. Ptak, W.; Czarnecki, J.; Brennenstul, M. Use of 3D scanning technique to determine tire deformation in static conditions. *J. Agric. Eng.* **2022**, *53*, 1. [[CrossRef](#)]
26. Ptak, W.; Czarnecki, J.; Brennenstul, M.; Lejman, K.; Małeczka, A. Evaluation of Tire Footprint in Soil Using an Innovative 3D Scanning Method. *Agriculture* **2023**, *13*, 514. [[CrossRef](#)]
27. Schjøning, P.; Lamandé, P.M.; Tøgersen, F.A.; Arvidsson, J.; Keller, T. Modelling effects of tyre inflation pressure on the stress distribution near the soil–tyre interface. *Biosyst. Eng.* **2008**, *99*, 133–199. [[CrossRef](#)]
28. Keller, T. Soil Compaction and Soil Tillage-Studies in Agricultural Soil Mechanics. Ph.D. Thesis, Swedish University of Agricultural Sciences, Uppsala, Sweden, 2004.
29. Komandi, G. The determination of the deflection, contact area, dimensions, and load capacity for driven pneumatic operating on concrete pavement. *J. Terramech.* **1976**, *13*, 15–20. [[CrossRef](#)]
30. Yadav, R.; Raheman, H. Development of an artificial neural network model with graphical user interface for predicting contact area of bias-ply tractor tyres on firm Surface. *J. Terramech.* **2023**, *107*, 1–11. [[CrossRef](#)]
31. Sharma, A.K.; Pandey, K.P. The deflection and contact characteristics of some agricultural tyres with zero sinkage. *J. Terramech.* **1996**, *33*, 293–299. [[CrossRef](#)]
32. Schjøning, P.; Stettler, M.; Keller, T.; Lassen, L.; Lamandé, M. Predicted tyre–soil interface area and vertical stress distribution based on loading characteristics. *Soil Tillage Res.* **2015**, *152*, 52–66. [[CrossRef](#)]
33. Kumar, S.; Noori, M.T.; Pandey, K.P. Performance characteristics of mode of ballast on energy efficiency indices of agricultural tyre in different terrain condition in controlled soil bin environment. *Energy* **2019**, *182*, 48–56. [[CrossRef](#)]
34. Pierzchała, M.; Talbot, B.; Astrup, R. Measuring wheel ruts with close-range photogrammetry. *Forestry* **2016**, *89*, 383–391. [[CrossRef](#)]

**Disclaimer/Publisher’s Note:** The statements, opinions and data contained in all publications are solely those of the individual author(s) and contributor(s) and not of MDPI and/or the editor(s). MDPI and/or the editor(s) disclaim responsibility for any injury to people or property resulting from any ideas, methods, instructions or products referred to in the content.

#### **4. Oświadczenia współautorów**

##### **4.1. Use of 3D scanning technique to determine tire deformation in static conditions**



Weronika Ptak  
imię i nazwisko

Wrocław, 14.06.2023 r.  
(miejsowość i data)

Instytut Inżynierii Rolniczej  
Uniwersytet Przyrodniczy we Wrocławiu  
ul. Chełmońskiego 37  
51-630 Wrocław  
afiliacja

### OŚWIADCZENIE

Oświadczam, że w pracy: Ptak W., Czarnecki J., Brennenstul M. 2022. Use of 3D scanning technique to determine tire deformation in static conditions. Journal of Agriculture Engineering, 53, 1-7 mój udział polegał na opracowaniu koncepcji i metodyki badań, prowadzeniu badań, obsłudze oprogramowania, analizie wyników i ich interpretacji, prezentacji wyników, pisaniu oryginalnego manuskryptu, odpowiedzi na recenzje i edycji manuskryptu oraz zapewnieniu finansowania.

14.06.2023 Weronika Ptak

data i podpis

Jarosław Czarnecki  
imię i nazwisko

Wrocław, 14.06.2023 r.  
(miejscowość i data)

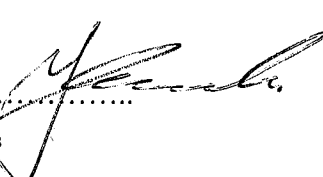
Instytut Inżynierii Rolniczej  
Uniwersytet Przyrodniczy we Wrocławiu  
ul. Chełmońskiego 37  
51-630 Wrocław  
afiliacja

### OŚWIADCZENIE

Oświadczam, że w pracy: Ptak W., Czarnecki J., Brennenstul M. 2022. Use of 3D scanning technique to determine tire deformation in static conditions. Journal of Agriculture Engineering, 53, 1-7 mój udział polegał na tworzeniu koncepcji badań i opracowaniu metodyki, zapewnieniu finansowania, analizie formalnej.

14.06.2023

data i podpis



Marek Brennensthul  
imię i nazwisko

Wrocław, 14.06.2023 r.  
(miejsowość i data)

Instytut Inżynierii Rolniczej  
Uniwersytet Przyrodniczy we Wrocławiu  
ul. Chelmońskiego 37  
51-630 Wrocław  
afiliacja

### OŚWIADCZENIE

Oświadczam, że w pracy: Ptak W., Czarnecki J., Brennensthul M. 2022. Use of 3D scanning technique to determine tire deformation in static conditions. Journal of Agriculture Engineering, 53, 1-7 mój udział polegał na prowadzeniu badań, obsłudze oprogramowania, analizie wyników i ich interpretacji, pisaniu oryginalnego manuskryptu oraz odpowiedzi na recenzje i edycji manuskryptu.

14.06.2023 Brennensthul

data i podpis

## 4.2. Evaluation of agriculture tires deformation using innovative 3D scanning method

Weronika Ptak  
imię i nazwisko

Wrocław, 14.06.2023 r.  
(miejsowość i data)

Instytut Inżynierii Rolniczej  
Uniwersytet Przyrodniczy we Wrocławiu  
ul. Chełmońskiego 37  
51-630 Wrocław  
afiliacja

### OŚWIADCZENIE

Oświadczam, że w pracy: Ptak W., Czarnecki J., Brennenstul M., Lejman K., Małecka A. 2022. Evaluation of agriculture tires deformation using innovative 3D scanning method. Agriculture, 12, 1108 mój udział polegał na opracowaniu koncepcji i metodyki badań, prowadzeniu badań, obsłudze oprogramowania, zbiorze danych, analizie wyników, ich interpretacji i analizie statystycznej, prezentacji wyników, pisaniu oryginalnego manuskryptu, odpowiedzi na recenzje i edycji manuskryptu.

14.06.2023 

data i podpis

Jarosław Czarnecki  
imię i nazwisko

Wrocław, 14.06.2023 r.  
(miejscowość i data)


Instytut Inżynierii Rolniczej  
Uniwersytet Przyrodniczy we Wrocławiu  
ul. Chęłmońskiego 37  
51-630 Wrocław  
afiliacja

### OŚWIADCZENIE

Oświadczam, że w pracy: Ptak W., Czarnecki J., Brennenstul M., Lejman K., Małecka A. 2022. Evaluation of agriculture tires deformation using innovative 3D scanning method. Agriculture, 12, 1108 mój udział polegał na tworzeniu koncepcji badań i opracowaniu metodyki, analizie wyników, zapewnieniu finansowania, analizie formalnej.

14.06.2023

data i podpis





Marek Brennensthul  
imię i nazwisko

Wrocław, 14.06.2023 r.  
(miejsowość i data)

Instytut Inżynierii Rolniczej  
Uniwersytet Przyrodniczy we Wrocławiu  
ul. Chełmońskiego 37  
51-630 Wrocław  
afiliacja

### OŚWIADCZENIE

Oświadczam, że w pracy: Ptak W., Czarnecki J., Brennensthul M., Lejman K., Małecka A. 2022. Evaluation of agriculture tires deformation using innovative 3D scanning method. Agriculture, 12, 1108 mój udział polegał na prowadzeniu badań, obsłudze oprogramowania, zbiorze danych, analizie wyników, ich interpretacji i prowadzeniu analizy statystycznej, pisaniu oryginalnego manuskryptu, odpowiedzi na recenzje i edycji manuskryptu.

14.06.2023. Brennensthul

data i podpis

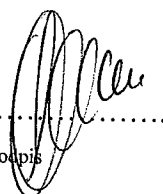
Krzysztof Lejman  
imię i nazwisko

Wrocław, 14.06.2023 r.  
(miejsowość i data)

Instytut Inżynierii Rolniczej  
Uniwersytet Przyrodniczy we Wrocławiu  
ul. Chełmońskiego 37  
51-630 Wrocław  
afiliacja

### OŚWIADCZENIE

Oświadczam, że w pracy: Ptak W., Czarnecki J., Brennenstul M., Lejman K., Małecka A. 2022. Evaluation of agriculture tires deformation using innovative 3D scanning method. Agriculture, 12, 1108 mój udział polegał na analizie wyników, analizie formalnej, zapewnieniu finansowania.

14.06.2023.....  
data i podpis 

Agata Małecka  
imię i nazwisko

Wrocław, 14.06.2023 r.  
(miejsowość i data)

Instytut Inżynierii Rolniczej  
Uniwersytet Przyrodniczy we Wrocławiu  
ul. Chelmońskiego 37  
51-630 Wrocław  
afiliacja

### OŚWIADCZENIE

Oświadczam, że w pracy: Ptak W., Czarnecki J., Brennensthul M., Lejman K., Małecka A. 2022. Evaluation of agriculture tires deformation using innovative 3D scanning method. Agriculture, 12, 1108 mój udział polegał na pozyskaniu danych, analizie i wizualizacji wyników.

14.06.2023 Agata Małecka

.....  
data i podpis

### 4.3. Evaluation of tire footprint in soil using innovative 3D scanning method

Weronika Ptak  
imię i nazwisko

Wrocław, 14.06.2023 r.  
(miejscowość i data)

Instytut Inżynierii Rolniczej  
Uniwersytet Przyrodniczy we Wrocławiu  
ul. Chełmońskiego 37  
51-630 Wrocław  
afiliacja

### OŚWIADCZENIE

Oświadczam, że w pracy: Ptak W., Czarnecki J., Brennenstul M., Lejman K., Małecka A. 2023. Evaluation of tire footprint in soil using innovative 3D scanning method. Agriculture, 13, 514 mój udział polegał na opracowaniu koncepcji i metodyki badań, prowadzeniu badań, obsłudze oprogramowania, zbiorze danych, analizie wyników, ich interpretacji i analizie statystycznej, prezentacji wyników, pisaniu oryginalnego manuskryptu, odpowiedzi na recenzje i edycji manuskryptu.

14.06.2023 Weronika Ptak  
data i podpis

Jarosław Czarnecki  
imię i nazwisko

Wrocław, 14.06.2023 r.  
(miejsowość i data)

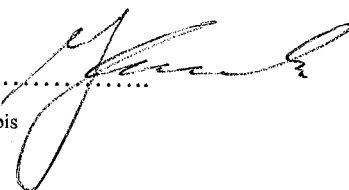
Instytut Inżynierii Rolniczej  
Uniwersytet Przyrodniczy we Wrocławiu  
ul. Chełmońskiego 37  
51-630 Wrocław  
afiliacja

### OŚWIADCZENIE

Oświadczam, że w pracy: Ptak W., Czarnecki J., Brennenstul M., Lejman K., Małecka A. 2023. Evaluation of tire footprint in soil using innovative 3D scanning method. Agriculture, 13, 514 mój udział polegał na tworzeniu koncepcji badań i opracowaniu metodyki, analizie wyników, zapewnieniu finansowania, analizie formalnej.

14.06.2023

data i podpis



Marek Brennensthul  
imię i nazwisko

Wrocław, 14.06.2023 r.  
(miejscowość i data)

Instytut Inżynierii Rolniczej  
Uniwersytet Przyrodniczy we Wrocławiu  
ul. Chełmońskiego 37  
51-630 Wrocław  
afiliacja

### OŚWIADCZENIE

Oświadczam, że w pracy: Ptak W., Czarnecki J., Brennensthul M., Lejman K., Małecka A. 2023. Evaluation of tire footprint in soil using innovative 3D scanning method. Agriculture, 13, 514 mój udział polegał na prowadzeniu badań, obsłudze oprogramowania, zbiorze danych, analizie wyników, ich interpretacji i prowadzeniu analizy statystycznej, pisaniu oryginalnego manuskryptu, odpowiedzi na recenzje i edycji manuskryptu.

14.06.2023 - Brennensthul

data i podpis



Krzysztof Lejman  
imię i nazwisko

Wrocław, 14.06.2023 r.  
(miejscowość i data)

Instytut Inżynierii Rolniczej  
Uniwersytet Przyrodniczy we Wrocławiu  
ul. Chełmońskiego 37  
51-630 Wrocław  
afiliacja

### OŚWIADCZENIE

Oświadczam, że w pracy: Ptak W., Czarnecki J., Brennensthal M., Lejman K., Małecka A. 2023. Evaluation of tire footprint in soil using innovative 3D scanning method. Agriculture, 13, 514 mój udział polegał na analizie wyników, analizie formalnej, zapewnieniu finansowania.

14.06.2023   
data i podpis

Agata Małecka  
imię i nazwisko

Wrocław, 14.06.2023 r.  
(miejsowość i data)

Instytut Inżynierii Rolniczej  
Uniwersytet Przyrodniczy we Wrocławiu  
ul. Chełmońskiego 37  
51-630 Wrocław  
afiliacja

### OŚWIADCZENIE

Oświadczam, że w pracy: Ptak W., Czarnecki J., Brennenstul M., Lejman K., Małecka A. 2023. Evaluation of tire footprint in soil using innovative 3D scanning method. Agriculture, 13, 514 mój udział polegał na pozyskaniu danych, analizie i wizualizacji wyników.

14.06.2023 Agata Małecka

.....  
data i podpis

#### 4.4. Evaluation of tires acting on soil in field conditions using 3D scanning method

Weronika Ptak  
imię i nazwisko

Wrocław, 14.06.2023 r.  
(miejsowość i data)

Instytut Inżynierii Rolniczej  
Uniwersytet Przyrodniczy we Wrocławiu  
ul. Chełmońskiego 37  
51-630 Wrocław  
afiliacja

### OŚWIADCZENIE

Oświadczam, że w pracy: Ptak W., Czarnecki J., Brennensthul M., Lejman K., Małecka A. 2023. Evaluation of tires acting on soil in field conditions using 3D scanning method. Agriculture, 13, 1094 mój udział polegał na opracowaniu koncepcji i metodyki badań, prowadzeniu badań, obsłudze oprogramowania, zbiorze danych, analizie wyników, ich interpretacji i analizie statystycznej, prezentacji wyników, pisaniu oryginalnego manuskryptu, odpowiedzi na recenzje i edycji manuskryptu.

14.06.2023   
data i podpis

Jarosław Czarnecki  
imię i nazwisko

Wrocław, 14.06.2023 r.  
(miejsowość i data)

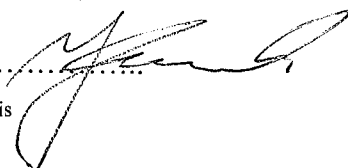
Instytut Inżynierii Rolniczej  
Uniwersytet Przyrodniczy we Wrocławiu  
ul. Chelmońskiego 37  
51-630 Wrocław  
afiliacja

### OŚWIADCZENIE

Oświadczam, że w pracy: Ptak W., Czarnecki J., Brennensthul M., Lejman K., Małecka A. 2023. Evaluation of tires acting on soil in field conditions using 3D scanning method. Agriculture, 13, 1094 mój udział polegał na tworzeniu koncepcji badań i opracowaniu metodyki, analizie wyników, zapewnieniu finansowania, analizie formalnej.

14.06.2023

data i podpis



Marek Brennensthul  
imię i nazwisko

Wrocław, 14.06.2023 r.  
(miejsowość i data)

Instytut Inżynierii Rolniczej  
Uniwersytet Przyrodniczy we Wrocławiu  
ul. Chełmońskiego 37  
51-630 Wrocław  
afiliacja

### OŚWIADCZENIE

Oświadczam, że w pracy: Ptak W., Czarnecki J., Brennensthul M., Lejman K., Małecka A. 2023. Evaluation of tires acting on soil in field conditions using 3D scanning method. Agriculture, 13, 1094 mój udział polegał na prowadzeniu badań, obsłudze oprogramowania, zbiorze danych, analizie wyników, ich interpretacji i prowadzeniu analizy statystycznej, pisaniu oryginalnego manuskryptu, odpowiedzi na recenzje i edycji manuskryptu.

14.06.2023 Brennensthul

data i podpis

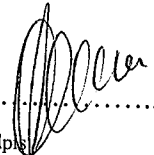
Krzysztof Lejman  
imię i nazwisko

Wrocław, 14.06.2023 r.  
(miejsowość i data)

Instytut Inżynierii Rolniczej  
Uniwersytet Przyrodniczy we Wrocławiu  
ul. Chelmońskiego 37  
51-630 Wrocław  
afiliacja

### OŚWIADCZENIE

Oświadczam, że w pracy Ptak W., Czarnecki J., Brennensthal M., Lejman K., Małecka A. 2023. Evaluation of tires acting on soil in field conditions using 3D scanning method. Agriculture, 13, 1094 mój udział polegał na analizie wyników, analizie formalnej, zapewnieniu finansowania.

14.06.2023 .....  
data i podpis 



Agata Małecka  
imię i nazwisko

Wrocław, 14.06.2023 r.  
(miejsowość i data)

Instytut Inżynierii Rolniczej  
Uniwersytet Przyrodniczy we Wrocławiu  
ul. Chełmońskiego 37  
51-630 Wrocław  
afiliacja

### OŚWIADCZENIE

Oświadczam, że w pracy: Ptak W., Czarnecki J., Brennenstul M., Lejman K., Małecka A. 2023. Evaluation of tires acting on soil in field conditions using 3D scanning method. Agriculture, 13, 1094 mój udział polegał na pozyskaniu danych, analizie i wizualizacji wyników.

14.06.2023 Agata Małecka

.....  
data i podpis